FLOW CONTROL OPTIMIZATION FOR IMPROVEMENT OF FAN NOISE REDUCTION

HANS R RAVEN E

Thesis submitted to the Faculty of Virginia Polytechnic Institute and State University in partial fulfillment of the requirement for the degree of

MASTER OF SCIENCE IN MECHANICAL ENGINEERING

Dr. Wing Fai Ng, Chair

Dr. Ricardo Burdisso

Dr. Clint Dancey

May 6, 2004

Blacksburg, VA

Keywords: Fan Noise Reduction, Flow Control, Wake Management, Trailing Edge Blowing, Suction Surface Blowing, Aerodynamic Loss, Fan, CFD, Computational Fluid Dynamics, Cascade Testing

FLOW CONTROL OPTIMIZATION FOR IMPROVEMENT OF FAN NOISE REDUCTION

HANS R RAVEN E

Abstract

The study of the flow of a fan blade was conducted to improve tonal fan noise reduction by optimizing an existing flow control configuration. The current configuration consisted of a trailing edge Slot with a flow control area of 0.045 in² per inch span with an exit angle of -3.3° with respect to the blade exit angle. Two other flow control configurations containing discrete jets were investigated. For the first configuration, the trailing edge jets (TEJ), the fan blade was modified with discrete jets spaced 0.3 inches apart with a flow control area of 0.01 in² per inch span positioned on the trailing edge aimed at -3.3° with respect to the blade exit angle. Similarly, discrete jets were also placed on the suction surface at 95.5% chord aimed at 15° with respect to the local blade surface. This configuration is referred to as the suction surface jet (SSJ). The discrete jets for both configurations were designed to be choked while injecting a mass flow rate of 1.00% of the fan through-flow. Computational Fluid Dynamics (CFD) was used to model new configurations and study subsequent changes in total pressure deficit using a blade design inlet Mach number of 0.73, Reynolds number based on chord length of 1.67×10^6, and design incidence angle of 0°. Experimental testing was later conducted in a 2D cascade tunnel. The TEJ and SSJ were tested at design blowing of 1.00% and at off-design conditions of 0.50%, 0.75%, and 1.25% fan through-flow. Results between the different flow control configurations were compared using a blowing coefficient. CFD showed the TEJ and SSJ offered aerodynamic improvement over the Slot configuration. Testing showed the SSJ outperformed the TEJ, as validated in CFD, producing wider and shallower wakes. SSJ area-averaged pressure losses were 25% less than TEJ at design. Noise predictions based on CFD findings showed that both TEJ and SSJ provided additional tonal sound power level attenuation over the Slot configuration at similar blowing coefficients, with the SSJ providing the most attenuation. Noise prediction based on experimental results concurred that the SSJ provided more total attenuation than the TEJ. Experimental results showed that the SSJ performed better aerodynamically and, based on analytical prediction, provided 2 dB more total attenuation than the TEJ.

I would like to dedicate my work to my parents. Their support throughout my years of college has made possible the achievement of this work and my degrees at Virginia Tech. Gracias, mamá y papá.

Acknowledgements

I would like to thank Dr. Ng, who gave me the opportunity to participate in various projects during my graduate studies. Without the opportunities presented, I may not have obtained my thesis.

David Arntz and Dr. Burdisso deserve my gratitude, too. They performed all the acoustic analysis for this project and were both great help in explaining the workings of acoustics and the prediction code.

Dr. Burdisso also deserves my thanks for having served me on my committee, as does Dr. Dancey. Thank you, Dr. Dancey, for also introducing me to the exciting world of fluids. My many instructors deserve my thanks, because without them I wouldn't know nearly as much as I do now.

Sarah Stitzel, Stephen Guillot, and Techsburg made CFD for this project possible. Sarah setup the CFD. Without her initial help, I would have never been able to run my CFD solutions, and it would have taken me twice as long to troubleshoot. Techsburg generated all of the grids used. Stephen and Sarah also graciously modified grids when I needed flow control at different locations.

My friends, particularly Bo Song, Todd Bailie, and Angie Rabe, also deserve recognition. Their knowledge, friendship, and/or experience were invaluable to me both in my research, my classes, and in life. I thank them for making my years at Tech all the better and warmer, and for helping me climb the obstacles I found along the way.

Lastly, I would also thank my wife, Marie Garber. Thank you for your patience, understanding, and support. I could not have done it without you.

Table of Contents

Index of Figures

Index of Tables

Index of Equations

Nomenclature

a	Speed of sound
A	Area
A_{jet}	Normal flow control area
A_L	Solid blade sound power level attenuation due to flow control
A_{LT}	Total solid blade sound power level attenuation due to flow control
$A_{orifice}$	Orifice area (bore)
A_{pipe}	Flow control supply pipe inner area
C	Fan blade chord length
$c_{blowing}$	Blowing coefficient
c_d	Orifice discharge coefficient
d	Diameter
$d_{orifice}$	Orifice diameter (bore)
d_{pipe}	Flow control supply pipe inner diameter
G	Momentum
L_w	Sound power level
L_{wT}	Total sound power level
m	Mass
$\dot{m}$	Mass flow rate
M	Mach number
$\overline{M}$	Average Mach number
$\hat{n}$	Normal unit vector
p	Pressure
p_o	Total pressure
p_s	Static pressure
Δp	Pressure drop across orifice meter
R	Gas constant

S	Pitch
T	Temperature
T_o	Total temperature
u	Uncertainty
V	Velocity
$\dot{V}$	Volumetric flow rate
w_d	Wake depth
X_1	Upstream (inlet) value of X
X_2	Downstream (exit) value of X
X_{jet}	Value of X pertaining to the flow control or to the flow control at the opening on the blade surface
Y	Wake half-width

Greek Letters

γ	Specific heat ratio
$\varepsilon_{\dot{m}}$	Non-dimensional mass flow error
ρ	Density
σ	Standard deviation
ω	Pressure loss coefficient

Abbreviations

BPF	Blade Passing Frequency
CFD	Computational Fluid Dynamics
SSJ	Suction Surface Jets (Suction Surface Discrete Jets)
TEJ	Trailing Edge Jets (Trailing Edge Discrete Jets)
VGJ	Vortex Generating Jets

Chapter 1. Introduction

1.1 Motivation

Engine system noise studies have shown that the dominant perceived noise source from turbofan engines at take off and landing operations is fan noise. Figure 1-1 below illustrates the dominance of fan noise for typical 1992-level technology turbofan engines [NASA Facts]. With the advent of higher bypass-ratio next-generation turbofan engines and stricter future noise regulations, fan noise reduction will become an integral part of turbofan engine design. Implementation of methods previously used for fan noise reduction, such as acoustic liners, optimized rotor-stator axial spacing, and rotor-stator blade count to achieve tonal "cut-off", will fail to meet these future regulations. Employment of new methods under study over the last eleven years will be a key factor for future ultra-high-bypass turbofan engines to be used commercially.

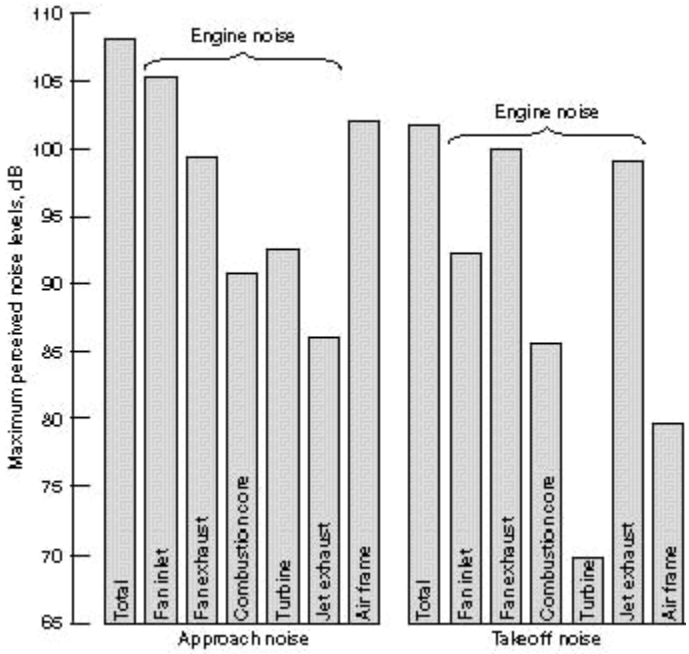

Figure 1-1 A breakdown of noise sources for a 1992-level technology turbofan engine for both approach landing and takeoff [NASA Facts]. Fan inlet and exhaust noise contribute largely to the total perceived noise level.

Interaction of the wake deficit produced by the fan rotor and the downstream stator vanes emits fan noise. The mean wake profile shed by the rotors creates unsteady pressure perturbations on the stators. When coupled to fan acoustic modes, this periodic unsteadiness creates tonal noise which shows up as multiples of the blade passing frequency (BPF), whereas non-periodic pressure fluctuations generate broadband noise [Brookfield].

Flow control, also referred to as wake management, has proven to be an effective means of reducing fan noise by suppressing the unsteady rotor-stator interaction (see section 1.2.2 for further discussion). Flow control is used to reduce pressure losses created by boundary layer viscous effects. This is achieved either by removing (suction) low momentum fluid to decrease boundary layer thickness or by adding (blowing) high momentum fluid to energize low momentum zones.

This thesis studies a fan blade geometry with a baseline flow control scheme. The baseline flow control consisted of a trailing edge slot blowing configuration. A 2D cross-section was studied in order to optimize a flow control scheme to achieve optimal fan noise reduction when compared to the default configuration. Both Computational Fluid Dynamics (CFD) and testing in a cascade were performed, and rotor wake velocity data was input by David Arntz and Dr. Ricardo Burdisso into NASA's CUP2D fan noise prediction code.

Previous research conducted has consisted of studies into the benefits of flow control. The first studies conducted to validate the usefulness of flow control were performed on flat plates. The research on blade geometries has mainly centered on the use of flow control in noise reduction and separation control. Some research has been conducted in the areas of high cycle fatigue (HCF) and into the effects of flow control on aerodynamic losses. These areas all deal with the unsteady interaction of wake deficits on downstream blade components (whether rotor or stator). The following section presents a summary of related research.

1.2 Literature Review

Presented below is previous research that has been conducted with emphasis in the areas of flow control and fan noise reduction. A discussion of flow control and its applications to fan noise, high cycle fatigue, separation control, and aerodynamic losses is initially presented followed by a brief discussion on alternative methods of fan noise reduction.

1.2.1 Flow Control Research on Flat Plates

Some of the first tests conducted to validate the use of flow control involved 2D flat plate testing in low speed (low Reynolds number) situations. Park and Cimbala [1991] conducted a study on the effects of flow control initial conditions on mean velocity and turbulence quantity decay rates in a 2D setting applying flow control to create a momentumless wake. The momentumless wake for this case is one where the momentum averaged across the wake equals the freestream value.

Park and Cimbala performed tests on a flat plate with a blunt end and different blowing configurations in an open-return low-speed wind tunnel. The freestream velocity was 4.2 m/s with

a Reynolds number based on the model diameter of 5400. Three types of flow control configurations were tested: central slot blowing, asymmetric slot blowing, and dual slot blowing. With each configuration, an overblown momentumless wake was achieved.

Smoke-wire flow visualization was collected up to 60 diameters downstream of the trailing edge of the test piece. These flow visualizations displayed that the dual slot excited strong vortex generation near the blunt trailing edge. Stronger turbulence was observed in the asymmetric and dual slot cases. Mean velocity profile data showed mean velocity overshoot decay rates of $x^{-0.92}$, $x^{-1.24}$, and $x^{-2.02}$ for central, asymmetrical, and dual slot configurations, respectively. Wake spreading rates were reported as slowest for the asymmetrical slot ($x^{0.30}$) and fastest for the dual slots ($x^{0.46}$). The rates for the central slot fell in between ($x^{0.36}$). Turbulence measurements showed axial turbulence intensity decay rates were equal for all three cases ($x^{-0.81}$), despite differences in magnitudes. Reynolds stress decay rates were much faster for dual jets than asymmetric ($x^{-2.49}$ to $x^{-1.84}$). Thus, Cimbala and Park concluded mean velocity decay rates and some turbulence quantities are dependent of initial conditions, with the exception of turbulence decay rates.

Naumann [1992] and Corcoran [1992] performed tests on a flat airfoil in a large scale water channel. Flow control was applied using trailing edge blowing through single slot, double slot, and double discrete jets. Four fractions of the blowing rate required to produce integrally momentumless wakes were used to study the sensitivity of wake attenuation to blowing rates. Trailing edge vortex generators were also used for some tests. The Reynolds number based on the chord was greater than 400,000. Particle image velocimetry (PIV) was used to obtain steady and unsteady wake measurements at 0.72 chords. For fully turbulent cases discrete jets proved best at reducing wake deficit and turbulence. When coupled with the jets, the vortex generators yielded quicker mixing of the wake.

Although tests of this kind were important to showing the feasibility of flow control geometries in affecting the steady and unsteady aspects of a wake and its decay and mixing rates, these tests lack applicability in modern turbomachinery. Flat plates subjected to low speeds experience different flow conditions than what is seen in modern stages with unsteady transonic flow, turning angles, and incidence angles. Other aspects not discussed or studied, such as the amount of mass flow used for the flow control and overshot wakes, are an important design criteria that will make the application of this technology feasible or unfeasible for modern and future engines. While application in modern turbomachinery was not as relevant, the initial findings were important to the development of the application of flow control in turbomachinery.

1.2.2 Flow Control Research in Fan Noise

The use of flow control in turbomachinery was not thoroughly studied until it became feasible and practical in modern and for future engines. Waitz, et al [1996] presented the first study of the application of flow control for the reduction of fan noise. The study evaluated the use of mass addition and removal for decreasing rotor-stator interaction and subsequent unsteady stator loading.

The blade geometry and inlet conditions used were representative of next generation high bypass turbine engines. A 2D cross-section of the midspan section of a 16 rotor blade 40 stator blade fan was chosen for this study. The blade was 0.25m in chord and 0.3m in span. Takeoff conditions were used for all tests. The first BPF was cutoff. Two flow control techniques were studied: boundary layer suction and trailing edge blowing.

Simulations were first conducted to study and predict the effects of varying wake width and depth and using boundary layer suction on unsteady stator loading. MISES was used to compute steady, viscous rotor results. UNSFLO was then used to obtain unsteady, Navier-Stokes solutions for the stator. Acoustic calculations were performed with LINSUB.

Gaussian wake distributions were manipulated to characterize the effects on unsteady stator loading and acoustic noise. Results showed that decreasing wake depth reduced unsteady stator loading harmonics and consequently acoustic tones. Changes in wake width, however, affected the harmonic content, because acoustic modes (1×BPF, 2×BPF, 3×BPF, etc.) peak when the wake width is the rotor pitch divided by that mode's number. Thus, by affecting wake width, the wake harmonic content can be changed. Since most fan stages have the 1×BPF tone cutoff, it is desired for wakes width to be 100% of the pitch. By doing so, the first acoustic mode will peak (contain the most energy), yet be cutoff. Simulations concluded that wide shallow wakes are desired for flow control.

Boundary layer suction numerical analysis was also conducted. With no suction, analysis showed the wakes merged downstream. With the application of small amounts of suction, wakes no longer merged, and the wake deficit was increased, i.e. the freestream increased since the wakes no longer merged. This scenario showed an increase in unsteady stator loading of 5%. For higher suction rates, this was not the case. By removing 3.5% of the fan through-flow, a loading reduction of 25% was achieved with suction located at 80% chord. However, the largest reduction in noise occurred by using approximately half the previous mass flow removal at 50-60% chord. This condition produced the smallest change in wake width to wake depth ratio.

Waitz tested with a three blade cascade used for aerodynamic measurements in a wind tunnel using a hot wire anemometer probe. Measurements were performed at 0.5, 1.0, 1.5, and 2.5 chords downstream of the trailing edge of the blade. Boundary layer suction was evaluated at 0.5 and 0.8 chords removing 1.5% and 2.2% of the fan through-flow. Blowing was performed at 0.7%, 0.8%, and 0.9% of fan through-flow. Measurements were performed using only one of the flow control conditions. The Reynolds number based on the blade chord was 3×10^5. Forty static pressure taps divided equally between suction and pressure sides were also used for comparison to solutions calculated with MISES (all taps were found to agree within 5% of MISES results).

Experimental results showed that reductions in wake width and depth using boundary layer suction coincided with numerical findings. With suction applied at 80% chord and removing 2.2% of the fan through-flow, 35% reduction in turbulent velocity fluctuation was achieved at 1.5 chords downstream. This produced a 3.7 dB reduction in broadband noise. Acoustic modes resulted with a 4.4 dB reduction in the 2×BPF mode with similar decreases in the higher-order modes.

Trailing edge blowing was conducted at various flow rates. Using 0.9% of fan through-flow, blowing produced a maximum reduction of velocity fluctuation of 50% at 1.5 chords downstream. This produced a 6 dB reduction in broadband noise. Acoustic calculations resulted in reductions of 11.4 dB at 2×BPF with 5-10 dB at higher-order modes.

Waitz et al concluded that trailing edge blowing was a better alternative to flow control when compared to boundary layer suction. The pressure required to use blowing could be obtained from core compressor stages. Boundary layer suction requires the use of a source to provide the mass removal. Trailing edge blowing is not limited by a finite trailing edge thickness like boundary layer suction. Also, radial pressure gradients seen in a rotating system hinder air movement to the hub for removal. Thus, trailing edge blowing uses less mass flow and passage area to produce better reductions than those seen with suction.

Sell's thesis [1997] presented the same study as Waitz et al, but with more detail. Sell concluded that the boundary layer suction design had its limits. Using suction at 80% chord with 1.25% of the fan through-flow, reductions in wake momentum thickness, wake half width, and wake deficit were 50%, 10%, and 43%, respectively. Increasing suction to 2.23% of the fan through-flow only demonstrated small improvements since the 1.25% case suctioned 102% of the boundary layer mass flow developed on the suction surface of the blade. Sells concluded in agreement with Waitz et al that the trailing edge blowing flow control was much more effective compared to suction surface boundary layer removal.

Sells mentioned that a good trailing edge design used as many small diameter holes as possible, directed to affect the wake's centerline. Three trailing edge blowing configurations were tested, one aimed at the metal angle, another at an estimated deviation angle, and another alternating between both angles. Integrally momentumless wakes were produced for each case, and off design conditions were tested. The best reductions in wake deficit and unsteadiness were performed by the momentumless wakes. Using 125% of the mass flow required for the momentumless wake yielded the worst results for both wake measurements and acoustic estimates. The deviation angle configuration proved the most effective, cutting back unsteadiness by 44.5% and steady profile nonuniformity by 68% (at 1.5 chords). Estimated reductions in acoustic tones of 22.4 dB, 18.6 dB, 13.2 dB, and 7.6 dB were seen for 2 to 5×BPF, respectively, with 7.0 dB reduction in broadband. Both Waitz et al and Sell concluded that testing in a two-dimensional cascade could not account for three-dimensional effects, and further testing would need to be conducted in the future using a rotating rig.

Eventually, Brookfield and Waitz [1998] tested in a rotating fan stage. These first-of-a-kind experiments were performed using a $1/6^{th}$-scale high bypass ratio fan with a mass-averaged total-to-static pressure ratio of 1.2, tip and inlet Mach number of 0.8 and 0.4, respectively, and tip diameter of 0.56 m. The rotor consisted of 16 wide-chord blades followed by a stator row of 40 blades. Flow field measurements were conducted 0.5 chords upstream and 0.1, 0.5, 1.0, and 1.5 chords downstream of the rotor using a probe with four flush mounted Kulite pressure transducers. Acoustic measurements were conducted by duct microphones pairs placed in the outer casing at $1/16^{th}$ of the circumference apart and 1 chord upstream and downstream of both blade rows. One stator blade was instrumented with 13 flush-mounted Kulites in order to obtain unsteady stator surface pressure measurements.

The trailing edge blowing rotor blades were designed such that changes to the external blade geometry were insignificant. Numerical simulations were used to design internal passages to yield a momentumless wake along the whole blade span. Using no injection, the trailing edge blowing rotors showed insignificant differences when compared to solid blade performance, although with some exception near the tip due to small differences in untwist characteristics and exterior shape. Average Mach numbers downstream of the rotor were within 4%, wake deficits 7%, and total pressures 1%.

A span-wise uniform momentumless wake was not achieved during testing. Instead, a tip-weighted (with the tip overblown) and midspan-weighted blowing distributions were realized. Less

than 2% of the fan through-flow was used for blowing during testing. Results showed time-mean relative Mach profiles were smoothed, yielding results of up to an 85% reductions in wake harmonic amplitudes. Brookfield and Waitz believed that reductions greater than 10 dB for radiated tonal noise may be possible. At BPF using a tip-weighted blowing distribution, stator unsteady loading showed a reduction of 10 dB.

Future testing for their program will attempt to obtain uniform span-wise blowing distributions so that radial coupling of the acoustic modes is not changed. Later, blowing only in specific span-wise locations will be tested to better understand three-dimensional flow and acoustic fields to gauge noise prediction tools.

Other work performed on a 3D test rig was done by Leitch, et al [1999]. The primary focus of this study was decreasing fan noise generated by rotors passing through wakes shed by upstream stators. The testing rig consisted of a 1/14 scale inlet designed as a combination of supersonic and subsonic designs (this combination was done for a wider range of applicability of results). The inlet used four stators with no turning angle located 0.75 rotor chords upstream of rotor. Trailing edge blowing was used on the stators and designed for a uniform profile using a minimal amount of air (testing used 1% of fan through-flow).

A Tech Development Inc. Turbofan Simulator, Model 460, was used to act as the high bypass ratio turbofan engine. The simulator was composed of a 4.1-inch diameter fan consisting of 18 fan blades followed by 26 exit guide vanes (EGV) one rotor chord length downstream. A 29 blade single-stage power turbine provides the power for the fan. The simulator was operated at 30,000, 50,000, and 70,000 rpm.

Testing was conducted at the Virginia Tech Anechoic Chamber facility. The chamber is considered anechoic above 200 Hz and has an ambient noise level of 30 dB, which is much lower than the measured levels. In order to prevent intake of ground vortices, the test rig was located four feet from the ground.

Aerodynamic and acoustic measurements were taken during testing with and without blowing. Aerodynamic performance of the fan was recorded by mapping total and static pressures at fan face and downstream stator wakes. Aerodynamic measurements were performed at the stators, fan face, and fan exit.

Acoustic measurements were performed with a Bruel and Kjaer Model 4136 condenser microphone at 12 horizontal locations along a circular arc from 0° to 110° at 48 inches from the

inlet. A Bruel and Kjaer Model 2030 spectrum analyzer was also used. Sound pressure level (SPL) for a particular location was comprised of 100 averaged spectral measurements.

For the aerodynamic results, a distortion parameter was calculated based on Aerospace Recommended Practice (ARP 1420) by the Society of Automotive Engineers. The parameter showed a 30% reduction for 30,000 and 50,000 rpm. Aerodynamic measurements were not taken at 70,000 rpm. It was also shown that trailing edge blowing did not change the fan operating point. Acoustic results showed an overall SPL reduction of 1 dB for all cases tested. Directivity plots showed for 30,000 rpm a maximum tone SPL reduction of 8.9 dB at 80° and an average 6.2 dB reduction in tone SPL btw 30° and 90°. For 50,000 rpm and 70,000 rpm, average reductions in tone SPL were found to be 2.6 dB and 1.2 dB, respectively.

Rao, et al [1999] presented the follow-up for this project implementing the use of active flow control. The stators used varied from those tested by Leitch. Like Leitch, four stators were used upstream. However, these stators used a different flow control configuration, where the blowing passage began at 1/8-inch diameter at the hub and ended at 1/16-inch diameter at the trailing edge hole. The flow rate was controlled by a Redwood Microsystems NO-3000 Fluistor Micro-Electro-Mechanical-System (MEMS) based microvalves. Each flow control hole was controlled by a microvalve.

A Single-Input-Single-Output (SISO) proportional, integral, and derivative (PID) controller actuated the microvalves. The controller used freestream pitot-static measurements as a reference. Blowing flow rates were optimized by matching total pressures measured 0.5 stator chords downstream of the stator with reference.

Bench testing of the stator blades was conducted prior to experimental testing. Blowing was optimized to set the wake axial velocities at 0.5 stator chords downstream of the control holes equal to freestream values at the same span-wise location. Velocity contours showed that flow control yielded good results, showing a more pitch-wise uniform contour with blowing than without.

The effectiveness of the controller was tested under flow conditions varying with time. Results showed the PID controller performed well. Under typical operating conditions, the controller was shown to be a practical means of reducing the wake deficit.

Acoustic measurements were conducted at the Virginia Tech Anechoic Chamber facility using a similar set-up to that described by Leitch. Testing was conducted at 29,500 rpm and 40,000 rpm. At 29,500 rpm, the BPF showed a 10 dB reduction with flow control implemented and 3 to 5 dB reductions in the first four harmonics. Directivity results showed a maximum reduction of 8.2

dB at 20° and 3 dB or more at most other locations. At 40,000 rpm, directivity showed a maximum reduction of 7.3 dB at 20° with flow control, with some reduction in the 0° to 40°. Between 60° and 110°, SPL remained equal to those seen with no blowing. A possible explanation given this was since the stator wakes were known to be completely reenergized, the presence of rotor-EGV interaction as source of noise was more dominant at 40,000 rpm than at 29,500 rpm. Estimated BPF power reductions were 4.4 dB at 29,500 rpm and 2.9 dB at 40,000 rpm.

1.2.3 Flow Control Research in Separation Control

Flow control has also been applied to situations where boundary layer formation of low momentum fluid causes adverse pressure gradients and thus separation of the fluid. Separation can have negative effects on performance and efficiency of components, causing major losses and other undesirable effects. In order to inhibit these effects, flow control has been implemented to mix or add high momentum fluid to low momentum boundary layers to delay separation and energize the fluid.

Qin et al [2000] presented a numerical study backed by experimental data on the effects of varying application of mass removal, mass injection, bumps, and synthetic jets to affect shock interactions. The goal of the study was to identify key parameters in changing the shock interaction zone via the different flow control methods. Using a variety of aerofoil, tests were conducted to validate the flow control's effectiveness in reducing shock strength and drag to lift ratios. Validation of the numerical method used was done by comparing results obtained with the numerical code to previous experiments performed on the aerofoil. Comparison between the results was found to be in good agreement.

Placing suction upstream of the shock was found to be detrimental to the aerodynamic performance of the blade. By placing the suction at or downstream of the shock, lift to drag ratios could be improved. Increasing the amount of mass removal tended to move the shock further downstream resulting in increases in performance in high lift regions of the blade and decreases in the low lift regions. Even though stronger suction delayed separation, an increase in shock strength was also observed.

Mass injection was tested similarly by placing the flow control upstream of, at, and downstream of the shock. Simulations revealed that blowing at or downstream of the shock would move the shock upstream, with slight shock strength reduction. The best results were obtained by blowing at the interaction zone. Blowing ahead of the shock created compression waves that would soften the effects of the shock and soften the adverse pressure gradient.

Other applications of flow control in fluid separation can be observed in low pressure turbines (LPT). LPT's usually experience separation at high-altitude where the Reynolds number based on the chord drops into the laminar region. Flow control in the form of a vortex generating jet (VGJ) can be applied in order to generate mixing and delay or inhibit separation on the LPT's suction surface. Bons et al [2002] studied the effects of using a VGJ on a LPT by adding pulsing to the flow control. A previous study performed by Bons showed that a narrow spike with a 1% duty cycle could provide the necessary flow control to inhibit separation. Bons's study attempted to further investigate the effects of the pulsing frequency and duty cycle on the effectiveness of the separation control.

Bons conducted tests in an open-loop, induction wind tunnel applying a flow field with a Reynolds number based on the chord of 25000 and low turbulence. VGJ's were applied onto the blade's suction surface at 0.63 chords. The flow control was aimed 30° in the pitch with a 90° skew and spaced every ten diameters with a 1-mm diameter. The cascade test section had a solidity of 1.13 and a turning angle of 85°. The pulsing was provided by a high-speed solenoid valve driven with a General Valve, Inc. Iota One.

Previous research performed on the blade by Bons showed that separation occurred between 68% and 73% of the chord. Results from these previous studies had shown that separation control could be obtained using pulsing jets with an order of magnitude decrease in required mass flow. Good results were obtained with a signal run at a low duty cycle, effectively creating a spike versus a step pulsing signal.

Tests performed in the Bons's study sought how changes in frequency affected the effectiveness of the VGJ's in preventing separation. One blowing ratio and two duty cycles (10% and 50%) were used to study the effects of changing dimensionless forcing frequencies from 0.012 to 7.7.

Phase locked wake and boundary layer measurements conducted by Bons recorded up to 60% reduces in losses. Raster plots were used to observe the time development of the flow under different pulsing frequencies. After the pulse occurred, the flow was observed to enter a transient state that settled into a steady "controlled" relaxation period before the flow returned to its "uncontrolled" separated state. Bons showed that as long as a pulse occurred prior to the end of the relaxation period, the "controlled" state was maintained. Further tests conducted showed that the "uncontrolled" state occurred within the same relaxation period (constant of the flow) regardless the

length of the pulse. Thus, Bons concluded that the beginning on the pulse was key to the dynamic response of the flow and not the length of the pulse.

Bons concluded that the study showed great promise for the effectiveness of pulsing VGJ's in separation of LPT's and for economy of mass flow. However, applicability of pulsing VGJ's would need to be studied for individual cases in order to optimize the design since the relaxation period is a function of the particular flow.

1.2.4 Flow Control Research in High Cycle Fatigue

Military engines experience more HCF failure than what is normally seen in commercial aircraft due to their high operating demands. Studies of high cycle fatigue (HCF) reduction using flow control are relatively new and few in number. Wake deficits produced by upstream stators or rotors produce forcing functions on downstream compressor blades. The unsteady nature of the flow produces forced excitations on the blades. Most of these vibrations lie within design limits. However, for resonance crossings occurring in the operating range, load cycles intensify quickly at high rotational frequencies which can lead to fatigue failure.

Bailie [2002] studied the effectiveness of trailing edge blowing on reducing forced vibrations using the Air Force Research Lab's Stage Matching Investigation transonic compressor rig. The test rig consisted of a row of 33 rotor blades followed by 49 stator blades. Wake generators (WG) with trailing edge blowing were placed upstream of the rotors to provide the forcing function. The wakes produced are similar to those created by a highly loaded, low-aspect ratio, modern front stage. Testing used 12 WG vane count and a 26% chord axial spacing between the WG and rotor row.

Results from earlier testing conducted in a transonic blowdown wind tunnel at Virginia Tech yielded the trailing edge blowing design for the compressor rig. Seven holes with a 0.082 in diameter and a 2.5 pitch-to-diameter ratio were placed outside of the endwall boundary layers in order to promote circumferential flowfield uniformity. The holes provided coverage along the entire span excluding the endwall boundary layer region. In the compressor rig test, strain gages were placed on nine rotor blades on three pressure-side locations on each blade. The strain gage's locations were selected for their sensitivity to anticipated critical modes.

Two modes were selected for testing: first torsional mode (~13,700 rpm) and the second leading-edge bending mode (~12,600 rpm). These two modes were within the primary operating range and chosen since lower harmonics normally exert greater forcing. Trailing edge blowing at 0.8% of the rig mass flow was shown to be able to suppress rotor response amplitude. For full span blowing, a 66% reduction in rotor strain was obtained at the first torsional mode, 46% reduction at

the leading edge bending mode, and an 87% reduction at second chordwise bending. Studies conducted with partial span blowing showed that excitation of current modes or creation of new ones was possible with certain configurations. Moderate increases in pressure ratio and efficiency were also detected.

1.2.5 Flow Control Research in Aerodynamic Losses

Few studies of flow control have concentrated solely on reducing aerodynamic losses. Carter, et al [2001] presented the study of a high-turning compressor blade with flow control consisting of boundary layer suction (BLS) and blowing from a single motive source. Whereas most flow control systems using BLS have implemented the use of a pump that expels removed mass flow to atmosphere, this ejector pump design mixed suctioned mass with the motive supply flow for ejection of the mixed flow through the jets.

Cascade testing of the compressor blade was performed at the transonic blowdown wind tunnel facility at Virginia Tech. The stator was based on the high-turning USAF TESCOM compressor, designed to use counter swirl to obtain higher loading. A 2D cross-section near the tip was chosen for study. The chord of the blade was 4 inches with a pitch of 1.8 inches and a turning angle of 69°. The test section consisted of a seven stator cascade with a 6-inch span.

Initial testing of the blade revealed separation near the trailing edge. As discussed previously, the excitation of a low momentum area from the boundary layer provides separation control. This can be done via removal of low momentum fluid or the addition of high momentum fluid. The use of both allows for further control of separation. Discrete suction holes (0.0625-inch diameter) were placed 0.805 chords downstream of the leading edge, slightly downstream of the separation point, and blowing holes (0.079-inch diameter) were placed at 0.895 chords. The 16 suction and 17 blowing holes were staggered in order to minimize interaction. Static and total pressure measurements were conducted at locations upstream and downstream of the stators. Downstream traverses were taken at 0.1 and 0.5 chords of the trailing edge.

Wake depth measurements showed a minimum normalized total pressure of 0.75 (where one is the freestream value) for no flow control or baseline. Applying motive supply sources of 0.7%, 0.9%, 1.2%, 1.4%, and 1.6% of the passage mass through-flow, minimum normalized total pressures of 0.8, 0.82, 0.83, 0.84, and 0.85 were obtained, respectively. Additionally, at 1.6% through-flow, a 65% reduction of total pressure loss coefficient was obtained. Flow turning angle was also found to increase, with wake centers shifting towards the pressure side. Up to 4.5° of additional turning were estimated using a motive supply of 1% of the mass through-flow. However, further study with an

angle probe is required to determine whether or not the turning is also seen in the freestream. Improvements in turning angles could lead to smaller chord lengths or stage sizes or fewer stages.

1.3 Goal of Current Research

Previous work conducted on flow control has shown that it is an effective means of reducing the unsteady rotor-stator interaction caused by wake deficits on the downstream stators. These studies have linked the benefits of reducing this interaction to reductions in noise generation, improvements in aerodynamic efficiency, and reductions in unsteady forcing functions known to cause HCF. However, few studies have been conducted solely in the optimization of flow control for purposes of reduction of unsteady rotor-stator interaction. Flow control is still a new technique which is slowly seeing its emergence as a practical and beneficial means of reducing rotor-stator interaction. Its implementation in modern engines will become necessary in order to meet noise regulations, improve efficiency of higher turning/loading components, and prevent fatigue of components on engines experiencing highly demanding operating conditions.

This project's primary goal is to optimize an existing flow control design that will allow for reduction in tonal noise generated by rotor-stator interaction of a fan. A fan blade geometry optimized for flow control was presented for study. Current blade design used a trailing edge blowing slot for wake management in order to provide fan noise reduction. An enhancement of this design was requested such that improvements in noise reduction could be maximized.

The first phase of this project was conducted studying a 2D cross-section of the fan blade geometry. CFD was used to iterate different proposed flow control configurations and study the effectiveness of given designs. Chordwise location as well as span-wise distribution was investigated, as well as jet direction. Acoustic simulations for the project were performed by David Arntz and Dr. Ricardo Burdisso using a numerical code. The most promising flow control schemes were chosen for experimental testing in a linear transonic blowdown cascade wind tunnel. Different mass flow rates were also tested in order to view the effectiveness of the different flow control schemes under off design conditions.

The research conducted is the first phase of an ongoing project. Results from the current study will be applied to a three-dimensional low speed test rig for measurements of the acoustic field. Eventually, research of this kind will allow the integration of flow control into commercial aircraft engines and future ultra high bypass ratio engines. In such a way, this type of research will

provide a basis for future work and show the benefits for noise control and subsequent aerodynamic and vibration improvements.

Chapter 2. Study Procedure

This chapter includes descriptions of the equipment and the procedures used. Description of the fan blade geometry (2.1) and flow control design (2.2) is followed by discussion of the testing facility (2.4). The cascade test section is discussed in section 2.5. Instrumentation and Data Acquisition are discussed in section 2.7 followed by a presentation of the flow control air supply used for this study (2.6). The Computational Fluid Dynamics (CFD) methodology used is discussed in section 2.3. Lastly, key calculations and data reduction techniques are discussed in section 2.8 before the beginning of Chapter 3 with the study experimental results.

2.1 Fan Blade Design

The fan geometry is based on NASA's efficient low-noise fan program modified with a thicker trailing edge for flow control purposes. The fan is an 18-blade 22-inch-diameter rotor followed by a 44-blade stator. Figure 2-1 shows a 3D rendition of the fan section.

Testing of the geometry was performed at conditions representative of take-off. For this study, a two dimensional cross-section of the fan geometry was taken at a radius of 9.89 inches (89.9% span). The cross-section's chord is 3.88 inches with a 3.63-inch pitch. The 2D blade has a 0° incidence angle at a design inlet Mach 0.73 assuming 8750 rpm with a turning angle of -15.4°. The flow exit Mach number is 0.45. The inlet and outlet flow angles are 55.4° and 40.0°, respectively. Figure 2-2 shows the 2D cross-section.

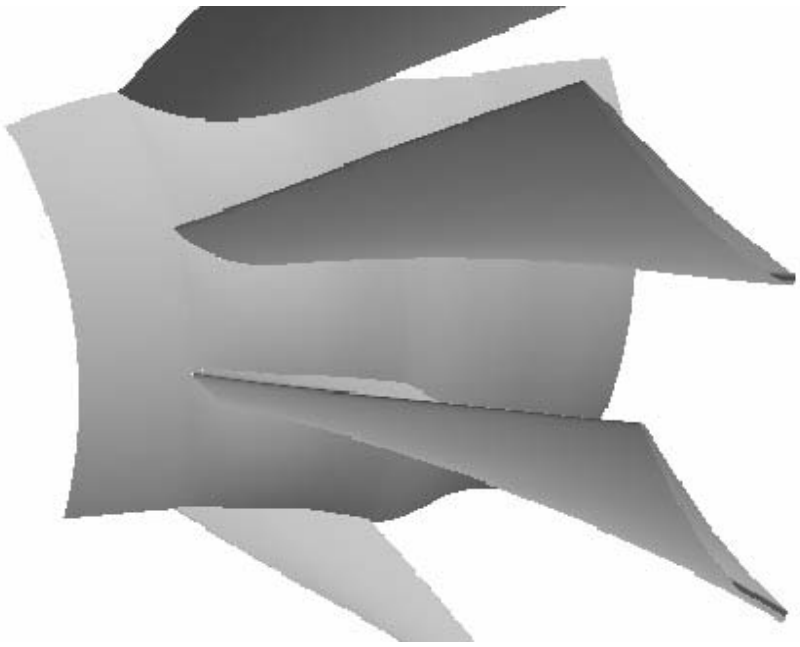

Figure 2-1 Three-dimensional fan rotor geometry

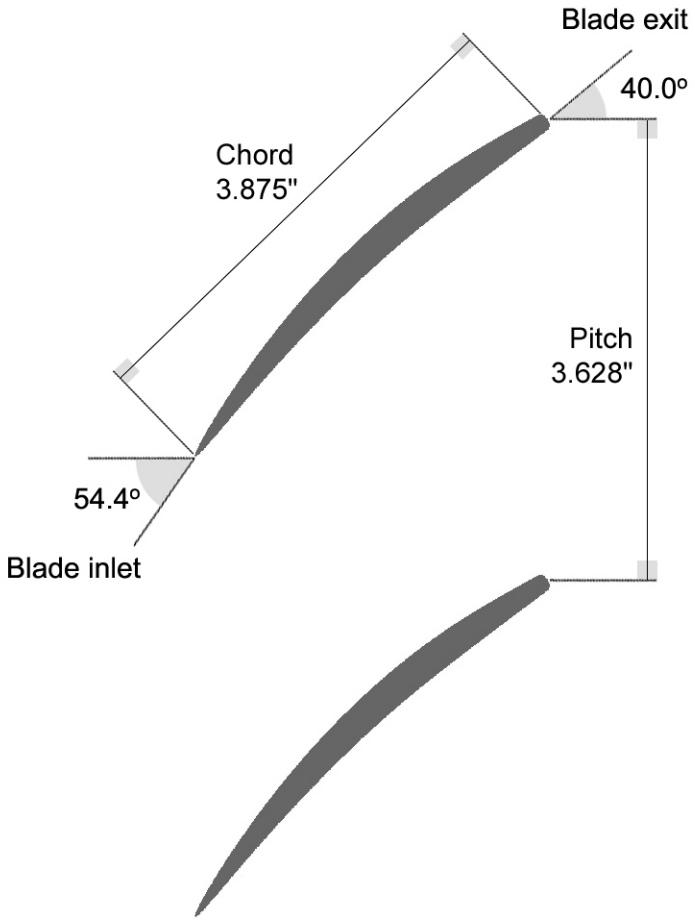

Figure 2-2 Fan blade cross-section studied

2.2 Flow Control Design

As mentioned in the previous chapter, the goal of the current project is to improve upon the effectiveness of an existing flow control configuration by attempting different configurations and concepts. CFD was used to test conceptual flow control schemes and evaluate their effectiveness in affecting the wake deficit produced by the blade. A detailed summary of these results are documented in Appendix A.

A design scheme was produced for investigating possible improvements in the existing flow control configuration, the Slot, by first recreating that flow control configuration using CFD. The use of discrete jets was then implemented with a study of spacing between holes assuming a constant mass flow rate per inch span. Following the study of discrete jets on the trailing edge, the jets were moved to the suction surface. Various locations and angles were studied. Lastly, other more complex jets implementing pitch and span angles were studied, but none proved more

effective than the designs presented in this study. Three flow control configurations were investigated for this study: Slot, trailing edge jets (TEJ), and suction surface jets (SSJ).

2.2.1 Slot

The blade was supplied with a trailing edge slot flow control scheme. The default scheme is shown in Figure 2-3, where the slot width and angle vary with radial location along the trailing edge of the rotor. For the cross-section studied, the baseline flow control was interpolated to be 0.0454 inches in width aimed at an angle of 36.7°. The area (inch^2) per inch span for the Slot was 0.0454 in^2/in. This flow control scheme is the baseline case to which other flow control schemes will be compared.

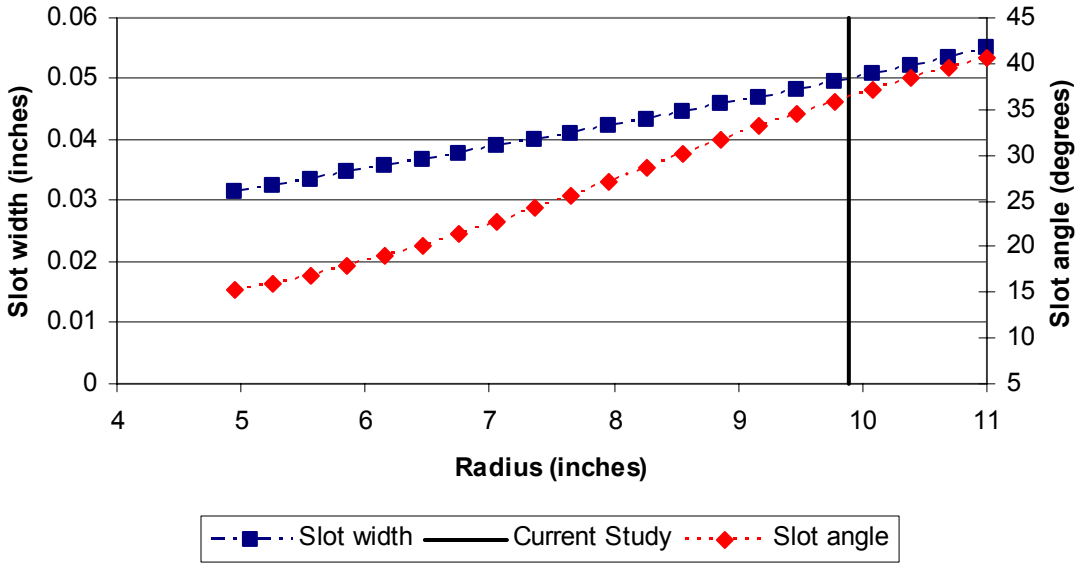

Figure 2-3 Three-dimensional baseline slot flow control provided by NASA

It should be noted that manufacturing and facility limitations prevented a proper internal passage design for the Slot. Bench testing of a manufactured Slot blade showed that the supply area to jet area ratio was unfavorable. Also, due to structural stresses, the blade deformed about the slot opening. The Slot was modeled in CFD and results discussed later in section 3.2. However, experimental results of the manufactured blade are documented in Appendix B and are not discussed in the results section. The blade manufactured is shown in Figure 2-4.

Figure 2-4 Photograph of blade used for testing with trailing edge slot – note the three part division

2.2.2 Trailing Edge Discrete Jets

After CFD studies with the slot concluded, the flow control scheme was changed to discrete jets on the trailing edge. The design criterion for the flow control was to deliver choked flow using a 0.01 in^2 jet passage area per inch span. This would constitute a use of 1% of the fan mass through-flow for the jets. Spacing between holes was optimized so that the flow at the location of the stators was uniform (no span-wise variation). Spacing was varied between 0.2 to 0.5 inches at 0.1-inch increments. Flow was also aimed at 36.7°, 40.0°, and 43.3°. Testing investigating spacing showed that the flow would properly mix with 0.2 and 0.3-inch spacing, but 0.4 began to show significant span-wise variation. A spacing of 0.3 inches was chosen resulting in a hole diameter of 1/16-inch. Variations in jets angles only showed a slight shift in the wake, and the final angle chosen was 36.7° to match the slot angle. The results of these CFD simulations are documented in Appendix A.

The blade manufactured for testing, shown in Figure 2-5, contained 14 jets designed to the previously mentioned criteria. Prior to testing, two jets on each side were sealed with epoxy due to the supply area to jet area ratio being unfavorable with 14 jets.

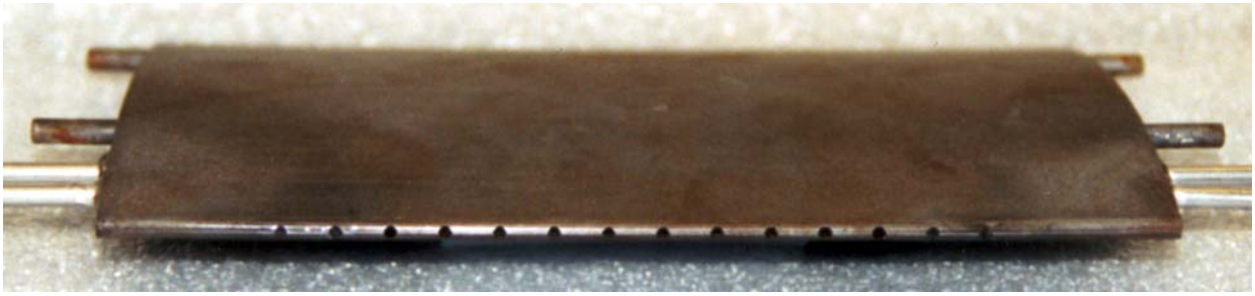

Figure 2-5 Photograph of blade used for testing with trailing edge jets

2.2.3 Suction Surface Discrete Jets

Suction surface jets were tested centered 86.6%, 95.5%, and 99.9% chords from the leading edge of the rotor. Using the same spacing as the final design for the discrete jets and an area per inch span was 0.01 $in^2/in.$, the flow was aimed at 15° from the blade surface for the 86.6% and

95.5% chord cases. Testing at larger angles decreased the benefits of the jets. The 99.9% chord case resided on the top portion of the blunt trailing edge and was aimed at 40.0°.

Best results were seen by the 95.5% chord jet which produced the smallest wake. CFD showed the jet not only increased momentum in the suction surface boundary layer, but also created additional mixing around the blunt trailing edge, decreasing some losses created by the thick blunt end. The manufactured blade that was tested contained ten jets spaced and sized to the previous specifications. The blade is shown in Figure 2-6.

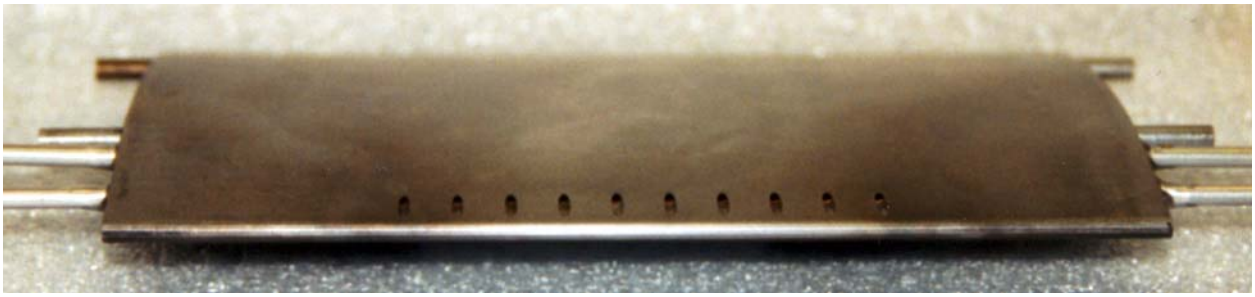

Figure 2-6 Photograph of blade used for testing with suction surface jets

2.3 CFD Method

CFD was performed on NASA's Advanced Ducted Propfan Analysis Code (ADPAC) version 1.02, an Euler/Navier-Stokes analysis code. Developed by the Allison Engine Company under NASA sponsorship, the code can be used for calculation of steady state or time-dependent flow fields of modern turbomachinery. It uses a discretized form of the Navier-Stokes equations. A flexible multiple-block grid discretization scheme allows the use of coupled 2D or 3D mesh blocks in a solution. Calculations are performed based on a four-stage, numerically-dissipating Runge-Kutta time-marching finite-volume solution technique. A multi-grid procedure allows accelerated prediction of steady flow. It is designed to be used either via serial or parallel computing machines running from one source code [Hall, et al, 1999].

The multiple-block grid used is shown in Figure 2-7. Minor modifications of the distribution of nodes were done depending on the location of the flow control on the blade's surface. The multi-block grid consisted of two blocks. The inlet block containing the blade passage was 389 by 45 nodes. The exhaust block consisted of 45 by 75 nodes. The analysis was run assuming an infinite cascade in the y direction and z direction (see Figure 2-7 for orientation). Boundary conditions were set by inputting a desired inlet total pressure and inlet flow angle and an exit static pressure. Inlet total pressure was 2116.22 psf (14.6960 psi) with an inlet flow angle of 55.4°. Exit static pressure was set to 1833.47 psf (12.7324 psi). This produced the proper

simulation take-off conditions for the flow. Jets were simulated using similar boundary conditions as those listed for the inlet. Turbulence levels were input into boundary conditions using turbulence levels typical of fully turbulent flow. A one-equation Spalart-Allmaras turbulence model was used for all CFD solutions. All CFD post processing was performed using Fieldview release 8 by Intelligent Light.

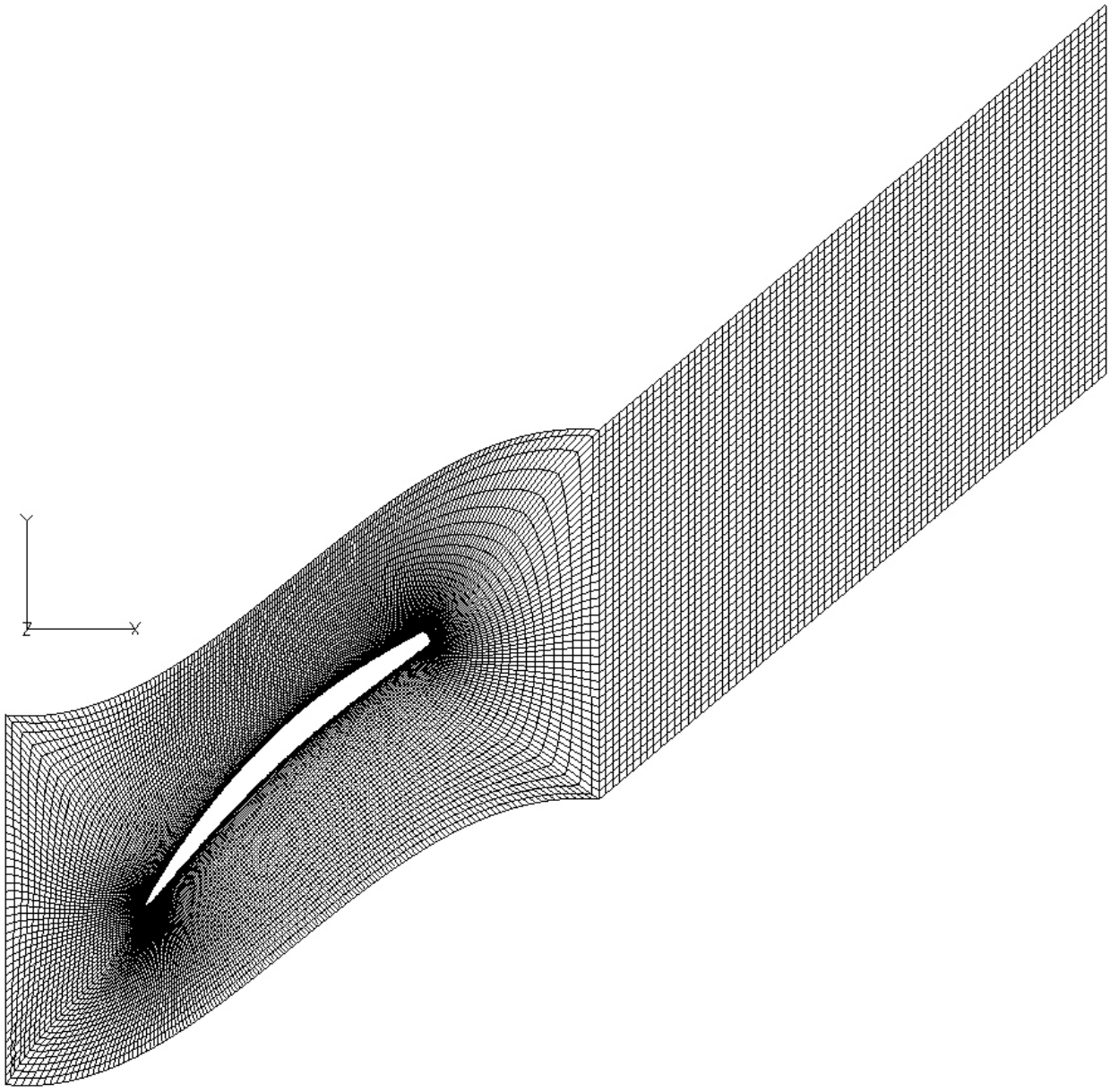

Figure 2-7 Multiple-block grid used for CFD

Grids used were generated by Techsburg, using Gridgen version 13.3. Gridgen is a 2D and 3D grid generation software capable of creating quadrilateral, hexahedral, triangular, and tetrahedral grid cells; mapped and hybrid meshes with single or multiple blocks; and abutting or overlapping

block interfaces. Along with grid generation, CFD of the fan blade with no flow control and some cases with VGJ's were also performed by Techsburg. All other CFD presented in this study was performed by the author.

Solid blade and Slot cases used a 2D grid, and TEJ and SSJ used 3D grids. CFD solutions were monitored by observing the convergence of two values with respect to iterations: application of continuity across the control surface and the pressure loss coefficient, defined later in this study. Other software used in the analysis of the code was Fieldview release 8 by Intelligent Light. All CFD post processing was performed using this software, as well as all contours presented in this study.

2.4 Testing Facility

Experimental testing was conducted at the transonic wind tunnel at Virginia Polytechnic Institute and State University, a blow-down type facility supplied by an Ingersoll-Rand four-stage, reciprocating compressor. Two storage tanks located outside of the wind tunnel facility provide the pressurized air. Prior to entering the facility, air is dried and cooled in an activated-alumina dryer. However, this does not handle the condensation collected by the compressor during the ambient air compression process. The compressor requires draining every ten to 12 runs.

An analog control panel in the lab controls activation, loading, and unloading of the compressor. Inlet total pressure into the test section is controlled by a pneumatically controlled butterfly valve with a 20 psig reference and 80 psig control air supply. A personal computer (PC) provides the control program required for the valve. The signal provided by the PC is sent through an electro-pneumatic converter. The control program is defined by seven constants, one of which is the objective inlet total pressure. This is set by the user in order to obtain the desired inlet Mach number. An upstream total pressure probe provides the feedback to the system. Typically, the valve takes about five seconds to reach steady state, and a constant total pressure is maintained for a further ten to 15 seconds.

Prior to entering the test section, the air is passed through flow straighteners and a meshed wire frame in order to provide uniform flow into the test section. The wire frame is far enough upstream so that turbulence is isentropic and has an intensity of 0.1% at the inlet to the test section. A turbulence grid upstream of the test section provides 1.6% turbulence to the cascade. After exiting the test section, a choke plate can be used in order to raise the exit static pressure of the wind tunnel facility and increase the total pressure inside the test section, should it be desired. For the

tests presented in this study, a 9.6-inch diameter choke plate was used in the 12-inch diameter exit pipe. This was done in order to raise the total pressure in the wind tunnel and better the response of the valve control system. A schematic of the wind tunnel facility can be seen in Figure 2-8.

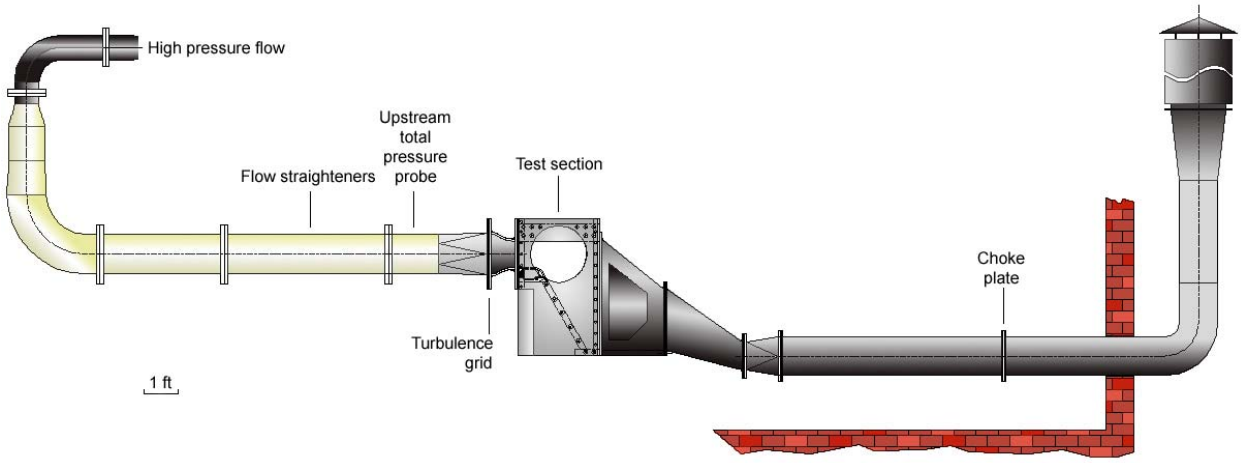

Figure 2-8 Virginia Tech transonic wind tunnel

The test section is an aluminum frame with openings on each side that allow for quick installation and change of the cascade. Top and bottom aluminum blocks with entry angles of 0.0° seal the test section. The aluminum blocks have exit angles of 51° and 60°, respectively. Plexiglas cascade windows (described in section 2.5) are sealed with an aluminum frame held by five brass screw clamps on each side. The clear Plexiglas allows visibility of the cascade from either side and, thus, the use of optics-based flow visualization, if desired. The cascade rotates freely within the aluminum test section to facilitate testing of multiple incidence angles.

The bottom block contains a smaller imbedded block. Different imbedded blocks can be inserted to allow a probe to traverse or measure at downstream locations. For this study, the imbedded block allowed downstream traverses at 1, 1.4, and 1.8 chords downstream parallel to the cascade trailing edge plane.

2.5 Cascade Design

The schematic of the cascade test section is shown in Figure 2-9. A five-blade cascade with 1.25-inch thick Plexiglas windows was used. Only the central blade, blade three, was machined for use with flow control. Nine static pressure wall taps with a 1/16-inch outer-diameter and 0.011-inch wall thickness were evenly distributed over two pitches and placed 2.9 inches upstream of the leading edge plane in the flow axial direction. Static wall pressure tap three was positioned axially upstream of the leading edge of blade three (see Figure 2-9). An upstream Kiel total pressure probe

was placed mid-pitch between blades two and three and 2.67 inches upstream of the leading edge plane. The upstream Kiel probe rested 1.25 inches from the interior Plexiglas surface. Downstream total pressure was taken by a Kiel traverse probe. Three downstream locations were traversed parallel to the trailing edge plane: 1, 1.4, and 1.8 chords downstream of the trailing edge. This was done to record wake propagation data. Only one pitch was traversed. Both top and bottom tailboards were used to improve flow uniformity. Figure 2-10 shows the actual test section in place at the Virginia Tech Transonic Wind Tunnel.

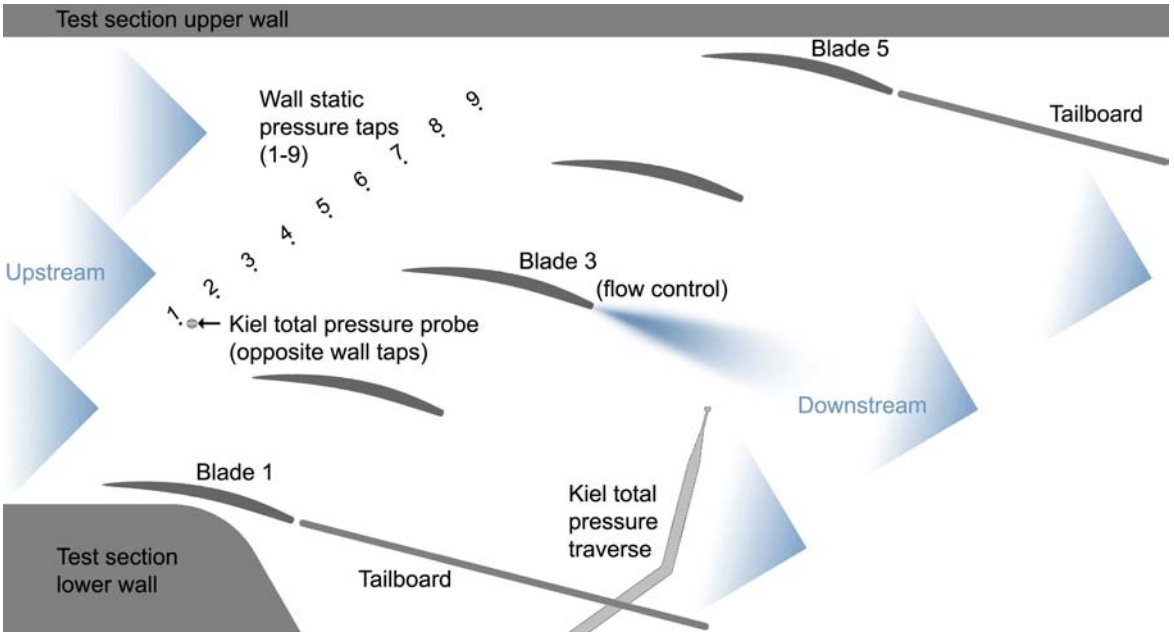

Figure 2-9 Schematic of the cascade in the wind tunnel test section

2.6 Flow Control Air Supply

The flow control air supply system is shown in a schematic in Figure 2-11. The blade flow control was fed by an Ingersoll-Rand 2475N5 5HP two-stage, reciprocating compressor. The compressor provided air pressurized to 175 psi at a rate 16.8 ambient cubic feet per minute. From the compressor, air was filtered through an Ingersoll-Rand filter in order to remove any dirt particles. The air then passed through an Ingersoll-Rand HRM regenerative dryer prior. Air is dried to below 4% relative humidity and collected in a storage tank.

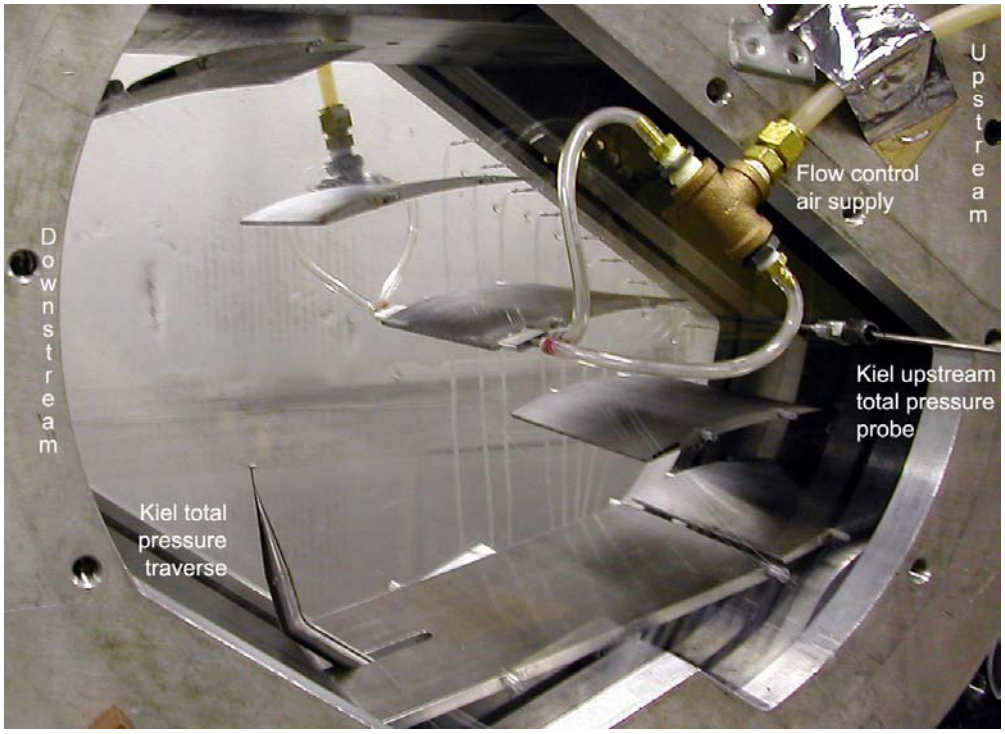

Figure 2-10 Cascade test section with both Plexiglas windows

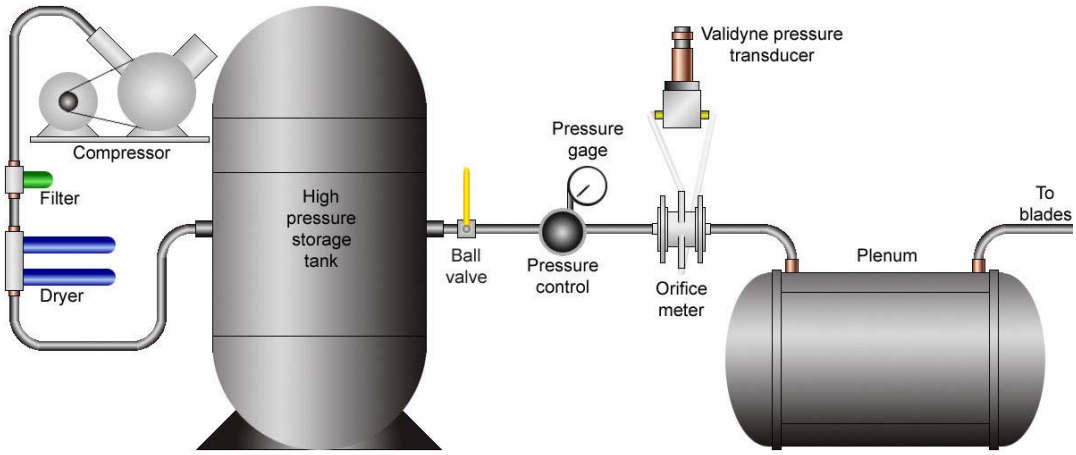

Figure 2-11 Flow control air supply system schematic

From the storage tank, air was passed through an on/off ball valve and then through a control valve where the supply total pressure could be adjusted from zero to 150 psi. Next, the air passed through a 0.28-inch bore diameter orifice meter with a discharge coefficient of 0.61. The change in pressure across the meter was measured by a Validyne pressure transducer hooked up to a display box. Using the supply total pressure and the Validyne pressure readout, the flow control mass flow rate was estimated (see section 2.8.1) and set for each case tested. The air lastly traveled through a 12-inch diameter, 7-gallon settling plenum chamber prior to entering the blades. The

supply air entered the blades through four steel tubes with 3/16-inch inner diameters. Two tubes were located on each side of blade in order to obtain a uniform flow distribution through the jets.

2.7 Instrumentation and Data Acquisition

Aerodynamic measurements of inlet static and total pressures and inlet-to-exit differential total pressures were recorded, along with pressure measurements on the flow control supply line for the flow control. Average run total temperatures were also collected via a K-type thermocouple readout with an accuracy of ±2°K.

Two Kiel probes were used to obtain total pressures downstream and upstream of the cascade (see Figure 2-12). Kiel probes have a sensitivity of ±30°. Total pressures were recorded with a MKS Type 223B Baratron® Differential Capacitance Manometer. The upstream total pressure was recorded using a ±20 psi ranged MKS transducer while the differential (inlet minus exit) was measured using a ±3 psi range. The MKS manometers were calibrated using reference pressures to obtain a calibration curve for each manometer.

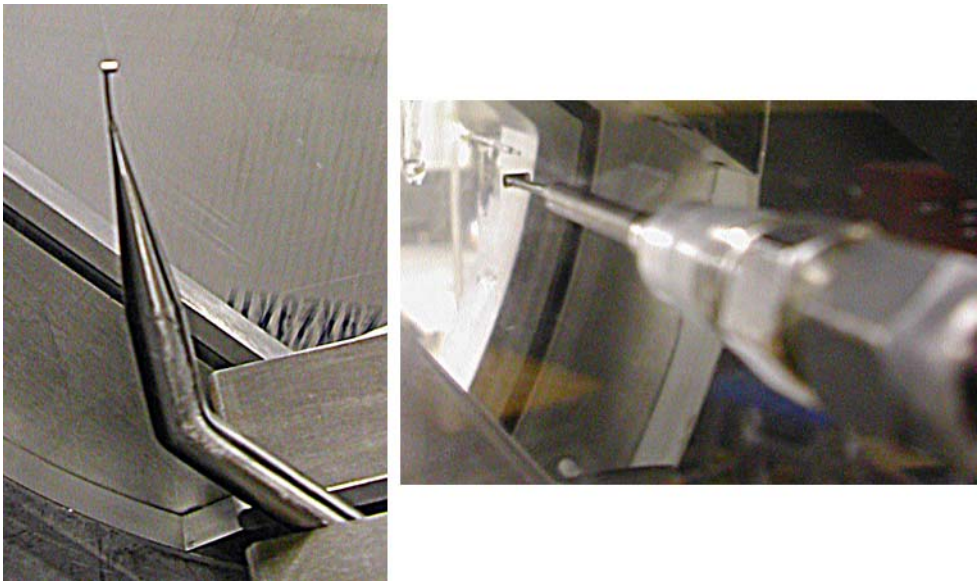

Figure 2-12 Kiel total pressure probes (downstream traverse and upstream left to right)

Static wall taps measurements were gathered using Pressure Systems 8400 System, a high-performance wind tunnel pressure data acquisition system. The System 8400 uses a miniature electronic pressure scanner (ESP) to measure differential pressure units using an array of silicon piezo-resistive pressure sensors, one for each pressure port. An ESP 32HD was used for this testing with a range of ±15 psi. Data was recorded at 50 Hz with ten averaged points per data point. Calibrations were performed every hour or every five runs, whichever came first, using the 8400

System's self-calibration function. Data acquired by the System 8400 was sent via a high speed IEEE-488 interface to the PC based LabVIEW® program, PSI Data Acquisition© version 2, written by the author.

A Validyne pressure transducer with a range of ±100 psi was hooked up to the flow control air supply orifice meter to estimate flow control mass flow rates. The downstream Kiel total pressure probe was traversed using the Techsburg T-1000 traversing mechanism. The T-1000 control program provided the input signals to the traversing mechanism, setting speed and travel distance: 0.4535 in/s and 3.63 inches (one pitch), respectively, for this study.

A PC was used to collect data from the three pressure transducers and the traverse control signal. Data from the transducers was sent to a National Instruments© A/D PC board via low impedance BNC cables connected to a 64-channel multiplexor. A LabVIEW® data acquisition program, 64 Channel DAQ and the PSI Data Acquisition©, were set to collect data at 50 Hz with 401 samples. A trigger signal was used to acquire all of the data and assure real-time overlap from the different sources and control programs.

2.8 Data Reduction Techniques and Key Calculations

Data obtained during testing was reduced in Microsoft Excel. A spreadsheet template was used to reduce the data into key parameters and plots. The effectiveness of the different flow control configurations under different mass flow rates was primarily evaluated using the area-averaged pressure loss coefficient for both CFD and experimental results. Later, the reduced data was introduced by David Arntz into CUP2D, a rotor-wake vane interaction noise prediction code by NASA. The results from the noise prediction code were the means by which the effectiveness of the flow control scheme was finally judged. The following discussion on data reduction techniques and key calculations has been broken down into four sections: aerodynamic performance (2.8.1), CFD convergence (2.8.2), flow control parameters (2.8.3), and acoustic calculations (2.8.4).

2.8.1 Aerodynamic Performance

Flow traveling across an aerofoil experiences viscous drag, creating a total pressure drop across the passage. The pressure loss coefficient presented in this study, ω, is defined as the change in total pressure across the passage, divided by the upstream dynamic pressure, as is shown in Equation 2-1.

Equation 2-1
$$\omega = \frac{p_{o2} - p_{o1}}{p_{o1} - p_{s1}}$$

The inlet Mach number was calculated using upstream total and static pressures assuming isentropic flow. The formula used is shown in Equation 2-2, where i is the sample number and j is the wall static pressure tap number. Using this method, inlet Mach number was calculated at each of the nine wall static pressures taps with respect to time.

Equation 2-2
$$M_1(i,j) = \sqrt{\frac{2}{\gamma - 1}\left[\left(\frac{p_{o1}(i,j)}{p_{s1}(i,j)}\right)^{\frac{\gamma-1}{\gamma}} - 1\right]}$$

The average time-dependent inlet Mach number for each experimental run was calculated by using a pitch-wise average of the inlet Mach numbers seen across wall static pressure taps one through five with respect to time (note that wall static pressure tap 3 is located directly upstream of the leading edge of Blade 3). This is shown in Equation 2-3.

Equation 2-3
$$\overline{M}_1(i) = \frac{\sum_{j=1}^{5} M_1(i,j)}{5}$$

The average inlet Mach number is defined in Equation 2-4.

Equation 2-4
$$\overline{M}_1 = \frac{\sum_{i=1}^{n} M_1(i)}{n}$$

The standard deviation of the inlet Mach number was calculated using Equation 2-5.

Equation 2-5
$$\sigma = \sqrt{\frac{\sum_{i=1}^{n}\left(M_1(i) - \overline{M}_1\right)^2}{n}}$$

Parameters measured from pressure loss coefficient generated wake profiles were used for comparison of aerodynamic performance between different flow control schemes. These parameters include area-averaged pressure loss coefficient, wake depth, and wake half-width.

Figure 2-13 shows how wake depth, w_d, and wake half-width, *Y*, are measured given a typical wake. The propagation of wake depth and wake width are important in noise reduction due to their effects on the strength of the wake-stator interaction (i.e. noise strength), and harmonic content,

respectively (Waitz, et al, 1996). The propagation of these parameters was used as inputs for the noise prediction code.

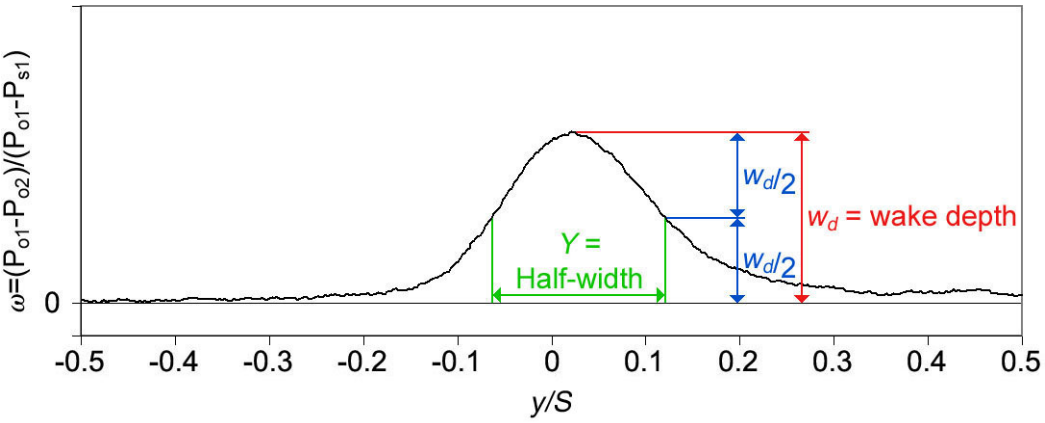

Figure 2-13 Typical wake showing measured parameters

The flow control performance was measured in terms of mass flow supplied. As mentioned in section 2.6, the pressure drop across the orifice meter was measured using a Validyne pressure transducer. Orifice meters function by creating an impediment in flow which causes a pressure drop. By measuring this pressure drop, it is possible to calculate the flow rate through the orifice. The complicated flow can be idealized to fit the Bernoulli equation neglecting viscosity and geometric distortions. Actual values are obtained through the use of coefficients that are properties of the orifice meter [Sabersky, et al., p.113-118]. Using the Bernoulli and the continuity equations, the ideal flow volumetric rate is obtained by applying Equation 2-6.

Equation 2-6

$$\forall_{ideal} = A_{orifice}\sqrt{\frac{2}{\rho}\Delta p}\Bigg/\sqrt{1-\frac{A_{orifice}^{\ 2}}{A_{pipe}^{\ 2}}}$$

Using the definition of the discharge coefficient, the actual volumetric flow rate can be calculated with Equation 2-7.

Equation 2-7

$$\forall_{actual} = c_d A_{orifice}\sqrt{\frac{2}{\rho}\Delta p}\Bigg/\sqrt{1-\frac{A_{orifice}^{\ 2}}{A_{pipe}^{\ 2}}}$$

The value of the discharge coefficient is a characteristic of the orifice meter; for the orifice meter used in this study, the value is 0.61. Applying the continuity equation, the mass flow rate through the orifice meter was calculated with Equation 2-8.

Equation 2-8
$$\dot{m} = \rho V A = \rho \bar{V}_{actual} = c_d A_{orifice} \sqrt{2\rho\Delta p} \Bigg/ \sqrt{1 - \left(\frac{d_{orifice}}{d_{pipe}} \right)^4}$$

By applying the ideal gas law, the density was estimated using the pressure measured with the pressure gage and an estimate for the upstream temperature. The ideal gas law is shown in Equation 2-9.

Equation 2-9
$$\rho = \frac{p}{RT}$$

2.8.2 CFD Convergance

Convergence of the CFD solutions was inspected by observing two key parameters' convergence to steady states. The two key parameters considered were continuity error and pressure loss. Convergence of CFD solutions can be said to occur when values are seen to reach a steady state. The value begins by fluctuating in a transient state, and as iterative calculations are performed, steady values based on inputs are reached.

Probe files were taken at the inlet plane, appropriate jet inlet, and exhaust plane. Figure 2-14 shows the location of the three probes on the mesh. Probe files contain values measured across the location of the probes at each CFD cycle run. Values outputted are mass flow, total and static pressures, total and static temperatures, and average velocities.

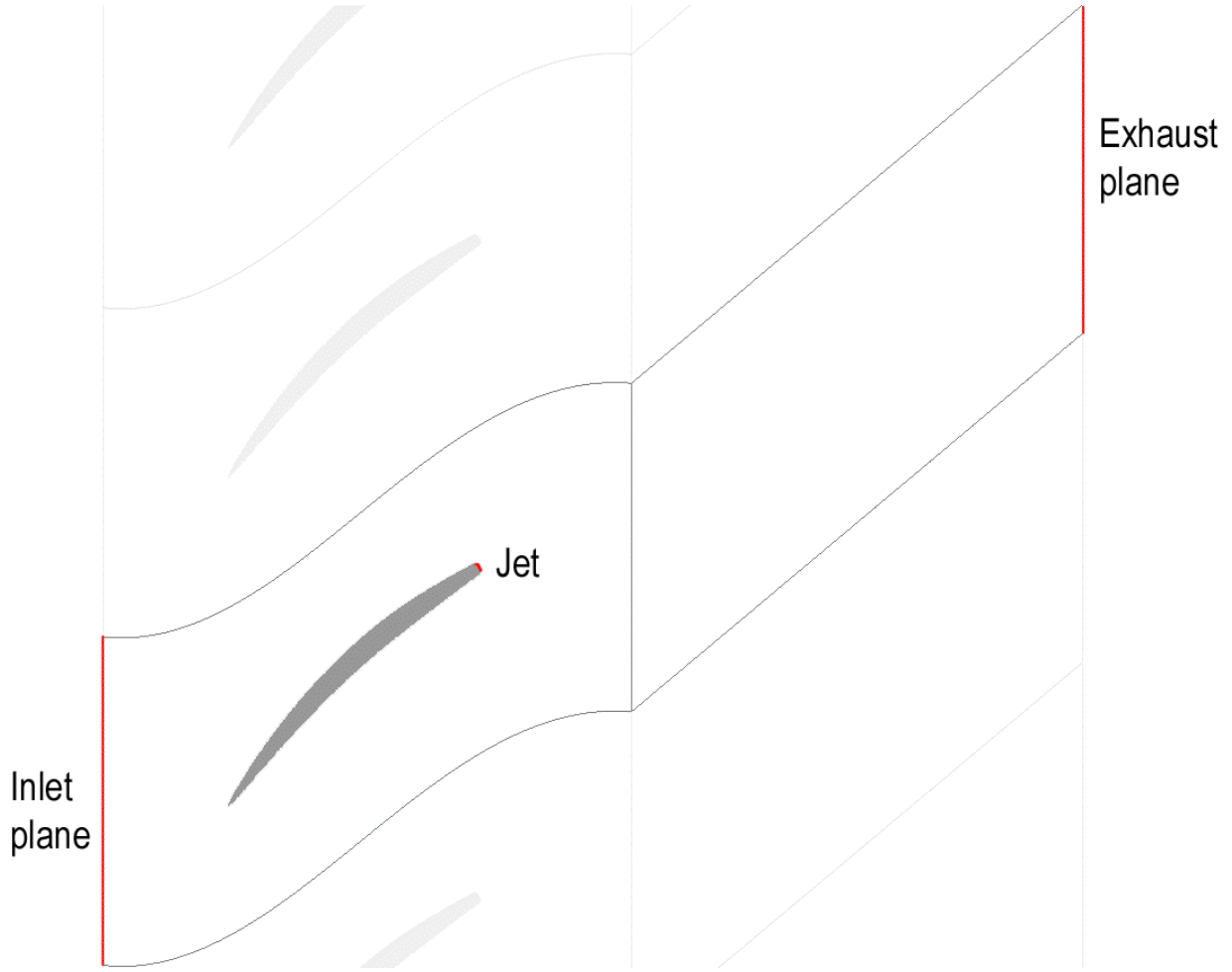

Figure 2-14 Location of the probes taken in CFD are shown highlighted in red

The application of the continuity equation on a flow that does not change with time can be said to state that for a closed system the mass flow into the system equals the mass flow out of the system. This is conservation of mass and is shown in Equation 2-10.

Equation 2-10 $$\dot{m}_{in} = \dot{m}_{out}$$

Conservation of mass can be applied in a system modeled in CFD and used to monitor the convergence of a solution. An error is generated where the mass flow into the system does not match the mass flow out of the system. By dividing this value by the mass flow out of the system, the error becomes non-dimensional. The formula used to compute non-dimensional mass flow error is shown in Equation 2-11.

Equation 2-11

$$\varepsilon_{\dot{m}} = \frac{\dot{m}_1 + \dot{m}_{jet} - \dot{m}_2}{\dot{m}_2}$$

When plotted against the cycle number, the non-dimensional mass flow error is observed to begin in a transient state and reach a steady state. A typical convergence plot of non-dimensional mass flow error for a CFD solution is shown below in Figure 2-15.

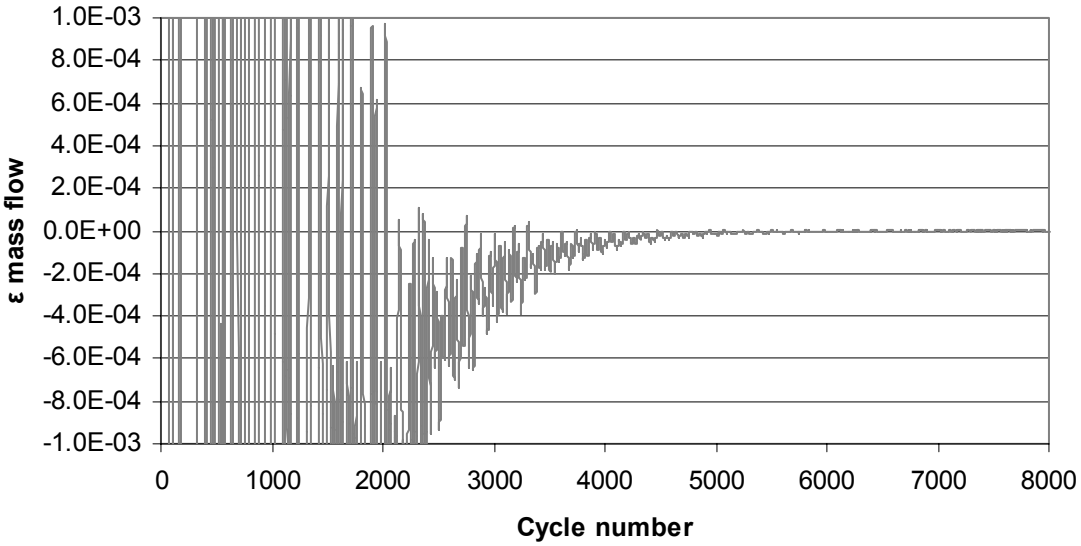

Figure 2-15 CFD non-dimensional mass flow error versus cycle number convergence plot

The second parameter used to study the convergence of the CFD solutions was pressure loss. The same definition shown in Equation 2-1 was used with values outputted by the inlet and exhaust plane probes. As seen with the non-dimensional mass flow error, the pressure loss is observed to begin in a transient state and reach steady state, assuming the appropriate number of cycles is run. A typical convergence plot of pressure loss for a CFD solution is shown in Figure 2-16.

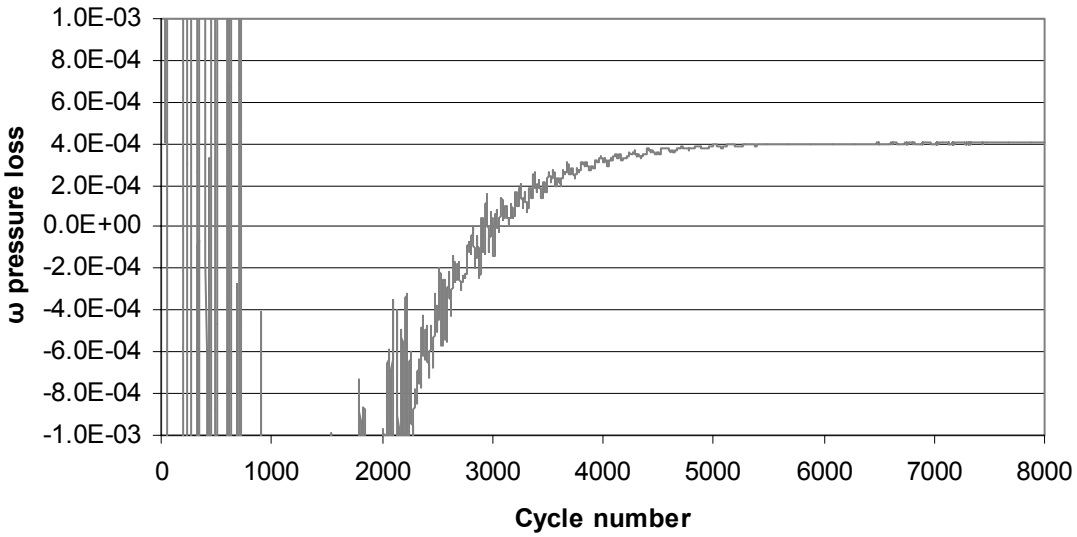

Figure 2-16 CFD pressure loss versus cycle number convergence plot

2.8.3 Flow Control Parameters

Flow control requires a high pressure fluid supply in order to produce the proper flow conditions to be effective. This high pressure supply would generally come from higher stages of an engine at a small penalty in efficiency in order for the flow control to achieve its goal. Thus, two of the most important factors in the viability of implementing flow control are mass flow rate and plenum pressure. Too much mass flow will be too detrimental to a particular stage, and the engine's performance will be hindered. Pressures that are too high also present a problem if the engine is not able to produce the required pressure. There are many other factors also worth considering, such as internal passage geometries and blade deformation; however they cannot be determined at this stage using 2D models.

A value with which to compare the different flow control cases became important in accurately evaluating the performance of the different cases since the distinct configurations do not output the same mass flow rate at equivalent supply pressures. Comparisons between the distinct flow control cases were drawn by considering the momentum associated with each flow control configuration. Momentum is defined as shown below.

Equation 2-12 $$\vec{G} = m\vec{V}$$

A blowing coefficient can be expressed by associating the jet momentum to the inlet momentum. The Equation 2-13 relates the momentum normal to a control surface for the jet and the inlet. For

the jet, the normal is parallel to the direction of the jet. For the inlet, it is perpendicular to the fan blade leading edge plane formed in the cascade.

Equation 2-13

$$c_{blowing} = \frac{\vec{G}_{jet} \cdot \hat{n}}{\vec{G}_1 \cdot \hat{n}} = \frac{m_{jet}\vec{V}_{jet} \cdot \hat{n}}{m_1\vec{V}_1 \cdot \hat{n}} = \frac{\dot{m}_{jet}V_{jet}}{\dot{m}_1\vec{V}_1 \cdot \hat{n}} = \frac{\dot{m}_{jet}M_{jet}}{\dot{m}_1\vec{M}_1 \cdot \hat{n}}$$

For this study, the blowing coefficient is presented as a percentage of the inlet linear momentum. Since the inlet conditions were matched, the blowing coefficient only relies on the jet dependent variables.

The mass flow rate used was measured via the orifice meter as described previously and assumed to be distributed uniformly along the blade's span. The speed of sound was assumed at 1117 ft/s. For the discrete jets, the jet flow is designed to be choked at 1.00% fan through-flow. For choked cases, the Mach number of the jet and hence the velocity is obtained through the definition of choked flow as seen in Equation 2-14.

Equation 2-14

$$M_{jet} = 1 \rightarrow V_{jet} = M_{jet}a$$

For cases where the flow control is not choked, the density is iterated through the use of isentropic relations and the ideal gas law. Hence, the speed of the jet is calculated using continuity, yielding a jet Mach number by using the speed of sound. This is shown in Equation 2-15.

Equation 2-15

$$V_{jet} = \frac{\dot{m}_{jet}}{\rho A_{jet}} \rightarrow M_{jet} = \frac{V_{jet}}{a} = \frac{\dot{m}_{jet}}{a\rho A_{jet}}$$

If the jet flow is not choked, static pressure was assumed to be constant throughout the boundary layer, so the static pressure was assumed to be the same as freestream. Thus the total pressure is now calculated using isentropic relations as seen in Equation 2-16.

Equation 2-16

$$p_{o-jet} = p_s\left[1 + \frac{\gamma - 1}{2}{M_{jet}}^2\right]^{\frac{\gamma}{\gamma-1}}$$

For cases where the jet flow was choked, the total pressure is calculated using Equation 2-17.

Equation 2-17

$$p_{o-jet} = \frac{\dot{m}_{jet}}{A_{jet}} \frac{\sqrt{RT_o}}{0.6847}$$

2.8.4 Acoustic Calculations

The noise prediction code results provided by David Arntz contained the sound power level generated for BPF tones in decibels (no broadband). All acoustic predictions were referenced to predictions for a solid blade. In order to calculate attenuation of the solid blade's individual tones, the difference in the sound power level between solid blade and flow control was performed at each BPF as shown in Equation 2-18.

Equation 2-18

$$A_L\big|_{i\times BPF} = \left(L_{w-ref} - L_{w-jet}\right)\Big|_{i\times BPF}$$

To obtain the total attenuation generated by each flow control case, the total sound power level produced by all eight tones must first be calculated using Equation 2-19.

Equation 2-19

$$L_{wT} = 10\log\sum_{i=1}^{8} 10^{L_w\big|_{i\times BPF}/10}$$

With the total sound power level calculated for the solid blade and each flow control case, the total attenuation of the solid blade's sound power level by each flow control case is yielded by means of Equation 2-20.

Equation 2-20

$$A_{LT} = L_{wT-ref} - L_{wT-jet}$$

Chapter 3. Results

This chapter provides a discussion of the results observed from the simulations and experiments conducted with three unique set of flow control configurations previously discussed. The specifications for each flow control configuration are summarized in Table 3-1 to refresh the reader with the particulars of each configuration. The discrete jets for the TEJ and SSJ were designed to be washed out 1.0 chord downstream of the trailing edge, so measurements taken directly downstream of the jets or between jets wouldn't differ significantly.

Table 3-1 Flow control configuration specifications

	Slot	TEJ	SSJ
Dimension (inch)	0.0454 height	1/16 diameter	1/16 diameter
Location	TE	TE	95.5% chord
Spacing	NA	0.3 inches	0.3 inches
Flow control exit angle	36.7°	36.7°	15° (local)
Area (in²) per inch span	0.0454 in²/in	0.01 in²/in	0.01 in²/in

Experiments were conducted after CFD results were obtained and studied. Comparisons between CFD and experiments displayed wakes generally of similar width and generally of similar height. However, CFD tended to have larger wake depths and slimmer wakes, and results showed a trend by CFD of under predicting losses by a small percentage.

The Slot is presented in this section for study solely in CFD between fan through-flow rates of 0.75% and 2.25% at half percent increments. As mentioned previously, machining and facility and time limitations prevented a proper design of the Slot's internal passages that permitted the Slot to behave as designed (see Appendix B). The two discrete jet cases, TEJ and SSJ, were studied between 0.50% and 1.25% at quarter percent increments using both CFD and experimental results. As mentioned previously, different flow control configurations are evaluated by using similar blowing coefficient as a basis of comparison. Figure 3-1 shows the relationship between the fan through-flow rate for each flow control configuration and the blowing coefficient. Although the TEJ and SSJ operate at similar conditions, the Slot operates at higher mass flow rates than the discrete jet cases at the same supply pressure. To produce the same mass flow rate requires a higher pressure for the discrete jets than the Slot. Both values are important to the implementation of flow control in an engine, since large requirements of either one can render the flow control unfeasible

due to penalties in engine efficiency. Results are discussed in terms of blowing coefficient, unless otherwise specified.

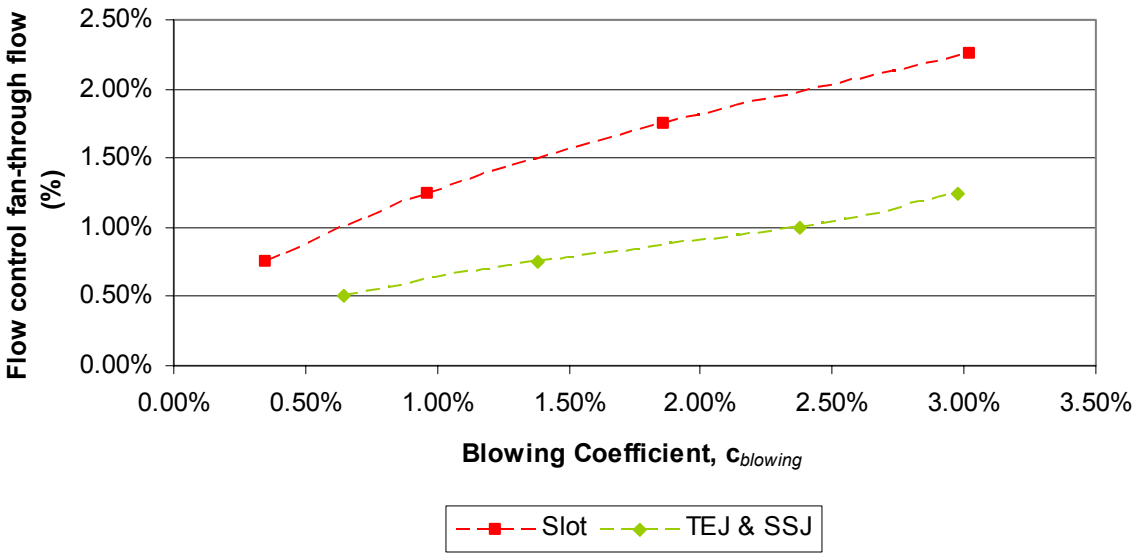

Figure 3-1 Flow control percent fan through-flow plotted against corresponding blowing coefficient for the configurations studied

CFD simulations and experimental tests were matched at operating conditions representative of take-off. The study of aerodynamic parameters for CFD is first presented followed by the experimental analysis. Average pressure losses and, more importantly, wake dimensional parameters (width and depth) are presented. Due to the effects of latter dimensional parameters on noise generation, their propagation was input into the noise prediction code, the results of which are presented last.

CFD simulations and experimental tests were matched at operating conditions representative of take-off. A discussion of boundary layer formation on the blade based on CFD simulations is first presented followed by the study of aerodynamic parameters for CFD and then followed by the experimental analysis. Average pressure losses and, more importantly, wake dimensional parameters (width and depth) are presented. Due to the effects of latter dimensional parameters on noise generation, their propagation was input into the noise prediction code. A brief highlight of results obtained by David Arntz will be presented. Note that only a partial analysis on the CFD based wake propagation data was performed.

Additional CFD results and studies conducted and previously mentioned can be seen in Appendix A. Appendix B, Appendix C, and Appendix D present wake data comparisons between

CFD and their respective experiment for the Slot, TEJ, and SSJ, respectively. Vortex Generating Jets are presented in Appendix E followed by an aerodynamic comparison of the solid blade to each of the flow control blades using no blowing in Appendix F. Lastly, the uncertainty analysis is presented in Appendix G.

3.1 Blade Boundary Layer Formation

Prior to discussion of the results obtained for this study, the flow physics inherent to the blade geometry with no flow control will first be addressed. This will yield a better understanding of the effects of the different flow control configurations presented.

Boundary layer formation is attributed to the retardation of flow due to viscous effects caused by the flow's interaction with the blade surface. The primary sources of boundary layer formation for the blade studied are the suction, pressure, and trailing edge surface. Boundary layer analysis is based on the assumption of a constant static pressure across the boundary layer. Within the boundary layer, fluid that is further removed from the freestream fluid experiences the viscous effects generated by the surface of the blade. This fluid experiences losses and a parabolic approach to a velocity of zero. Thus, across the boundary layer, a total pressure gradient is formed.

Figure 3-2 shows a total pressure contour rendered in Fieldview that highlights the boundary layer formation seen on the blade surface without flow control added, i.e. solid blade. As a reminder, solid blade CFD solutions use a 2D grid. Of the three surfaces mentioned previously, the pressure side generates a much thinner boundary layer when compared to the suction surface, which is roughly three times as thick. The blunt trailing edge nearly doubles the thickness of the boundary layer generated by the suction side. Thus, the majority of the boundary layer formation comes from the suction surface and the blunt trailing edge.

The thick trailing edge of the blade multiplies the boundary layer generated losses of the suction surface. This is best illustrated by observing Figure 3-3. Calculated streamlines and velocity vectors have been added to the total pressure contour shown previously. The vectors illustrate the direction and relative magnitude of fluid's velocity. The streamlines allow a better visualization of the mechanics of the fluid.

From the figure, it can be surmised that the blunt trailing edge only affects the fluid from the suction side. As fluid from the suction side is forced to turn and fill the area behind the blunt trailing edge, strong adverse pressure gradients are formed. This leads to the formation of separation points along the trailing edge, and recirculation zones (vortices) are generated. These

areas of fluid recirculation serve in producing larger losses, thickening the boundary layer, and thus generating a larger wake.

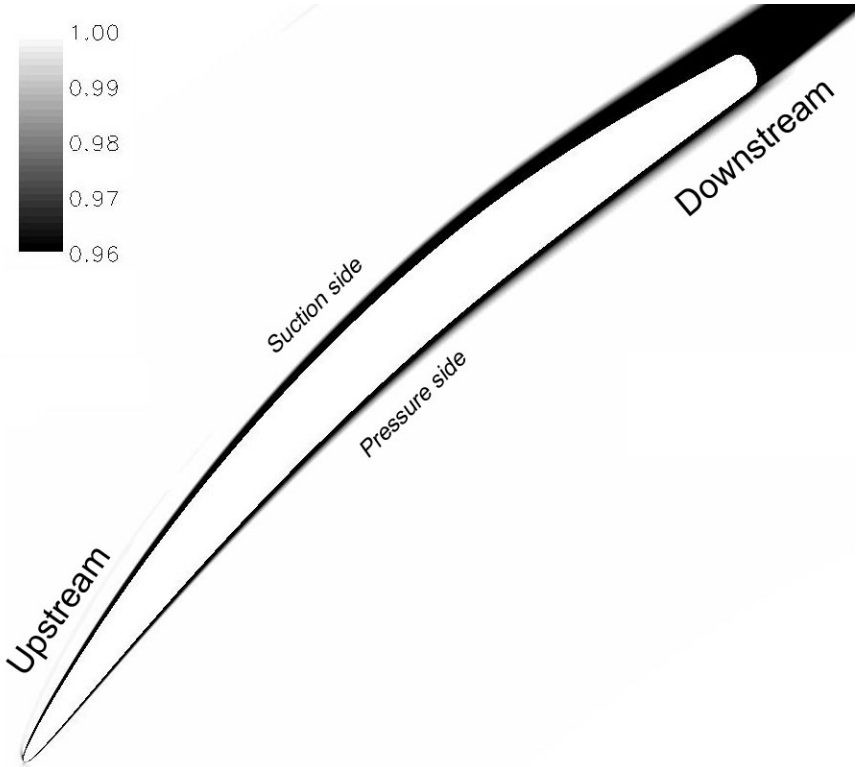

Figure 3-2 CFD total pressure contour referenced to freestream total pressure highlighting boundary layer formation on the solid blade

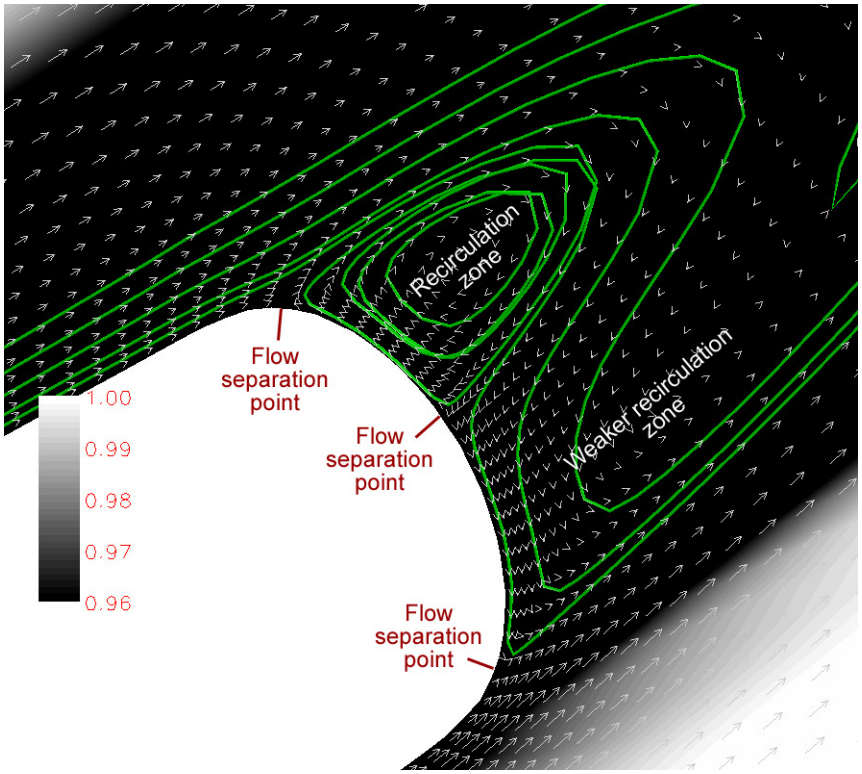

Figure 3-3 CFD total pressure contour focused on the trailing edge of the solid blade with calculated streamlines and velocity vectors

As mentioned previously, the original blade geometry upon which the current blade being studied was modified to implement flow control in the form of a slot along the trailing edge. This modification was performed by thickening the trailing edge. The primary focus of the flow control applied will be to lessen the effects of the major sources of boundary layer formation (the suction surface and trailing edge), and thus, overall losses for this blade in order to lessen the rotor-stator wake interaction and reduce fan noise.

3.1.1 Trailing Edge Slot

As mentioned in 2.2.1, the trailing edge slot consisted of an opening 45.4×10^{-3} inches in width along the trailing edge of the blade aimed at an angle of 36.7°. Shown below in Figure 3-4 is a CFD total pressure contour for the Slot similar to the one seen in Figure 3-3, where the freestream total pressure is referenced to highlight boundary layer formation. As a reminder, Slot CFD solutions use a 2D grid.

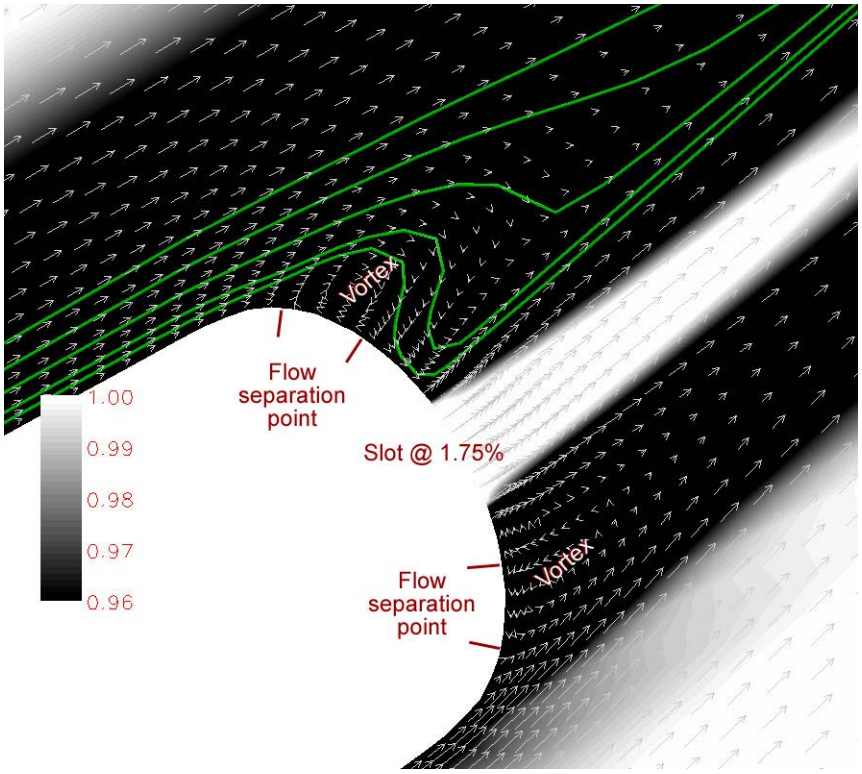

Figure 3-4 CFD total pressure contour focused on trailing edge of the Slot at 1.75% fan through-flow with calculated streamlines and velocity vectors

This total pressure contour shows the slot blowing 1.75% of the fan through-flow. Compared to the case with no blowing, the vortices produced along the trailing edge of the blade are much less pronounced. Although vortices are present towards both the pressure and suction side, they are of smaller magnitude than those seen in Figure 3-3. Thus, the recirculation zones hinder the flow much less. The flow surrounding the slot is energized and sped up due to the high energy jet, as can be seen by the velocity vectors surrounding the high energy flow in the figure. However, because there is less mixing, this may produce a narrower wake than the solid blade.

3.1.2 Trailing Edge Discrete Jets

The TEJ configurations consists of 1/16 inch in diameter holes aimed at an angle of 36.7° and spaced 0.3 inches apart in the span along the trailing edge of blade, as mentioned in section 2.2.2. Figure 3-5 shows the CFD total pressure contour sliced at the center of the discrete jet hole. As a reminder, TEJ CFD solutions use a 3D grid.

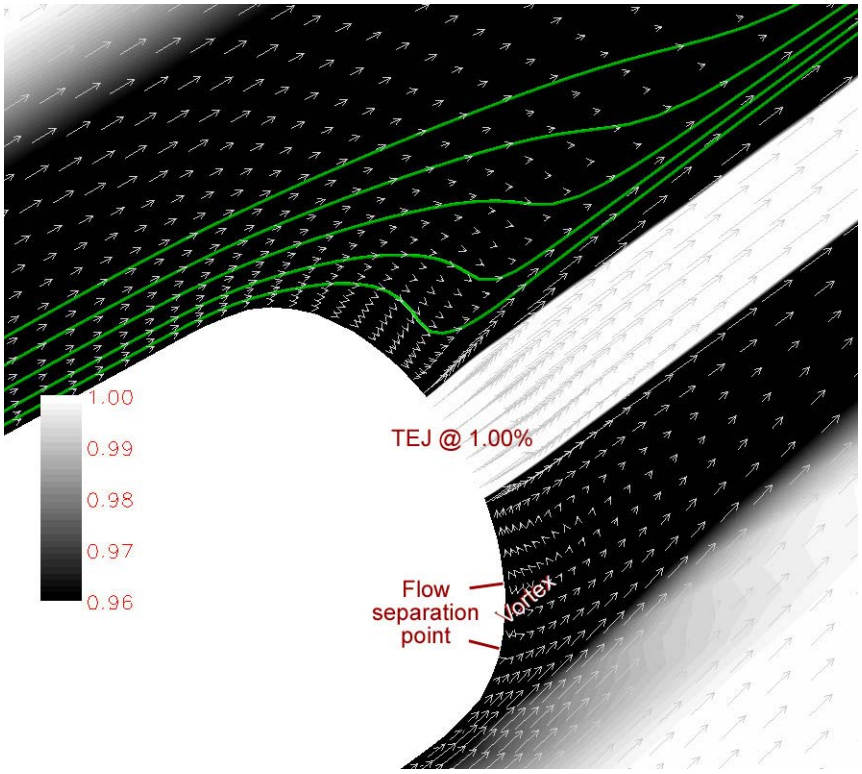

Figure 3-5 CFD total pressure contour focused on trailing edge of the TEJ at 1.00% fan through-flow with calculated streamlines and velocity vectors

The jet is shown operating at design, 1.00% fan through-flow. As in the previous total pressure contours, the freestream total pressure is referenced to highlight boundary layer formation around the trailing edge of the blade. If Figure 3-4 is referenced, immediately evident is the change in the stream lines, number of separation zones, and corresponding vortices. The flow shows no separation along the suction surface of the blade. The streamlines shown along the suction surface are smoother since there is no vortex to hinder flow. The pressure side still experiences two separation points, but they are more closely spaced. The vortex is of lesser magnitude. Even though three-dimensional effects can not be observed in this figure, it is evident that from this point of view that the TEJ is energizing the surrounding flow more greatly than the slot, as can be seen via the velocity vectors surrounding the jet and the changes in the surrounding flow.

3.1.3 Suction Surface Discrete Jets

Like the TEJ, the SSJ configuration consists of 1/16 inch in diameter holes spaced 0.3 inches apart in the span along the trailing edge of blade, as described in detail in Section 2.2.3. However, the jets are located at 95.5% chord from the leading edge of the blade on the suction surface and aimed at 15° from the surface. The CFD total pressure contour for this blade is shown in Figure 3-6, with the cross-section taken at the center of the discrete jet hole. As a reminder, SSJ

CFD solutions use a 3D grid. The flow control is shown blowing at design, 1.00% fan through-flow. Once again, total pressure is referenced to freestream total pressure, highlighting boundary layer formation. Velocity vectors are also shown to highlight the direction and magnitude of the flow. There are differences between the pressure contours for this blade and no flow control (Figure 3-4) and TEJ (Figure 3-5) cases. First, there are three flow separation points symmetrically located about the trailing edge of the blade.

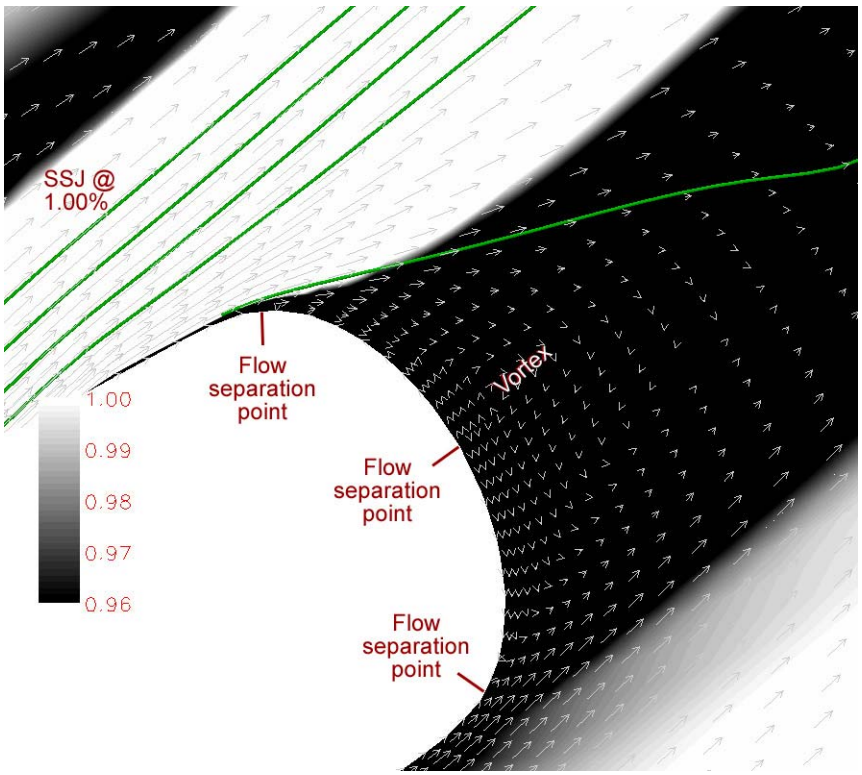

Figure 3-6 CFD total pressure contour focused on trailing edge of the SSJ at 1.00% fan through-flow with calculated streamlines and velocity vectors

Second is the presence of a vortex centered about the trailing edge. This vortex forms a wedge shape along the trailing edge, and the pressure and suction surface streamlines join smoothly and closer to the trailing edge than with the other cases previously studied (carefully observe the velocity vectors). This will yield a narrower wake. Although a weaker vortex is seen in the TEJ contour, it remains towards the pressure side and does not behave in the same way.

Third, the SSJ is energizing the stagnant flow formed by the suction surface through the effects of a viscous ramp. This will decrease losses generated by the suction surface and shift the wake towards the pressure side. However, the blunt trailing edge still remains a major source of losses and subsequent boundary layer. Even though the original geometry of this blade was

thickened for the use of trailing edge blowing, this flow control could possibly be implemented onto thinner blade, which would consequently mean a smaller wake and lessened strength of the rotor-stator wake interaction.

3.2 CFD Aerodynamic Results

As discussed previously, many CFD simulations were conducted in order to determine the flow control cases with the most potential for improvement of the existing configuration, the Slot. This section outlines the CFD findings for the most promising cases studied: the TEJ and SSJ. Simulations were conducted at fan through-flows matching those used for experiments. The Slot was simulated using between 0.75% fan through-flow to 2.25% at half-percent increments. This corresponds to blowing coefficients between 0.4% and 3.0%. The TEJ and SSJ were both simulated using between 0.50% and 1.25% fan through-flow at quarter percent increments. This corresponds to blowing coefficients between 0.7% and 3.0%. Along with comparisons between different flow control configurations, it was also important during CFD to observe if the flow control offered improvement at different blowing coefficients over a solid blade (i.e. no flow control). Thus, CFD results shown here contain not only the flow control configuration results, but also the solid blade results.

Area-averaged pressure loss coefficients (see Equation 2-1) for the three flow control configurations and solid blade are shown in Figure 3-7 at the three downstream measurement locations. Both the discrete jet cases offer an improvement over the Slot in performance, but the SSJ configuration produces the greatest reduction in area-averaged pressure loss coefficient for all blowing coefficient values. The CFD average pressure losses also show that the Slot does not improve solid blade aerodynamic performance at lower blowing ratios. Air was being blown and not suctioned via the flow control at lower blowing ratios, but fluid being introduced into the boundary layer was of lower momentum than freestream yet higher than surrounding boundary layer. Thus, this resulted in overall decrease in aerodynamic performance.

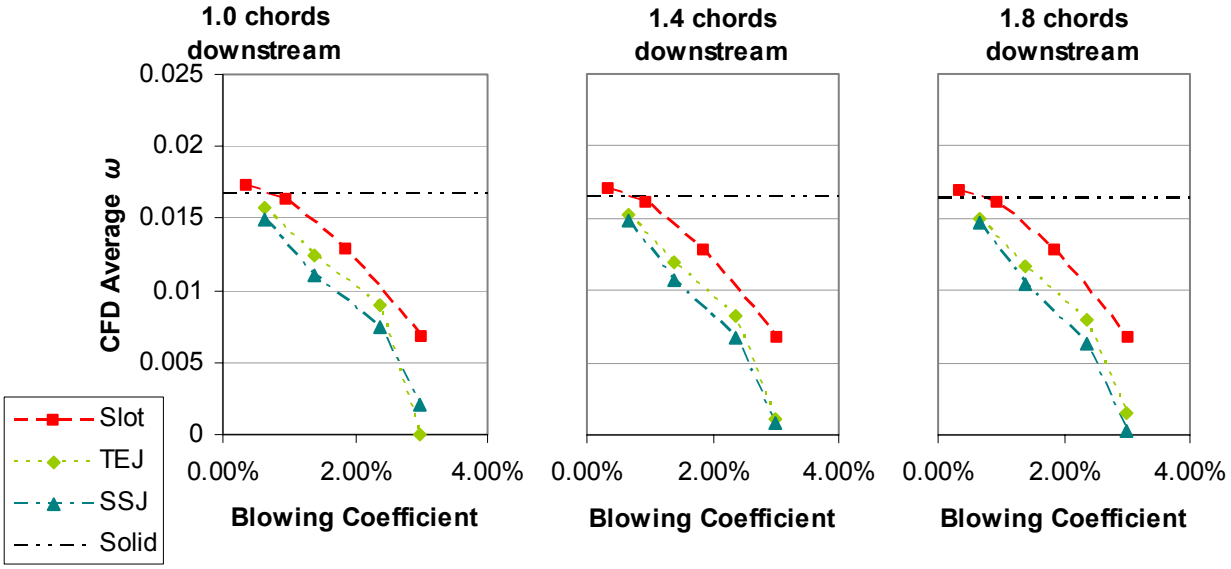

Figure 3-7 CFD area-averaged ω for all flow control configurations at all three downstream locations

Wake profiles showed that the discrete jets produced overblown wakes at the highest simulated blowing coefficients (3% $c_{blowing}$ or 1.25% mass flow rate). Because the noise prediction code was not designed to handle overblown cases, additional aerodynamic parameters for these operating conditions are not further shown or discussed.

Wake depth is shown in Figure 9 at three downstream locations. Comparisons between the different flow control cases reveal that the discrete jets once again offer improvement over the Slot, with the SSJ producing slightly shallower wakes. Shallower wakes produce weaker noise levels. Comparisons to solid blade show that the Slot produces deeper wakes at lower blowing coefficients. The reasons for this can once again be explained by the total pressure associated with the Slot-added fluid being lower than the freestream value.

Lastly, the wake half-width is shown in Figure 10 at the three downstream locations. From CFD it can be noted that the narrowest wakes were produced by the Slot and were narrower than those seen by the solid blade. CFD simulation of the solid blade revealed that the mixing of pressure and suction surface boundary layers occurred centered along the blunt trailing edge. Vortices present along the blunt trailing edge of the solid blade are either gone or greatly decreased in magnitude for the slot. Since the Slot flow control blows along the entire span of the blade, the Slot is hindering mixing of the suction and pressure surface boundary layers that would normally take place for the solid blade. This lack of mixing produces a much narrower wake than that seen

for the solid blade. This lack of mixing also results in deeper wakes for the Slot, as discussed previously.

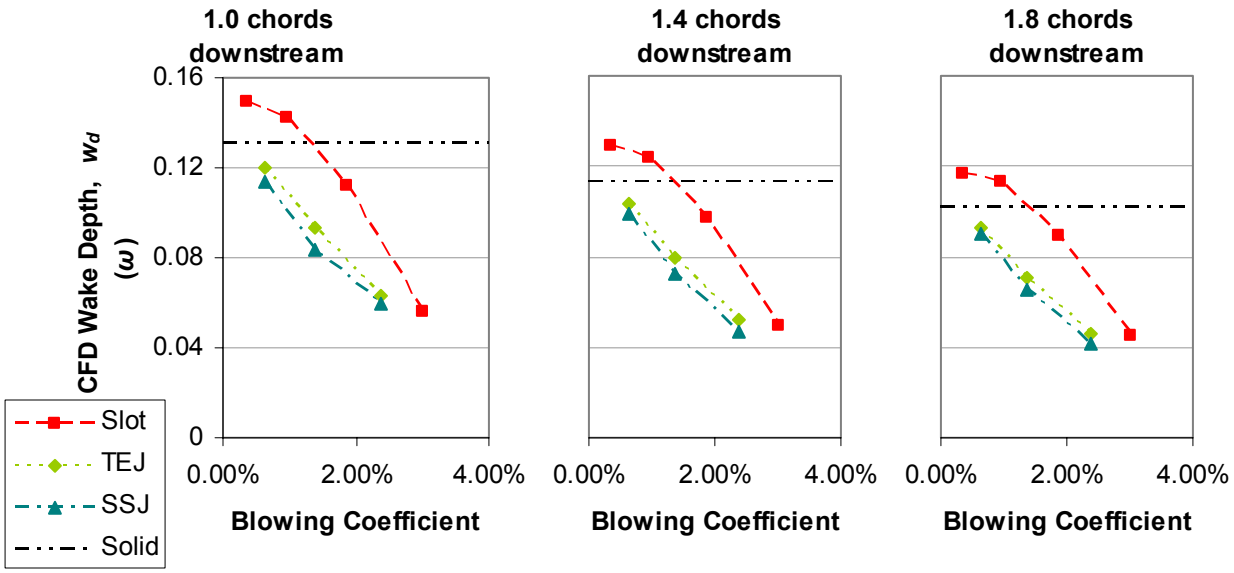

Figure 3-8 CFD wake depth for all flow control configurations at all three downstream locations

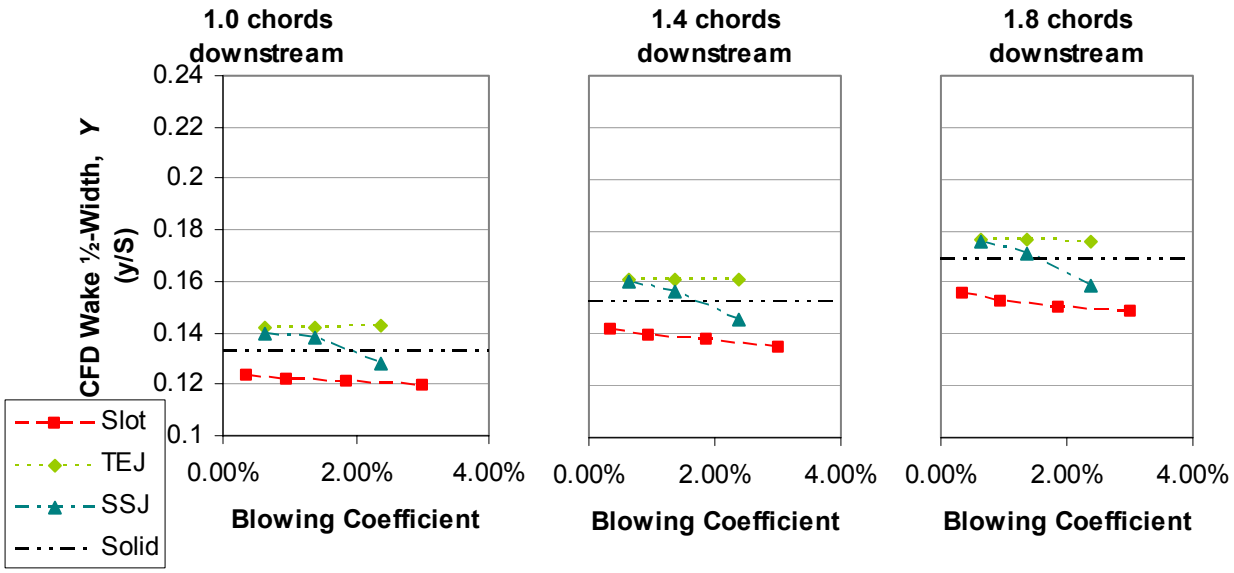

Figure 3-9 CFD wake half-width for all flow control configurations at all three downstream locations

This is not the case for the discrete jets. Because the jets are spaced, they allow for mixture of the suction and pressure side boundary layers. This produces a much more complex three dimensional flow structure than that seen with the Slot and the solid blade. However, CFD predicting the discrete jets would produce wider wakes than those seen by the solid blade is in disagreement with experimental results discussed later. This could be attributed to differences

between CFD 2D solutions (the solid blade and Slot) and 3D solutions (TEJ and SSJ). There were some differences in the ADPAC input file parameters between the 2D and 3D solutions. These changes were necessary in order to stabilize the 3D solutions and to allow them converge. The parameters changed affect the eigenvalue scaling terms in the implicit residual smoothing algorithm (Hall, et al, 1999) and may have caused some discrepancies when switching between 2D and 3D solutions. Likewise, any discrepancies may have been propagated by the difference in the complexity of the 3D and 2D simulations. Nevertheless, it is still expected that the TEJ and SSJ will produce wider wakes than those produced by the Slot due to the discrete jets having more complex flow structures.

Note that the SSJ half-width decreases as the blowing coefficient is increased, whereas the TEJ show a slight increase in width. This is due to the location of the suction surface jets. CFD also showed that the SSJ did not adhere to freestream main direction, unlike the TEJ. Whereas the TEJ were aimed at affecting the center of the wake, the SSJ affected the suction side boundary layer. This led to CFD predictions of a narrowing of the SSJ wake as blowing rates were increased due to the addition of higher momentum fluid to one side of the wake instead of to the middle of the wake as performed by the TEJ.

Thus, the CFD solutions show that the SSJ produce the shallowest wakes and the least area-averaged pressure loss coefficient, but the TEJ offer wider wakes than the SSJ. Since shallower and wider wakes produce less noise than sharper and narrower ones, the TEJ and SSJ should offer an improvement in noise reduction over the Slot based on CFD data. An acoustic prediction based on partial CFD data (not all blowing coefficients for all cases were studied in detail) will be presented and further discussed after the experimental results.

3.3 Experimental Aerodynamic Results

This section highlights the results of the wind tunnel testing conducted for this study. As has been mentioned in previous sections, due to the design of the Slot, no adequate plenum design was found given facility, machining, and time limitations. Slot plenum designs bench tested showed poor flow uniformity along the span (see Appendix B for a more detailed discussion). Thus, only the solid blade and the discrete jets were tested in the Virginia Tech wind tunnel facility. The TEJ and SSJ were both tested using 0.50%, 0.75%, 1.00%, and 1.25% fan through-flow, which corresponds to blowing coefficients between 0.7% and 3.0%. Wind tunnel tests conducted on the solid blade are also shown. The results of the solid blade will allow for a better comparison between

the experimental cases and the CFD cases, since experimental results for the Slot have been omitted due to prior discussions regarding the plenum design.

Figure 3-10 shows the area-averaged pressure loss coefficients for the discrete jets and solid blade at the three downstream locations. Compared to CFD, area-averaged pressure loss coefficients were found to be under-predicted. However, overall trends show agreement, and the SSJ outperforms the TEJ at every blowing coefficient, as seen in CFD. Experimental improvements in solid blade performance by the discrete jets also seem to follow the same trend as seen in CFD. As mentioned previously, the highest blowing coefficient tested will not be further discussed since results produced an overblown wake. Wake propagation data collected from overblown cases cannot be input into the noise prediction software used in this study.

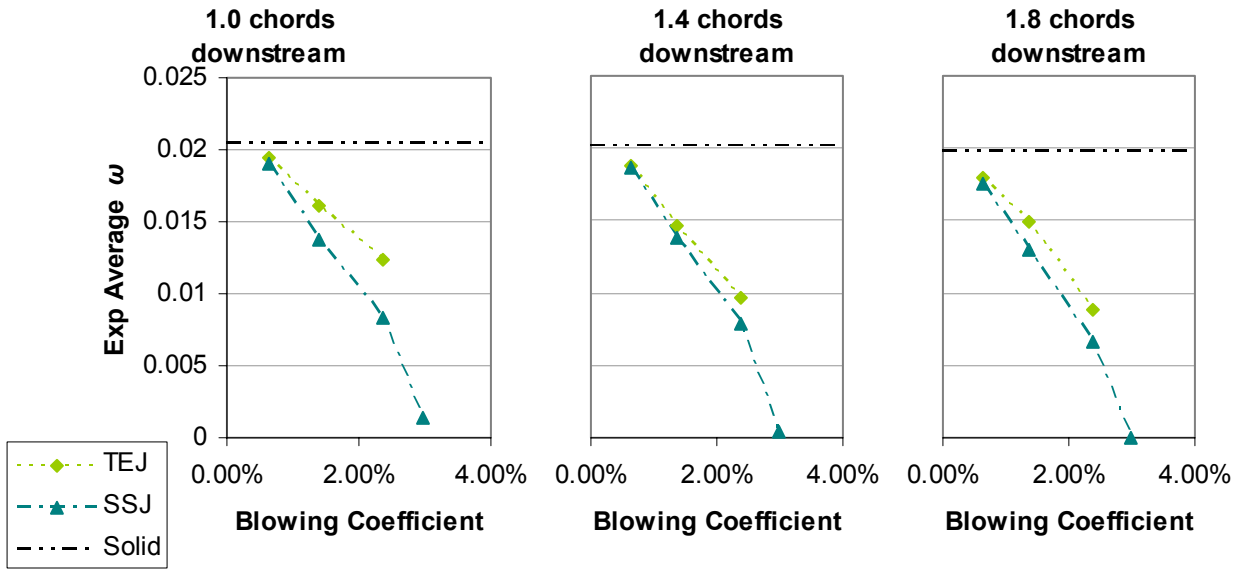

Figure 3-10 Experimental area-averaged ω for TEJ and SSJ at all three downstream locations

Figure 3-11 shows the wake depth. Compared to CFD, similar trends are observed. Both the TEJ and SSJ offer shallower wakes than those produced by the solid blade, but not as much when compared to solid blade as was predicted by CFD, especially at the lower blowing coefficient. The SSJ produces the shallowest wakes which is in agreement with CFD. However, there is a larger difference between the TEJ and SSJ depth at about 1.5% blowing coefficient (0.75% fan through-flow). This difference can be better explained by first studying the experimental wake half-width results.

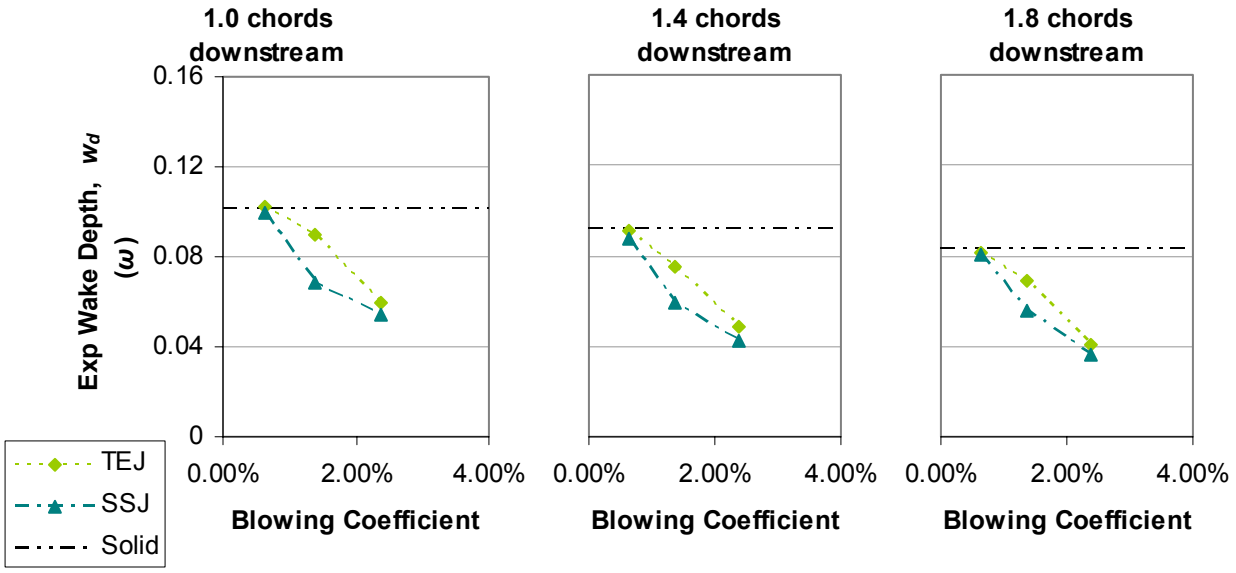

Figure 3-11 Experimental wake depth for TEJ and SSJ at all three downstream locations

Observation of the experimental wake half-width with respect to blowing coefficient in Figure 3-12 shows that the SSJ are producing the widest wakes at about 1.5% blowing coefficient (0.75% fan through-flow). The trends seen here differ greatly from the CFD results. In the experimental results, the SSJ produce the widest wakes at lower blowing coefficients, whereas the TEJ seems to produce the widest wake at the highest blowing coefficient.

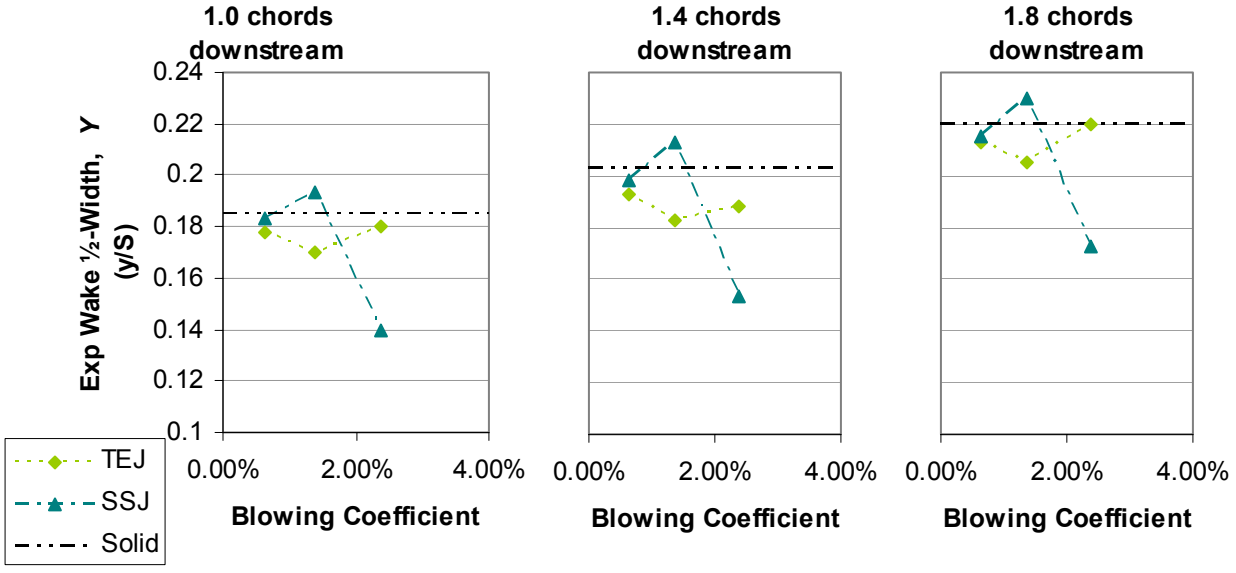

Figure 3-12 Experimental wake half-width for TEJ and SSJ at all three measurement locations

The SSJ's increased half-width at lower blowing coefficient values can be explained by studying the configuration in more detail. The SSJ creates a viscous ramp effect on flow traveling

on the suction surface. At 1.00% fan through-flow, both discrete jet configurations were designed to be choked. At this point, flow control momentum and total pressure are much higher than that of freestream fluid. This produces a very strong jet that energizes the surrounding retarded fluid, but does not quickly merge to the direction of the surrounding flow. Most of the suction surface boundary layer fluid will be forced around the jet instead of over it. Thus, the suction surface boundary layer is energized but not redirected. At lower mass flow rates, the momentum and total pressure are still higher than freestream values, but the SSJ is no longer as strong. Therefore, the jet will adhere more easily to the direction of the surrounding flow. In this case, more of the retarded boundary layer fluid will travel up the jet as in a viscous ramp, while some will still go around it. This produces a much greater level of mixing than seen with the stronger choked jet. And since the wakes produced by the SSJ at 1.5% blowing coefficient are wider due to mixing, this would produce shallower wakes and explain the increased difference observed in the experimental wake depth plots at the same blowing rate. However, contrary to CFD results, the discrete jet configurations do not produce wakes wider than those seen by the solid blade in the range tested, with the exception at the 1.5% blowing coefficient for the SSJ.

This difference between CFD and experimental is not unexpected. CFD is an analysis tool whose accuracy is dependant on the assumptions made for the analysis. As mentioned before, a Spalart-Allmaras one-equation model was used for this study. Like other one equation models, the eddy viscosity is assumed to be a function of the mixing length, which simplifies the transfer of momentum by turbulence. Additionally, it has been shown that the Spalart-Allmaras model poorly simulates jet spreading ratios (Wilcox, 1998). Thus, this yields some limitations in the applicability of the CFD model used. The more assumptions that are made, the more the physics of a modeled system are simplified. This simplification allows the modeled system to deviate from the actual system, and can lead to inaccuracies when details are meticulously studied. Nevertheless, CFD still provides a powerful analysis tool when overall trends are observed. Therefore, inaccuracies in wake half-width can be expected despite accurate forecast of trends in average ω and wake depth. This discrepancy does not affect the validity of CFD simulations or of the assumptions made on the system modeled; it just defines the limits of its applicability.

Thus, experimental results show that the SSJ produce less losses and shallower wakes compared to the TEJ. The widest wakes were produced by the SSJ at lower blowing rates, but at higher blow coefficients, the TEJ produce wider wakes than the SSJ at the same blowing coefficient.

3.4 Noise Analysis Results

This section provides a conclusion to the effectiveness of the flow control configurations in decreasing rotor-stator interaction. The aerodynamic data was post processed and input into the noise prediction code by David Arntz. The data output by the prediction code was then examined and conclusions made. As mentioned previously, overblown cases have been omitted due to prediction code limitations.

The noise analysis offered in this section was performed with NASA's CUP2D code, a rotor-wake vane interaction noise prediction code. The code yields a two dimensional approximation of the periodic and unsteady rotor-stator interaction which causes distinct tones to be produced at frequency multiples of the BPF. It accounts for frequency coupling and for flow swirl in the area between rotor and vanes. Coupling of acoustic modes and reflection of these modes propagate upstream interacting with the rotating fan, creating further modes and harmonic changes. This produces different cut-off and cut-on frequencies than those seen downstream of the stators. Therefore, upstream predictions will not necessarily show the same harmonic content as downstream due to reflections and coupling of acoustic modes. Modes propagating upstream are also moving against local flow velocity vectors and undergoing a Doppler Effect, thus creating changes in frequencies.

Wake profile propagation data is input through wake depth and width. The data output by the code gives sound pressure and power calculated at positions upstream of rotor and downstream of stator. Only sound power levels for each BPF will be shown here. The data has been formatted to be presented in comparison to the noise prediction for the solid blade case. The sound power level and total sound power level changes are shown in decibels. Note that the number of rotors and stators is designed for the first BPF to be cut-off.

Figure 3-13 shows the total attenuation of tonal noise based on CFD data. Only a partial acoustic analysis of CFD findings was conducted. Only one point of comparison is presented between the TEJ, SSJ, and Slot. This occurs at 1.00% fan through-flow for the TEJ and SSJ, and 2.0% for the Slot. CFD predicts that the discrete jets will offer the most attenuation of solid blade over the Slot. SSJ offers about 4 dB more attenuation than the Slot both upstream and downstream and 1 dB and 0.5 dB more attenuation over TEJ upstream and downstream, respectively. Note that below a blowing coefficient of 1.7% (1.67% fan through-flow), the Slot begins to produce more noise than the solid blade due to increases in wake size experienced due to the addition of low momentum fluid by the flow control (see section 3.2).

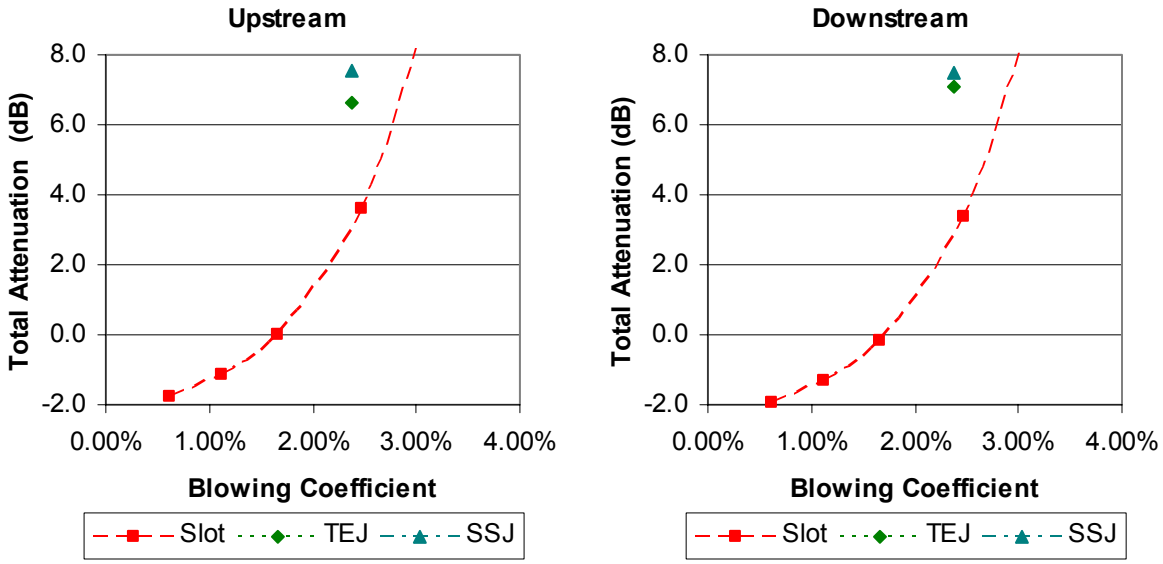

Figure 3-13 Total attenuation of solid blade tonal noise based on CFD propagation data

Shown in Figure 3-14 is the noise prediction for the TEJ at the different blowing ratios tested based on experimental data collected. Attenuation to solid blade as expected increases with increased blowing rate. However, for the 0.50% fan through-flow case, the downstream prediction shows an increase in noise. Observation of the aerodynamic wake data reveals that the wake dimension at this point are very similar to solid blade, with the exception of creating a slightly sharper wake. This leads to more noise, since the unsteady interaction is strengthened by a sharper wake. Acoustic coupling produces upstream predictions that do not reflect the downstream results for the 0.50% case.

The predictions for the SSJ based on experimental data are shown in Figure 3-15. As expected, attenuation increases with increased blowing rates. The harmonic content varies greatly from that seen for the TEJ. Upstream noise predictions show increased attenuation compared to the TEJ at equivalent fan through-flow. Downstream data also shows more attenuation. At a blowing rate of 1.00%, the SSJ shows a lack of downstream attenuation about 5×BPF. This results from wake width changes. At this blowing rate, the SSJ produces a small, but very narrow wake, approximately 1/5 the pitch in width, which causes an excitation of the 5×BPF tone.

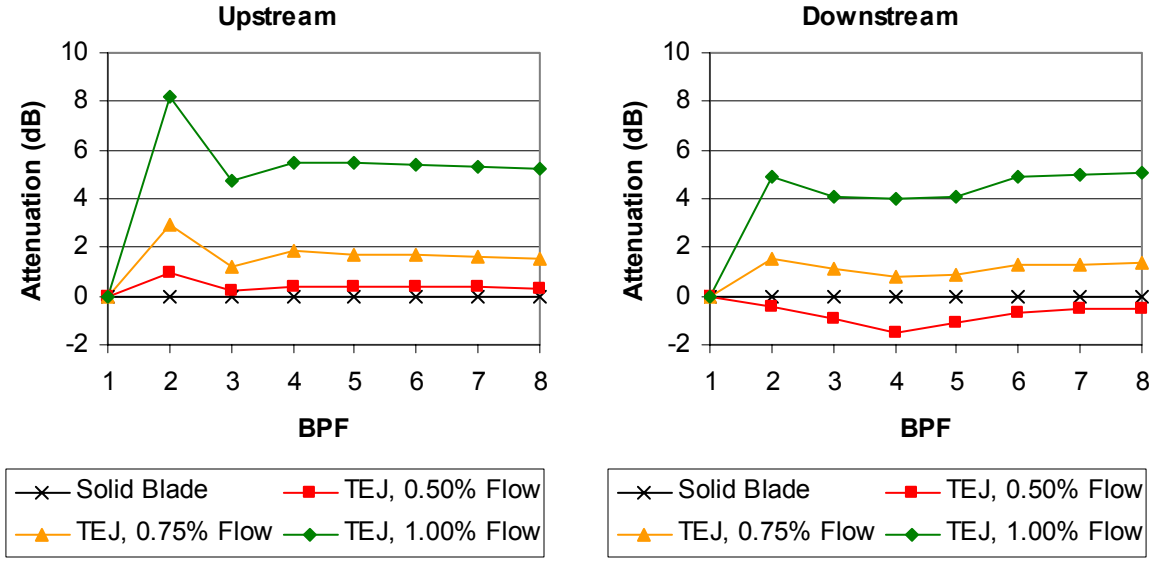

Figure 3-14 Tonal noise prediction based on TEJ experimental data

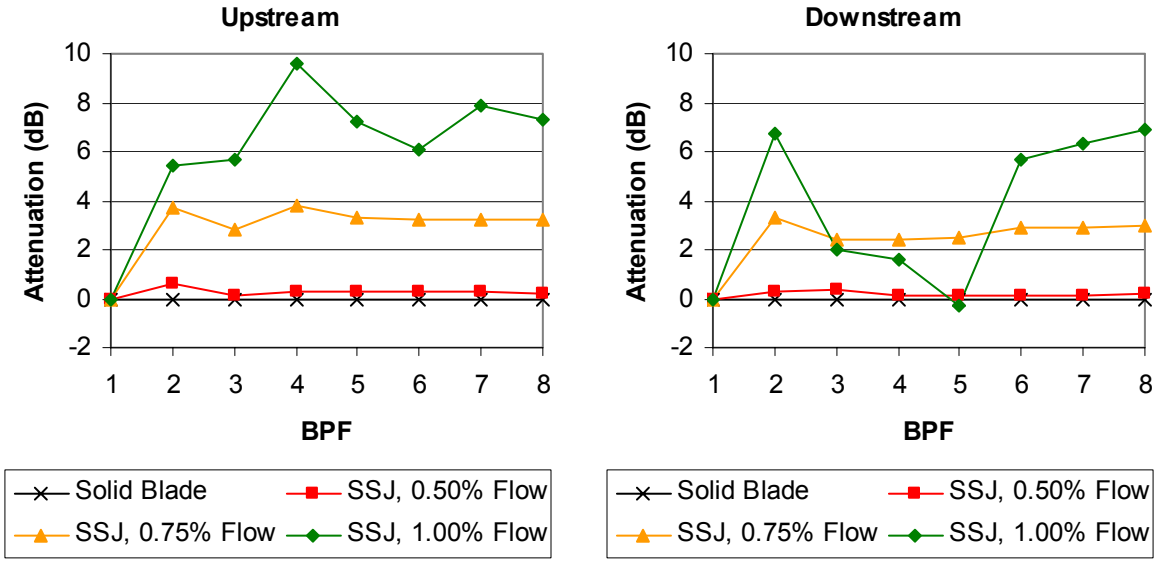

Figure 3-15 Tonal noise prediction based on SSJ experimental data

Total attenuation of tonal noise based on the predictions for the two discrete jet cases is shown in Figure 3-16. This data shows that the SSJ attenuates solid blade noise attenuation by about 2 dB more than the TEJ both upstream of the rotor and downstream of the stator for most every blowing coefficient. The total noise attenuation predictions based on experimental data are different from those observed using CFD data due to the aerodynamic differences discussed previously. However, for both CFD and experimental based predictions at 1.00% flow, the SSJ do offer more attenuation over the TEJ and more so upstream than downstream.

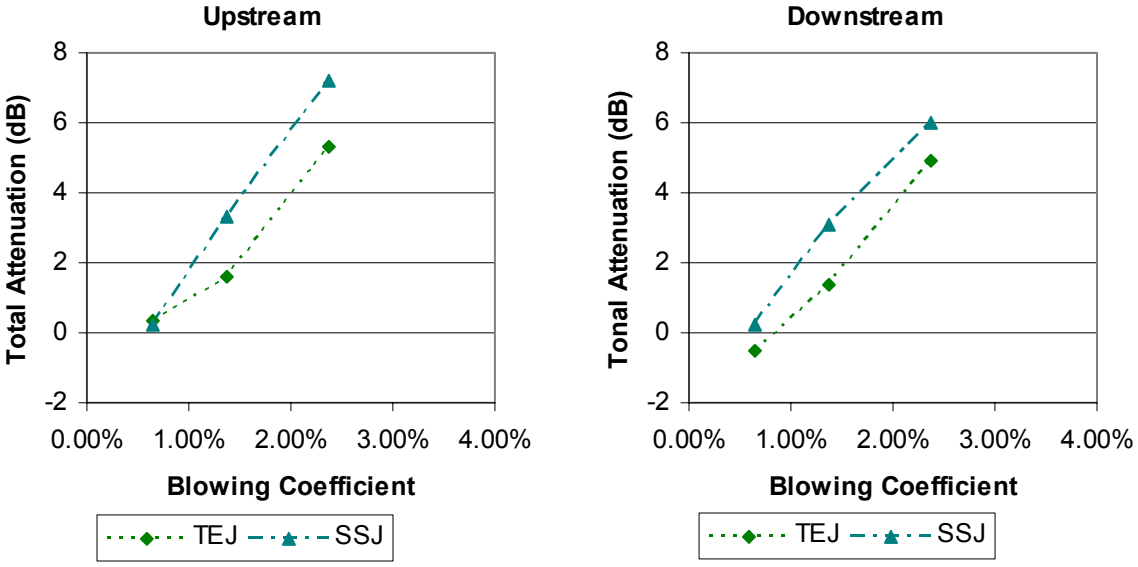

Figure 3-16 Total attenuation of solid blade tonal noise based on experimental propagation data

The implications of the acoustic predictions based on experimental wake propagation data are significant. As mentioned previously, the blade geometry was modified to accommodate the trailing edge Slot flow control. To accommodate that configuration, the trailing edge was thickened. Previous discussions on the formation of the boundary layer on the solid blade also pointed out the main sources of boundary layer formation: the suction surface and the thick trailing edge. These two sources account for the majority of the losses attributed to the blade geometry studied. As mentioned, the implications of the acoustic predictions are significant. The location of the SSJ and plenum and design requirements could allow for a blade with a thinner trailing edge than the one studied to be used. This implies fewer losses due to a diminished size in the recirculation zone created by the thick and blunt trailing edge. The application of the SSJ on this thinner trailing edge blade would account for a drastic decrease in losses and wake size that would greatly increase the noise attenuation obtained. Neither the Slot of TEJ could be applied to a thinner blade or a blade without a blunt trailing edge.

Chapter 4. Conclusions and Recommendations

A two-dimensional study of a fan blade was conducted to improve tonal fan noise reduction by optimizing an existing flow control configuration. The fan consists of an 18-blade 22-inch-diameter rotor followed by a 44-blade stator. The study was conducted on a 2D cross-section of the fan blade at 89.9% span with design inlet conditions Mach 0.73, Reynolds number based on chord length of 1.67×10^6, and 0° design incidence angle. The cross-section has a turning angle of 15.4°, chord of 3.9 inches, and pitch of 3.6 inches.

Conceptual flow control configurations were modeled with CFD to study the reductions in total pressure deficit and flow velocity deficit using blade design conditions. From these conceptual configurations, two configurations along with the existing flow control scheme were chosen for further study in a transonic wind tunnel: TEJ and SSJ. The existing flow control configuration, the Slot, consisted of an opening 45.4×10^{-3} inches wide and centered along the trailing edge of the fan blade aimed at an angle of 36.7°. The TEJ and SSJ flow control schemes consisted of discrete jets with 1/16-inch diameter spaced 0.3 inches center to center designed to be choked. The TEJ were positioned on the trailing edge of the blade aimed at 36.7°, and the SSJ were positioned at 95.5% chord angled at 15° from the blade surface.

Testing at the blow-down type transonic wind tunnel facility at Virginia Polytechnic Institute and State University was conducted in order to cross-validate results obtained through CFD. The test section consisted of a five blade cascade with the middle blade machined for flow control. All three configurations were simulated and tested at four distinct mass flow rates. The Slot was tested at 0.75%, 1.25%, 1.75%, and 2.25% fan through-flow. Both TEJ and SSJ configurations were tested using 0.50%, 0.75%, 1.00%, and 1.25% fan through-flow. Comparison between configurations was achieved through the use of a blowing coefficient which related the momentum of the flow control as a percentage of the freestream momentum.

CFD demonstrated that the discrete jets would both offer an improvement over the Slot in area-averaged pressure loss coefficient. Wake dimensional propagation based on CFD showed that the SSJ would produce the shallowest wakes at every blowing coefficient. In terms of noise, this would indicate a lessening in strength in unsteady rotor-stator wake interaction, or a decrease in noise strength. CFD wake half-width showed the TEJ producing wakes wider than the SSJ at all blowing ratios, with the difference between the two cases becoming greater as the blowing coefficient was increased. This would imply a change in the harmonic content of the noise

generated. However, the trend shown in CFD for the wake half-width was questioned by the experimental results. Nevertheless, CFD showed that the SSJ flow control configuration would aerodynamically outperform the TEJ and Slot.

The experimental data showed that the SSJ produced better results that the TEJ. Experimentally, the SSJ generated the least losses and produced the shallowest wakes at all blowing rates, and produced the widest wakes at lower blowing coefficients, including a wake wider than that seen with the solid blade at 0.75% fan through-flow. Noise predictions based on CFD showed that the SSJ would offer more attenuation than the TEJ and Slot at the same blowing coefficient. Noise prediction results based on experimental data also displayed that the SSJ produced 2 dB more total attenuation than the TEJ at all blowing rates, both upstream of the rotors and downstream of the stators. And, unlike the other configurations tested, the SSJ could potentially be used on a blade with a thinner trailing edge than the one used in this study. The blade used for this study was modified from an earlier design with a thicker trailing edge in order to allow for the addition of flow control. The reduction of this thick trailing edge would remove one of the major components in the production of boundary layer and losses. The use of a blade with a thinner trailing edge would imply fewer losses associated with the blade, which would signify a decrease in unsteady rotor-stator wake interaction and less noise. Neither the Slot nor the TEJ could be implemented on a blade with no blunt trailing edge.

Both the SSJ and TEJ configurations could also offer a simpler implementation onto a 3D rig, offering more structural stability and simpler internal passages than the Slot configuration, whose large opening presented structural and internal passage problems on a 2D cascade blade. Even though all of the flow control configurations used very similar plenum and air supply designs, the poor settling of incoming air into the plenum which attributes to poor uniformity did not manifest itself with the discrete jet flow control. Because the flow control openings are of smaller size, the losses associated with the holes allowed the settling chamber to perform more adequately than it did for the Slot.

This brings up an interesting point regarding the application of the Slot configuration in a 3D and more realistic setting. As seen in studies by Brookfield and Waitz [2000], flow control passage design of a blade is an important aspect towards the applicability of a flow control system. Properly designed passages will allow the flow control system to function correctly while providing little change to the blade untwist characteristics.

The opening created by the Slot along the trailing edge greatly changes the structure for the blade, affecting the blade untwist characteristics. Because it requires large amounts of mass flow, the flow supply into the blade must have a large area or receive high pressure air, which must be settled in order to perform as designed. Because the trailing edge would present such a large opening, the air must be properly settled and straightened, or it will suffer from poor uniformity. As seen by Brookfield and Waitz, despite careful analysis and design of interior passages so that the flow control would create a momentumless wake, a momentumless wake was not achieved when tested. Thus, the use of discrete jets offers a great advantage over larger open slots, not only due to their aerodynamic effects but they are more feasible to implement on a realistic blade.

Additionally, the SSJ flow control configuration could be improved. By maintaining the flow control area per inch span (0.01) while decreasing spacing between the discrete jets, additional mixing could be occur even at higher flow rates, which could produce wider wakes. This would benefit noise reduction by lessening the strength of the unsteady wake-stator interaction. Experimental results showed the SSJ producing a wake wider than that seen with the solid blade while decreasing aerodynamic losses. Performance of the SSJ at 1.00% fan through-flow may show improvement if the holes were machined at a smaller diameter and spaced more closely while still maintaining a choked design point at 1.00% mass flow rate. The goal would be to allow the high momentum air expelled by the SSJ to more easily adhere to the surrounding flow while allowing the SSJ to behave like a viscous ramp; thus, producing a wider wake. This would change the noise harmonic content and prevent the predicted 5×BPF peak downstream of the rotor, thus providing better attenuation. This may also allow the needed high energy flow added by the 1.00% fan through-flow case to more thoroughly mix into the central wake region. If the SSJ were to be optimized to allow for the wake to be widened while contributing to lessening losses, this may produce less fan noise than the best results seen in the current study using similar blowing coefficients and yield a superior design to the one tested. With the possibility of applying the SSJ configuration onto a blade with a thinner trailing edge, suction surface jets could be a superior design to the all-too-commonly-used trailing edge blowing.

Appendix A. CFD Results

The CFD investigation conducted for this study can be broken up into four stages. The first stage of the CFD analysis consisted of an assessment of the Slot configuration at a variety of mass flow rates. Second, the use of discrete jets was introduced with design constraints of choked flow at 1.00% fan through-flow. Spacing between jets was investigated at this stage to determine optimal spacing in order to insure proper integration of the jets into downstream flow. Third, the discrete jets were moved to the suction surface at three locations, and their effects on the wake profile were studied. The final stage consisted of using more complex flow control configurations involving the addition of angles in the span-wise direction. The first three stages of the investigation are outlined here, along with some Mach contours demonstrated in the last section. The final stage of the CFD investigation deserves its own discussion in Appendix E and is shown with experimental results.

A.1 Slot Investigation

The goal of this project was to optimize the existing flow control on a fan blade in order to improve fan noise reduction. As such, it was important to fully understand the existing flow control configuration and its properties. Thus, the Slot was studied using a wide range of mass flow rates from 0.95% to 3.11% of the fan through-flow. Total pressure wakes normalized by the freestream total pressure 2.34 chords downstream of the trailing edge are shown in Figure A-1 with the solid blade thrown-in for reference.

The figure shows the wake profiles shift from the solid blade towards the suction surface. This effect is expected since the Slot flow control affects the flow generated by the blunt trailing edge of the blade. Another interesting feature displayed by the figure is that low mass flow rates produce wake that are deeper than baseline. This phenomenon occurs because the fluid being added by the flow control is of lesser energy than the freestream fluid. However, the added fluid still has more energy than the immediately surrounding retarded boundary layer fluid. Thus, even though the Slot is adding fluid to the boundary layer, the added fluid is not energetic enough to lessen the losses associated with the wake. According to CFD results, the addition of fluid into the wake does not start to improve conditions until the mass flow rate becomes greater than 1.66% of the fan through-flow. Overblown wakes, just as undesired as wakes worse than baseline due to the production of increased unsteady wake-stator interaction and thus noise, start to occur somewhere between 2.59% and 2.67%. Thus, it can be surmised that the desired operating range of the Slot is between 1.66% and 2.67% fan through-flow.

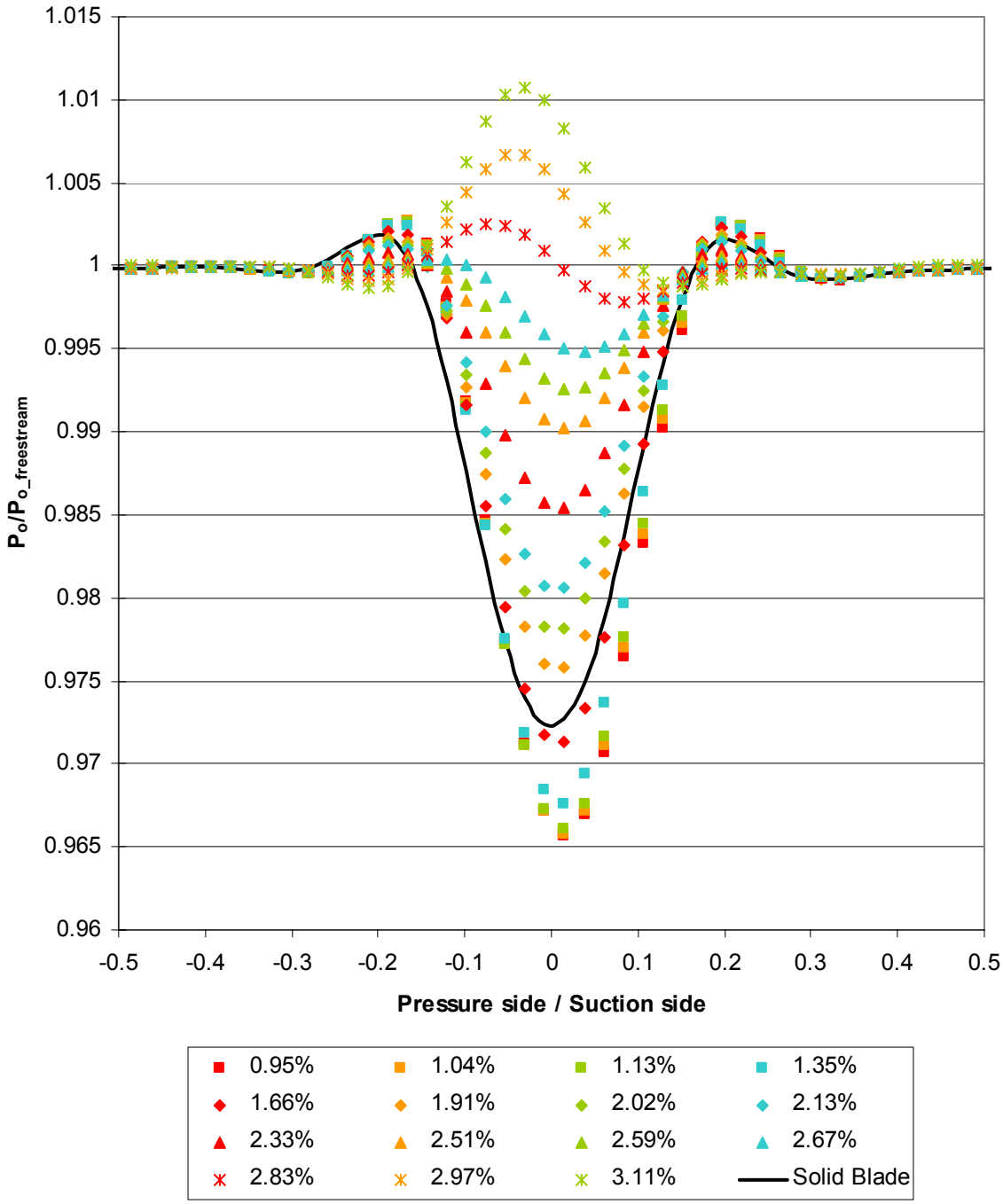

Figure A-1 CFD total pressure wakes referenced to freestream for the Slot at various mass flow rates

A.2 Discrete Jet Span-wise Spacing

After the Slot flow control configuration had been investigated, the use of discrete jets was introduced for use on the trailing edge of the blade. The discrete jets were modeled to yield 1.00% of the fan through-flow at choked conditions. This criterion was self-imposed since the only

requirement for the project was to optimize the flow control in order to improve the fan noise reduction of the Slot.

The aspect that needed to be considered was the spacing between jets that would allow the jets to be properly mixed into the surrounding flow without creating further unsteady rotor-stator interaction due to variation of the flow in the span-wise direction. It was desired for there to be little if any sign of the jet's presence 1 chord downstream. It was also considered important that the jets be spaced far apart enough to not require large amounts of machining on the blade surface. However, what was not considered at this point was that more carefully spaced holes mix more quickly into the surrounding fluid. This stage of the CFD study therefore gives the upper limit of how far apart the jets should be spaced in order to yield properly mixing in the span-wise direction.

Three distinct distances between discrete jets demonstrating the downstream Mach contours at 1.0, 1.4, and 1.8 chords are shown below. The following figures illustrate a perspective view looking from downstream to upstream (left to right). The location of the discrete jet is shown on the trailing edge of the blade. Figure A-2 shows contours using a spacing of 0.2 inches, Figure A-3 uses 0.3 inches, and Figure A-4 utilizes 0.4 inches. The contour edges have been highlighted for accentuation.

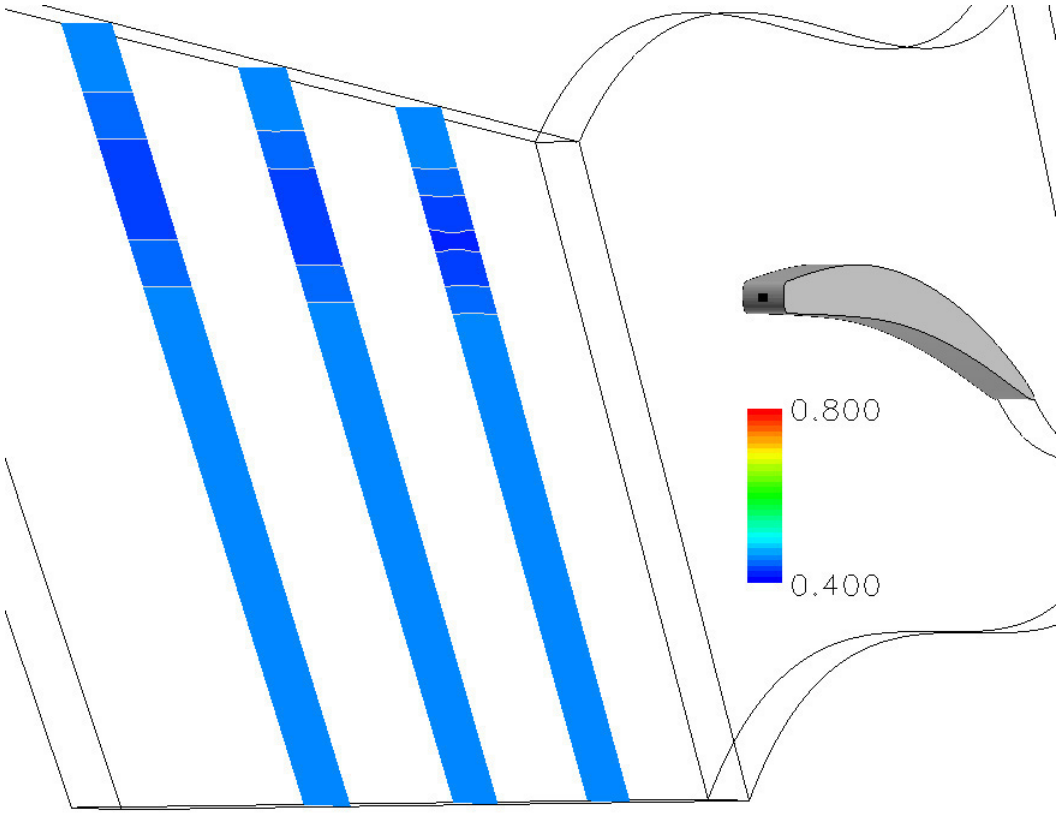

Figure A-2 Downstream Mach contours for TEJ at 1.00% mass flow rate spaced 0.2 inches apart

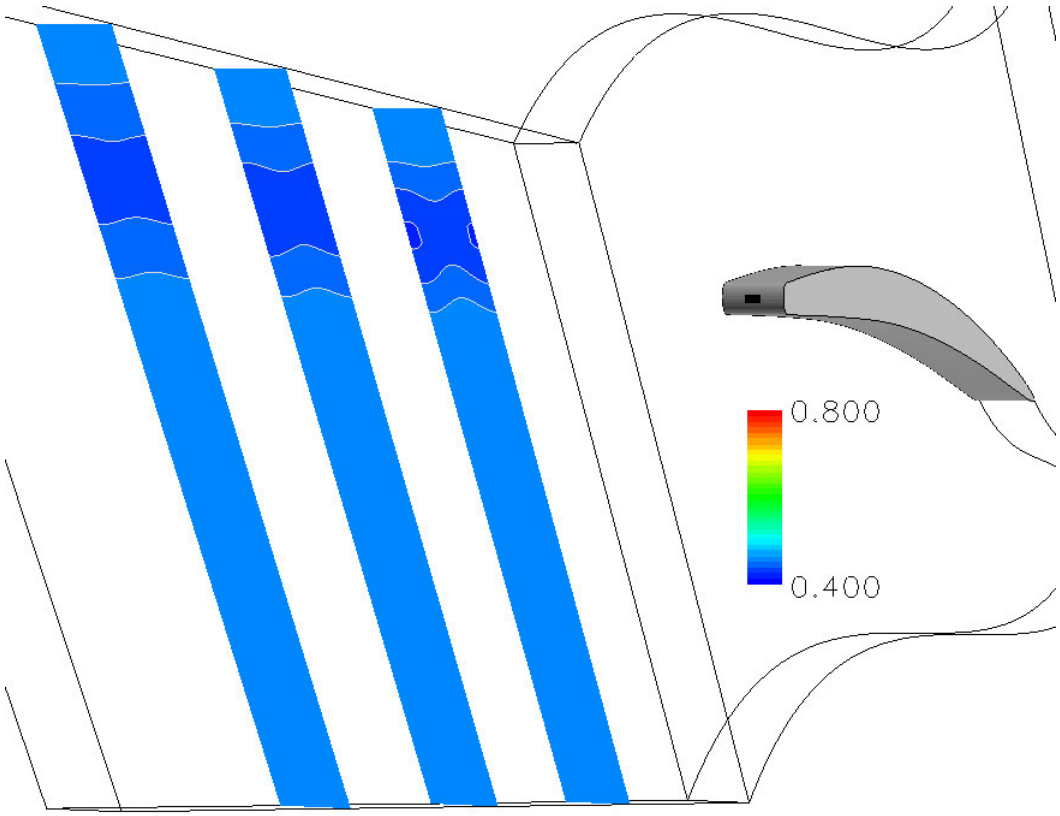

Figure A-3 Downstream Mach contours for TEJ at 1.00% mass flow rate spaced 0.4 inches apart

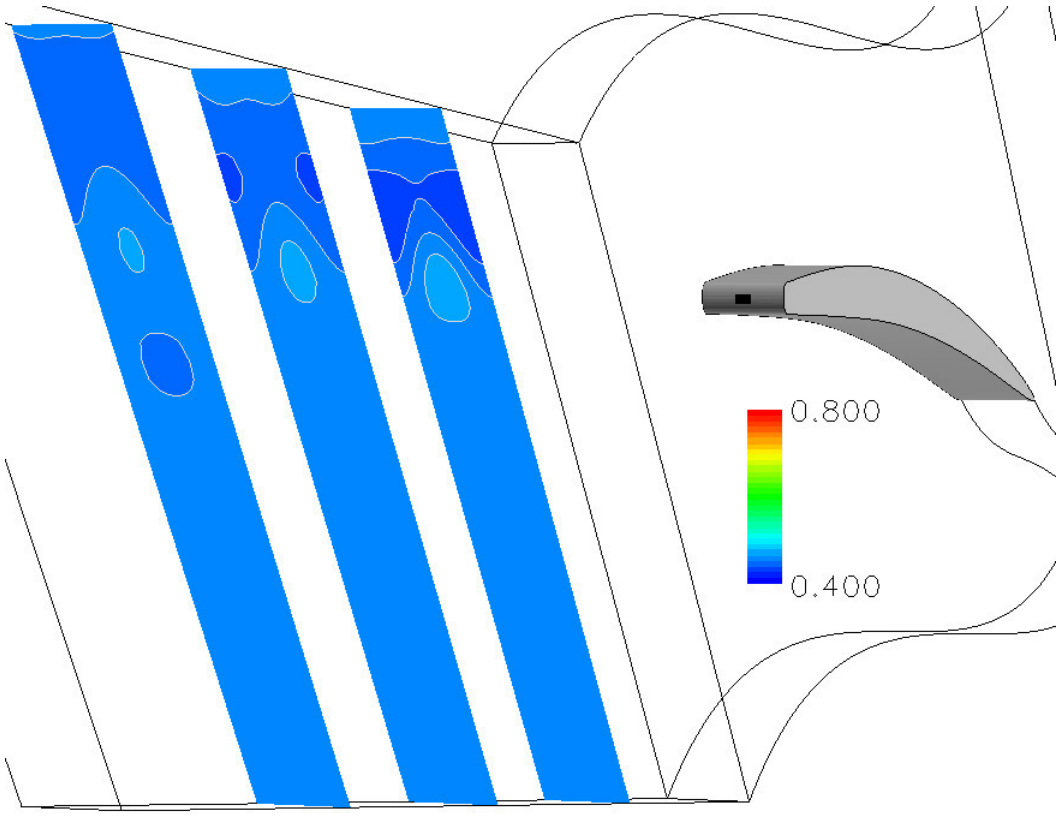

Figure A-4 Downstream Mach contours for TEJ at 1.00% mass flow rate spaced 0.4 inches apart

From the contours, it can be stated that the 0.2 inch displays little span-wise variation at every downstream location. The 0.3 inch shows moderate variation. But neither of these cases shows evidence of the jet not having mixed with the surrounding flow. There is no fluid associated with the jet that is of higher velocity than the surrounding or freestream velocity. The described condition does occur at a spacing of 0.4 inches where the jet can still be easily distinguished from surrounding flow even 1.8 chords downstream of the trailing edge. Thus, because CFD will under-predict losses and mixing associated with these losses, 0.3 inches was determined as the upper limit of how far apart the discrete jets could be spaced in order to insure proper mixing of the jet with the surrounding flow without creating large span-wise variations. This spacing was chosen for testing and the rest of the CFD simulations conducted.

The angle at which the TEJ were aimed was also varied ±3° from 36.7° using CFD for further analysis. With the exception of a small shift in the center of the wake, negligible variation of aerodynamic losses was detected by CFD. In order to provide a more accurate comparison between the Slot and TEJ, it was decided to angle the TEJ at 36.7° to the axial direction, the same angle used for the Slot.

A.3 Suction Surface Location

The discrete jets were moved to the suction surface to attempt suction surface blowing once spacing between the jets had been decided upon. Three locations for the SSJ were considered utilizing CFD: 86.6%, 95.5%, and 99.9% chords from the leading edge of the blade. For each location, the same conditions as those used for the TEJ were imposed: choked flow control using 1.00% fan through-flow. For both the 86.6% and 95.5% chord locations, the SSJ was aimed at 15° from the local surface. The 99.9% chord location was located on the upper portion of the blunt trailing edge and aimed at 40.0° to the axial direction (as defined in Figure 2-2).

Total pressure wakes normalized by the freestream total pressure for the three SSJ locations and solid blade are shown in Figure A-5. The wake profiles were taken 2.34 chords downstream of the trailing edge. All wakes show a shift from baseline towards the pressure side. This is expected given the location and mechanics of the SSJ.

The SSJ located at 95.5% chord produced the shallowest and narrowest wake of the three locations tested. The 86.6% chord SSJ creates the deepest wake, followed by the 99.9% chord wake. The 99.9% chord location is seen to behave very similarly to the TEJ, with the exception of shifting the wake towards the pressure side. This shift is expected since the SSJ is aimed 3° more into the

suction side and will energize the suction side boundary layer instead of the trailing edge boundary layer despite its location on the blunt edge.

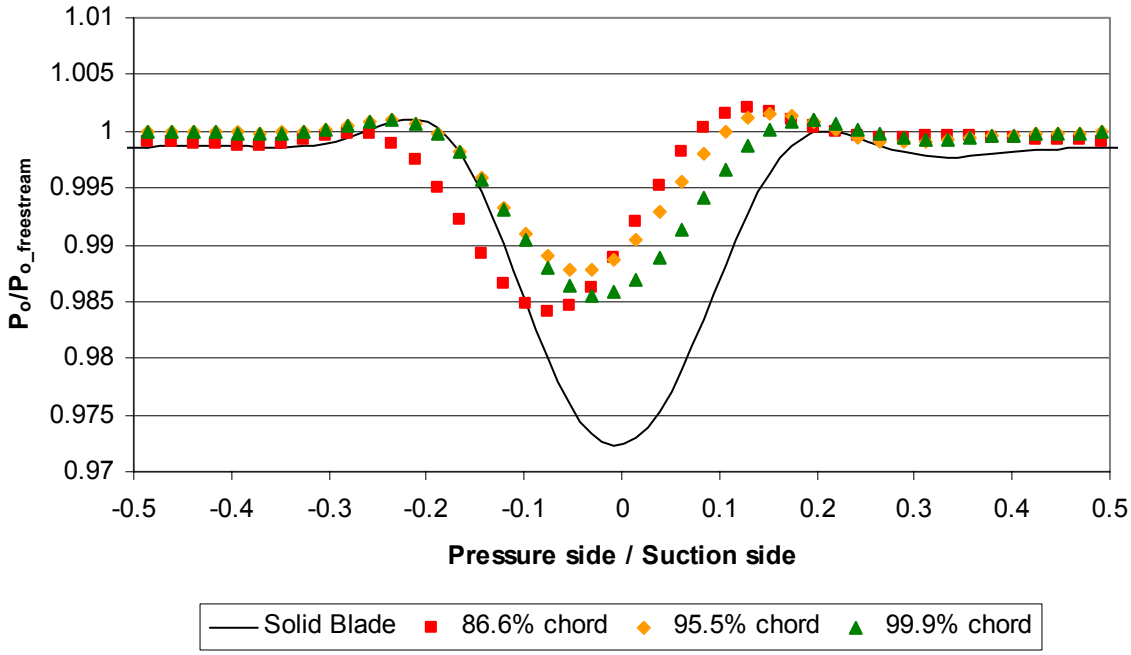

Figure A-5 Normalized total pressure wakes for SSJ at three distinct blade suction surface locations with solid blade for comparison

Because of the location of the holes and the strength of the fluid being introduced into the retarded boundary layer fluid by the SSJ at 86.6% chord, the flow control fluid does not completely mix into the boundary layer fluid. The flow control does improve surrounding flow conditions, but not to the extent that the SSJ at 95.5% chord does. The SSJ at 86.6% chord does not adhere to the surrounding flow as well as the SSJ located at 95.5% chord; the latter is forced to turn with the fluid attempting to maintain attached to the blade surface. The SSJ at 86.6% chord is farther upstream and is not as affected by the fluid turning around the blunt trailing edge. It will be seen in the Mach contours following this section that the SSJ is very pronounced when compared to TEJ and even more so when compared to the Slot.

A.4 Mach Contours

Contours showing total pressure and Mach number were important tools in evaluating the usefulness of flow control schemes for this study, facilitating comparisons of different cases to one another in CFD. They are of particular interest around the trailing edge and in the exit passage downstream of the blade. Shown below are Mach contours of various configurations run. To start,

a solid blade Mach contour is shown first in Figure A-6. The study of the solid blade was an important part of determining how to optimize the flow control. It was important to understand the way the flow behaved without the use of flow control at design conditions. The question of where to locate and implement flow control could be more readily answered.

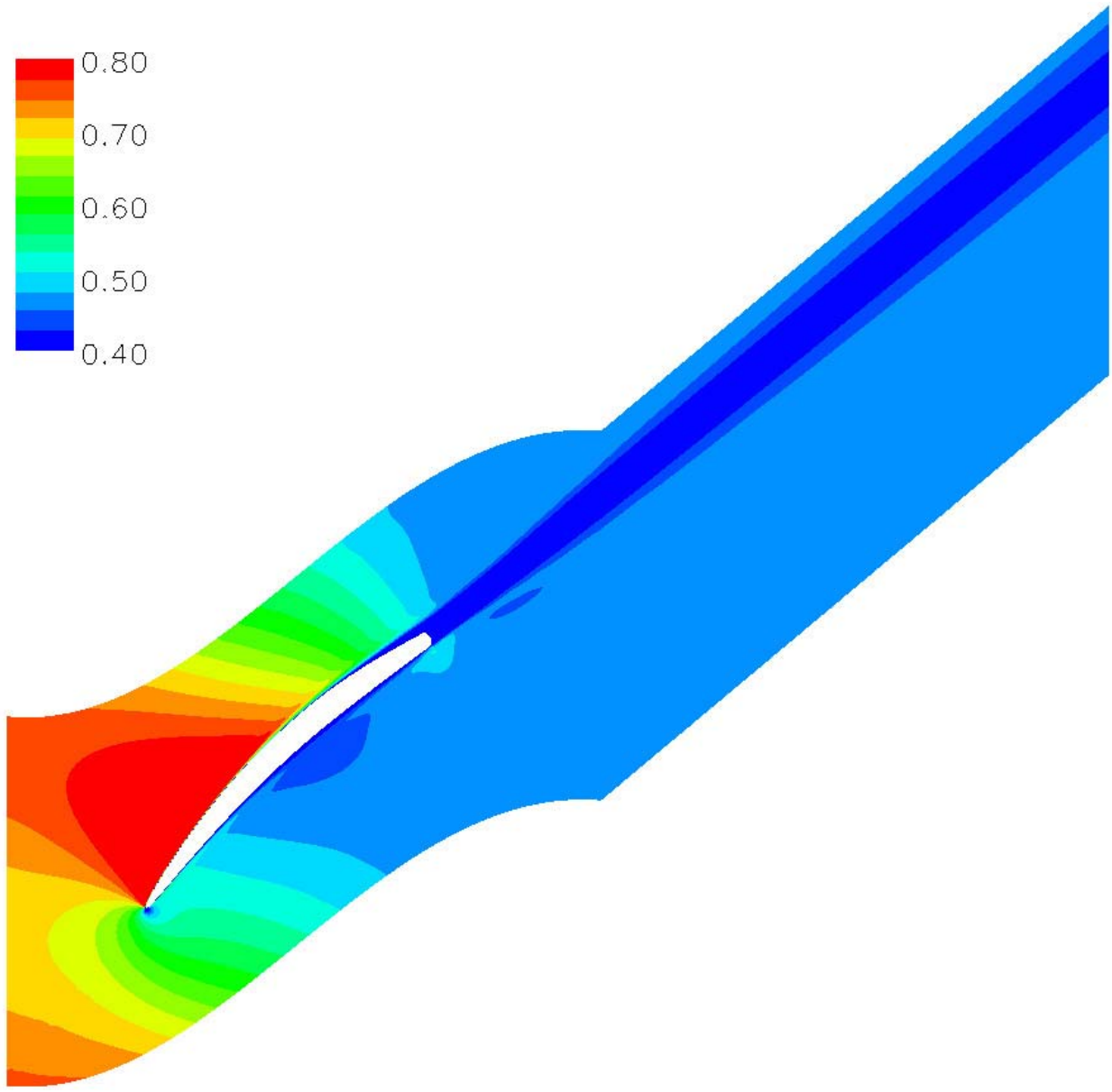

Figure A-6 CFD Mach contour for solid blade

The next three contours shown are for the Slot operating at three fan through-flows. The first flow rate of 1.00% is shown in Figure A-7. Notice that appearance of the flow control is minute and difficult to see in this particular perspective. The flow control fluid is slightly faster than the surrounding flow, but it is not contributing in lessening the wake deficit of the blade.

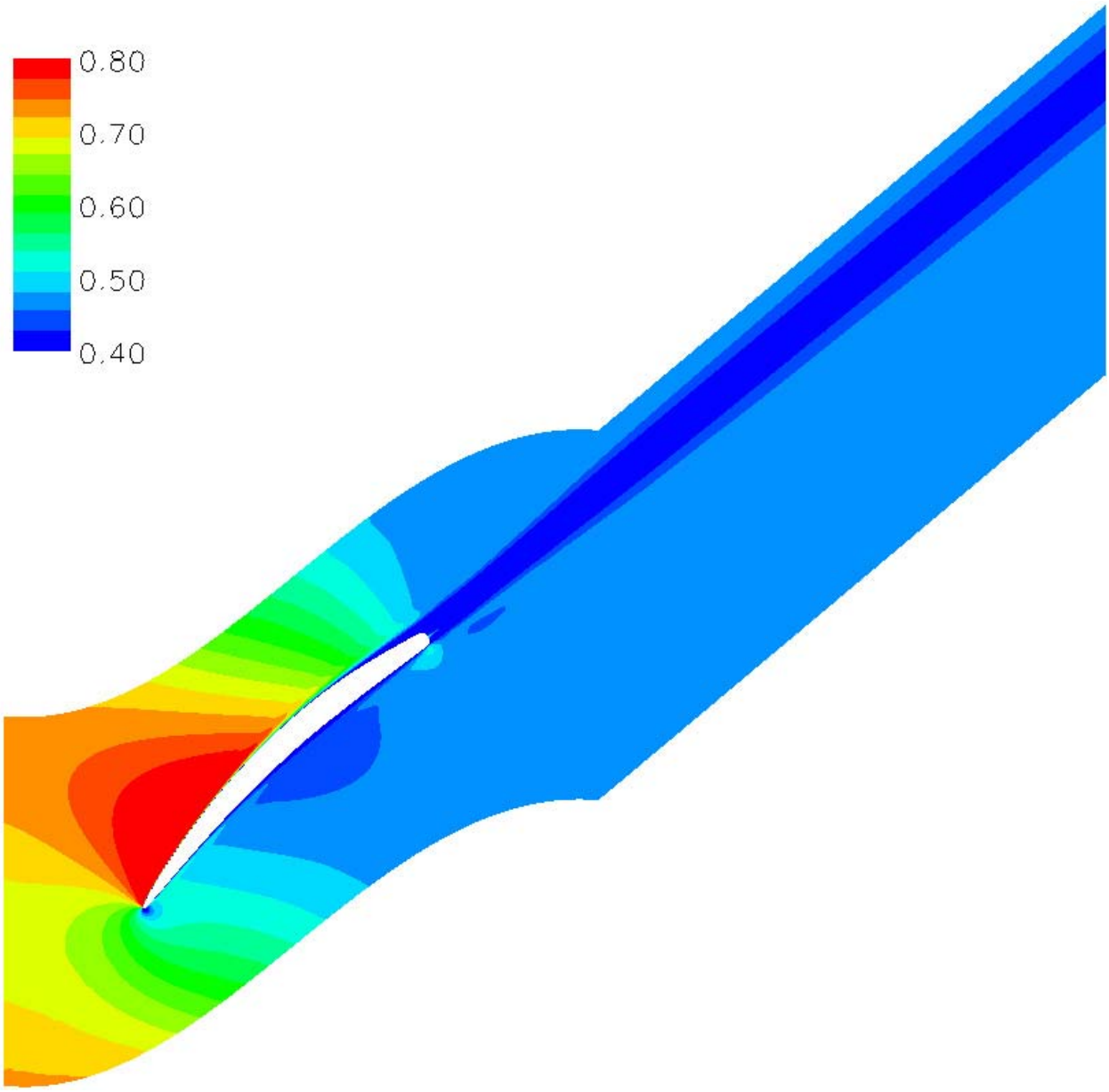

Figure A-7 CFD Mach contour for Slot at 1.00% mass flow rate

The next Slot case shown is for 1.91% fan through-flow in Figure A-8. The jet is only slightly more pronounced than what was seen in the previous case, despite that the flow rate has nearly doubled. This time the downstream wake shows some improvement as the darker shade of blue has begun to thin.

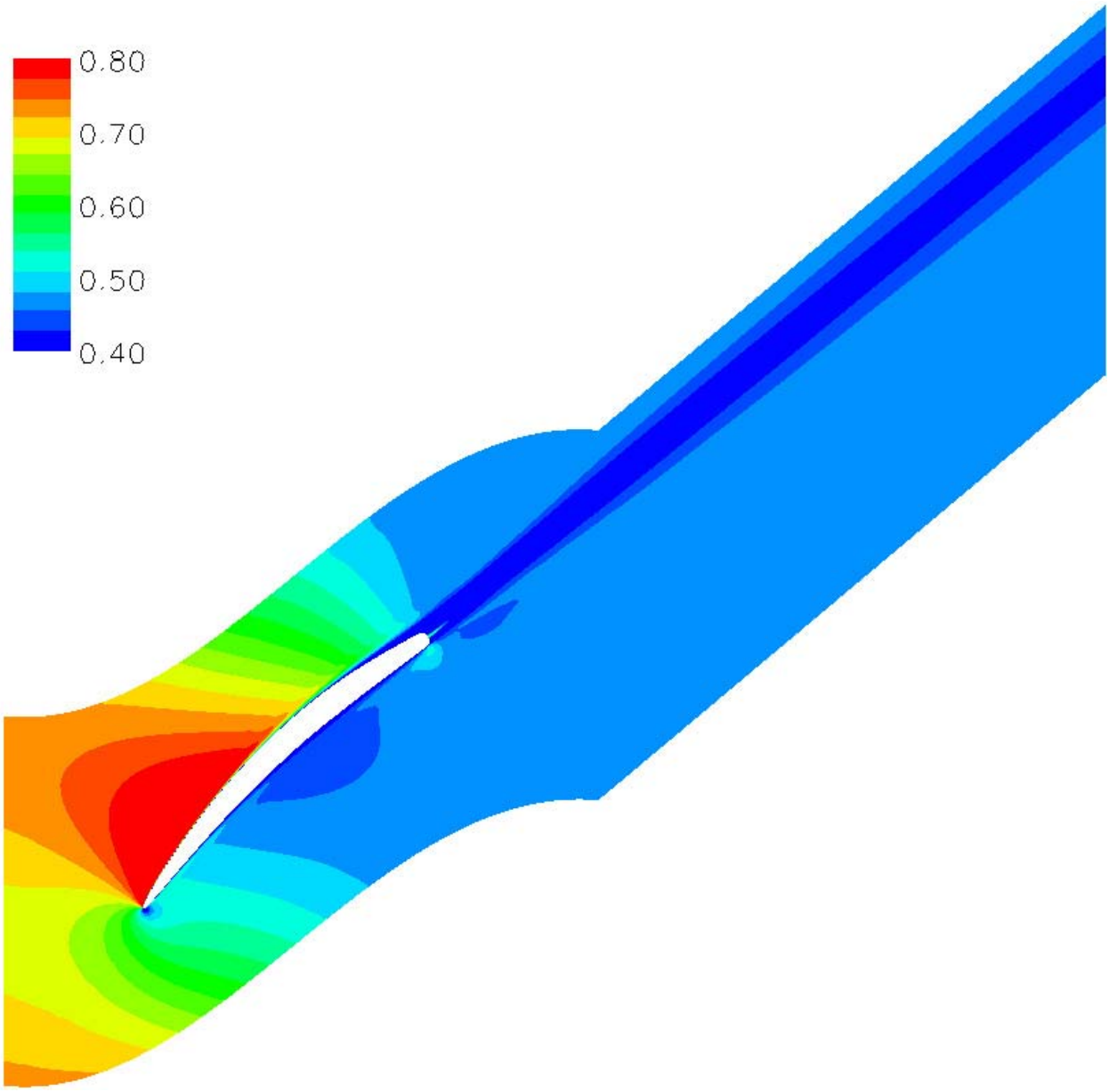

Figure A-8 CFD Mach contour for Slot at 1.91% mass flow rate

Finally, the Slot is shown in this final contour using 2.13% fan through-flow in Figure A-9. The flow control fluid is more visible. The effect on the wake has become more noticeable in this contour than in the previous. The darker shade of blue in the downstream wake has thinned to nearly half its original solid blade width.

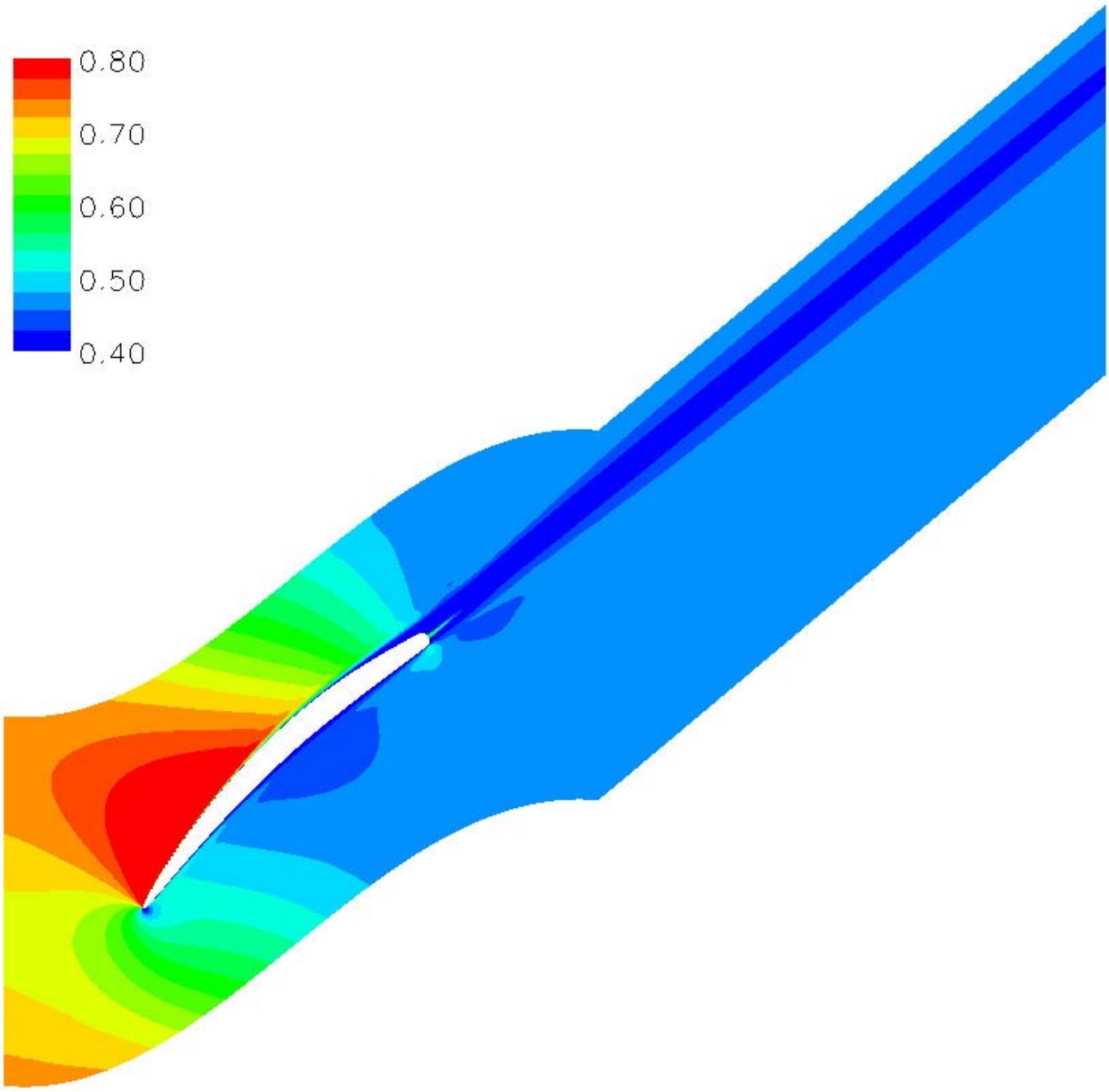

Figure A-9 CFD Mach contour for Slot at 2.13% mass flow rate

The next Mach contour, Figure A-10, is for the TEJ operating at 1.00% fan through-flow. The Mach contour cross-section is taken across the center of the jet. There is a large difference between this Mach contour and the solid blade and Slot cases. The jet is easily visible since the fluid escaping the jet exits at Mach 1. The effect is also easily seen. The downstream wake region pertains to only one shade of blue as opposed to two in the previous contours. The immediate contours surrounding the trailing edge have also changed compared to the solid blade.

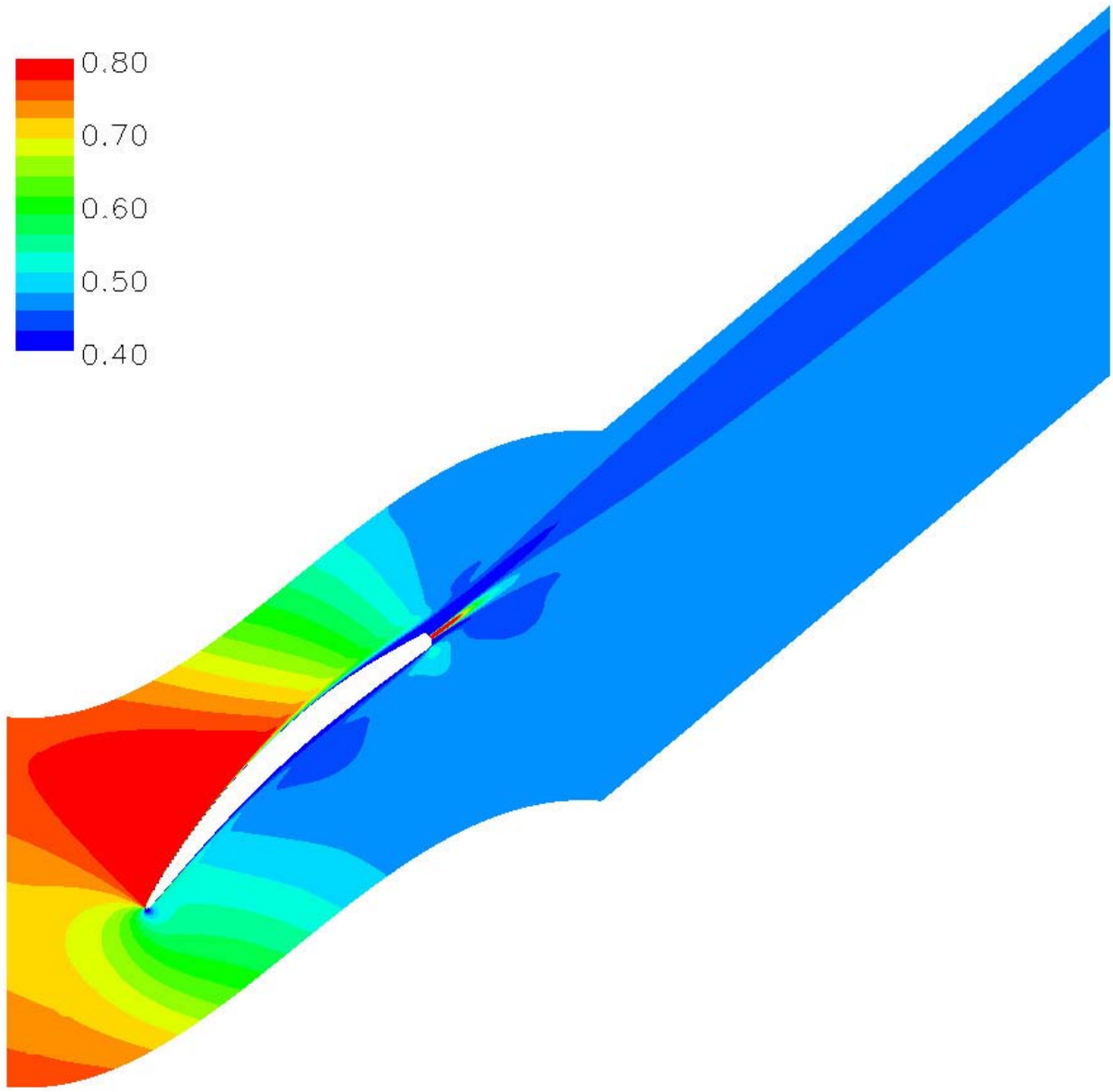

Figure A-10 CFD Mach contour for TEJ at 1.00% mass flow rate

As with the TEJ, the SSJ show a pronounced jet. Figure A-11 is the Mach contour for the SSJ at 95.5% chord using design conditions. As before, the cross-section was taken across the center of the jet. The jet seems larger than that seen in the TEJ, and this is attributed to the mixing of the flow control fluid into the surrounding flow. This cross-section shows the complete removal of the suction surface boundary layer from the wake. When compared to the solid blade, the wake is also shifted towards the pressure side (downwards). As in the TEJ, the SSJ wake deficit only uses one shade of blue, but this deficit is thinner than the one seen for the TEJ.

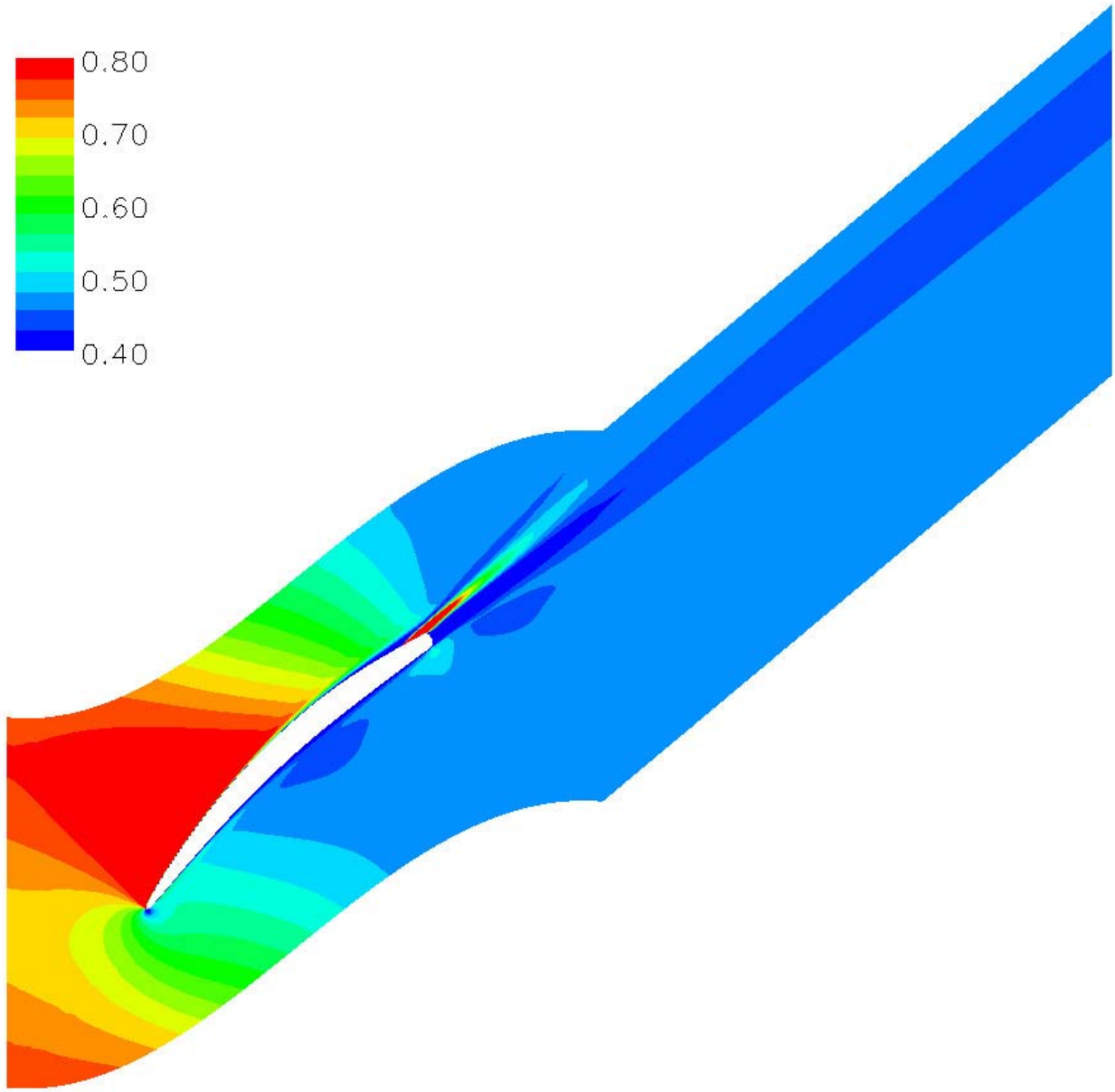

Figure A-11 CFD Mach contour for SSJ at 1.00% mass flow rate

Appendix B. Slot Wake Data

The following section contains a wake based brief comparison between CFD and experimental results obtained for the Slot flow control configuration. Note that for the following section, when comparing CFD and experimental data, CFD wake data is shown in blue squares and experimental wake data is shown in red circles.

As mentioned in 2.2.1, facility limitations and internal passage designs requirements prevented the proper wind tunnel testing of the Slot. The blade that was manufactured contained a slot that covered the central 3.88 inches of the 6-inch span and was shown in Figure 2-4. The trailing edge slot consisted of an opening 45.4×10^{-3} inches in width along the trailing edge of the blade aimed at an angle of 36.7°. Due to structural stresses, the slot was fitted with two 1/8-inch-wide support beams that divided the slot area into three parts. The center division measured 13/16 inches wide, and the two side divisions measured approximately 1.4 inches each. Bench testing showed that the supply area to jet area ratio was unfavorable, and the two side divisions were sealed with aluminum tape. Experimental cases were conducted for four different fan through-flows: 0.75%, 1.25%, 1.75%, and 2.25%. Ideally, this rate refers to uniform blowing along the trailing edge, but as will be seen, despite attempts to salvage the manufactured blade for feasible data, this was not the case.

The results from cascade testing plotted with corresponding CFD results for the pressure loss coefficient are presented next. Figure B-1 through Figure B-3 correspond to the downstream pressure loss coefficient wakes for 0.75% fan though-flow. Figure B-4 through Figure B-6 show the wake propagation for 1.25% mass flow rate. A pressure loss coefficient plot for fan through-flow rate of 1.75% is presented from Figure B-7 to Figure B-9. Lastly, Figure B-10 through Figure B-12 illustrates the spread of the wake with 2.25% fan through-flow for the slot. For all cases, the wakes are shown at 1.0, 1.4, and 1.8 chords downstream of the trailing edge.

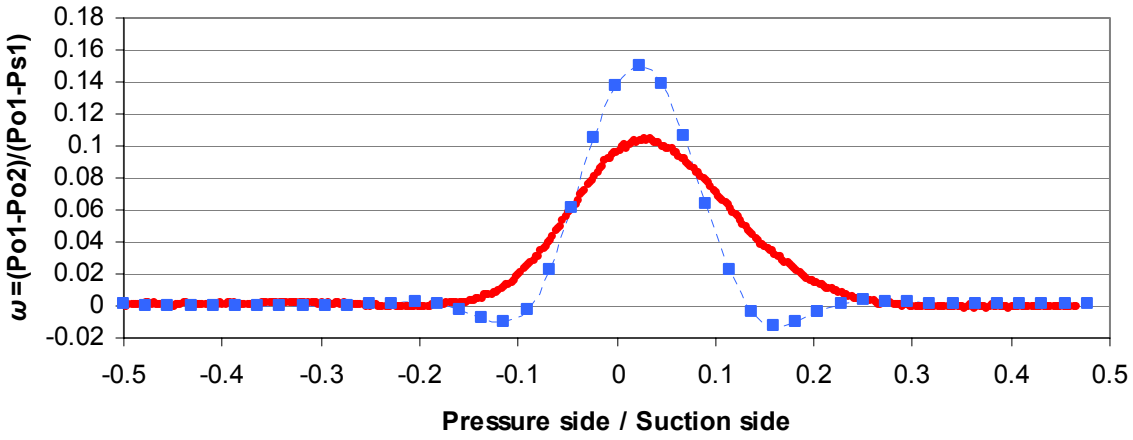

Figure B-1 CFD and experimental pressure loss for slot with 0.75% mass flow rate at 1.0 chords

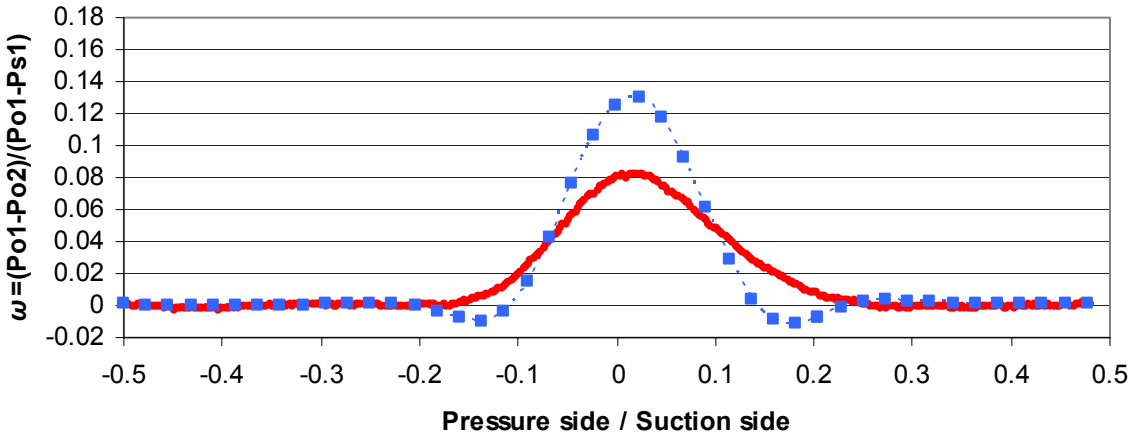

Figure B-2 CFD and experimental pressure loss for slot with 0.75% mass flow rate at 1.4 chords

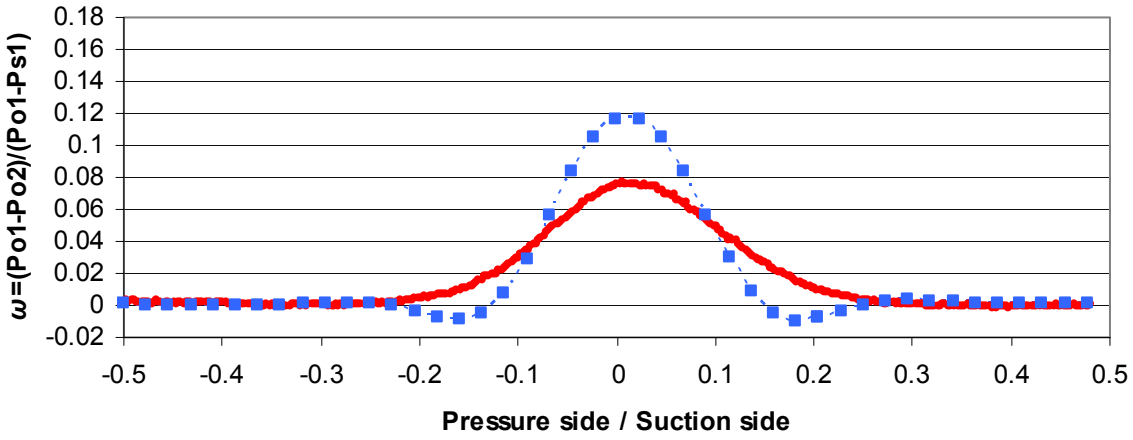

Figure B-3 CFD and experimental pressure loss for slot with 0.75% mass flow rate at 1.8 chords

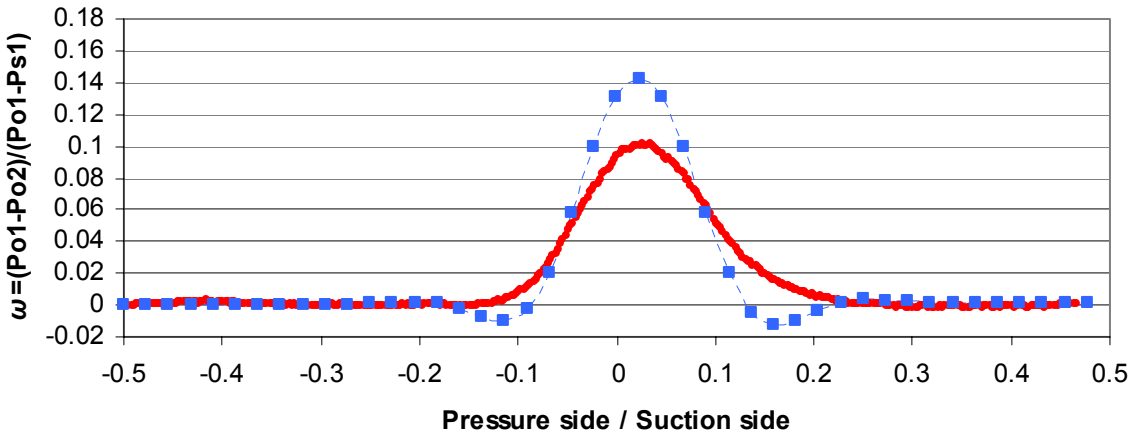

Figure B-4 CFD and experimental pressure loss for slot with 1.25% mass flow rate at 1.0 chords

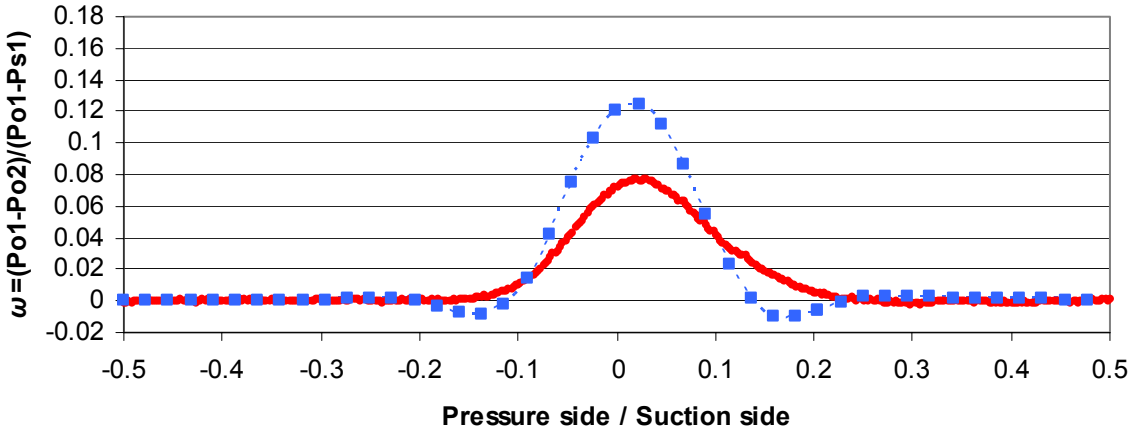

Figure B-5 CFD and experimental pressure loss for slot with 1.25% mass flow rate at 1.4 chords

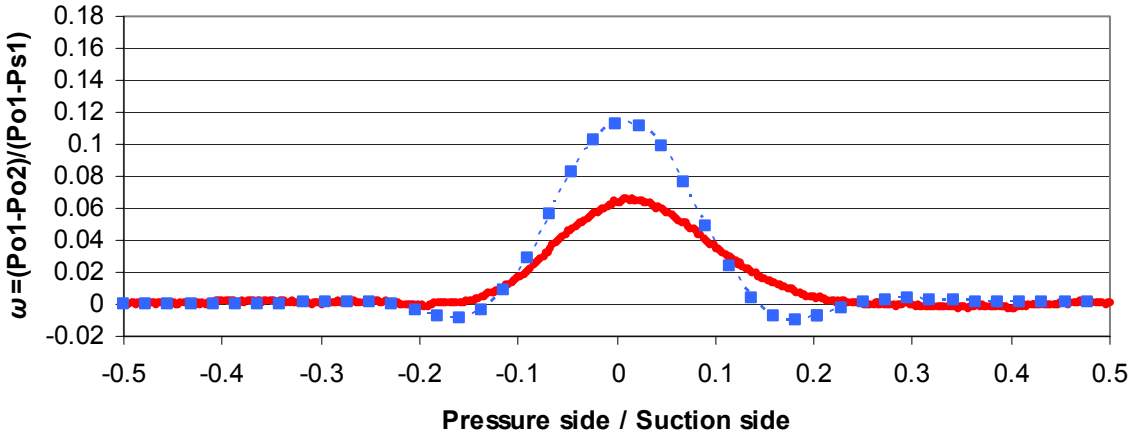

Figure B-6 CFD and experimental pressure loss for slot with 1.25% mass flow rate at 1.8 chords

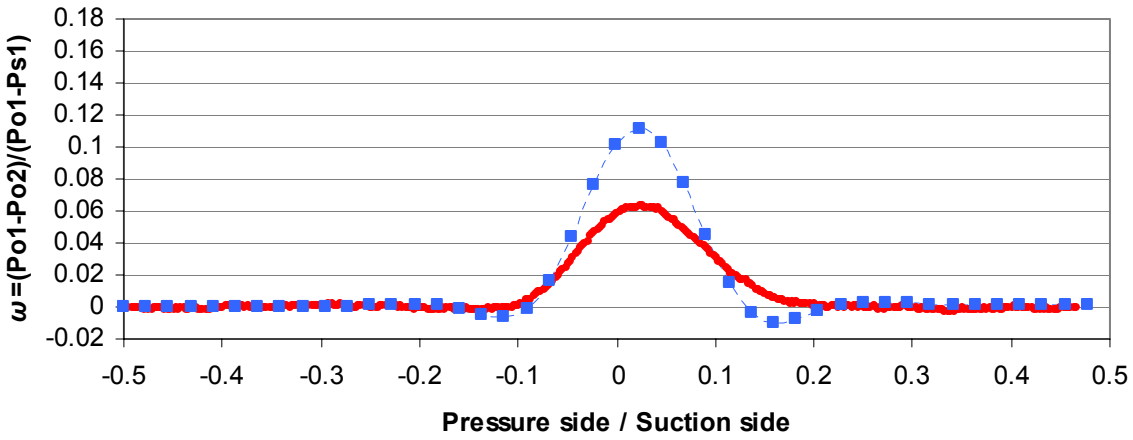

Figure B-7 CFD and experimental pressure loss for slot with 1.75% mass flow rate at 1.0 chords

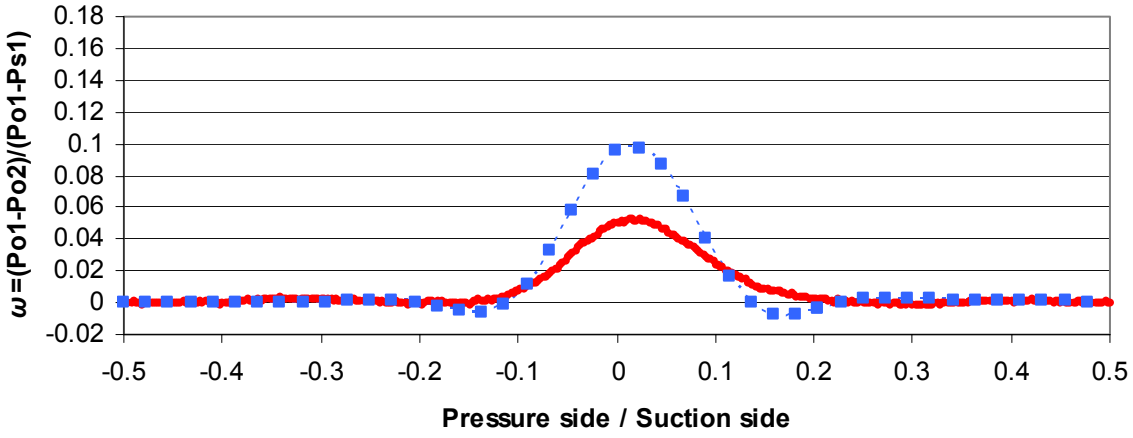

Figure B-8 CFD and experimental pressure loss for slot with 1.75% mass flow rate at 1.4 chords

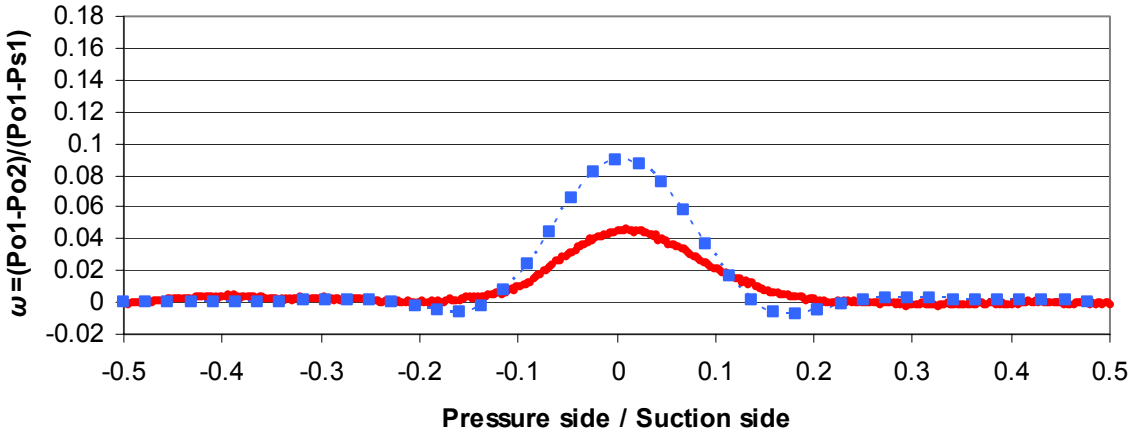

Figure B-9 CFD and experimental pressure loss for slot with 1.75% mass flow rate at 1.8 chords

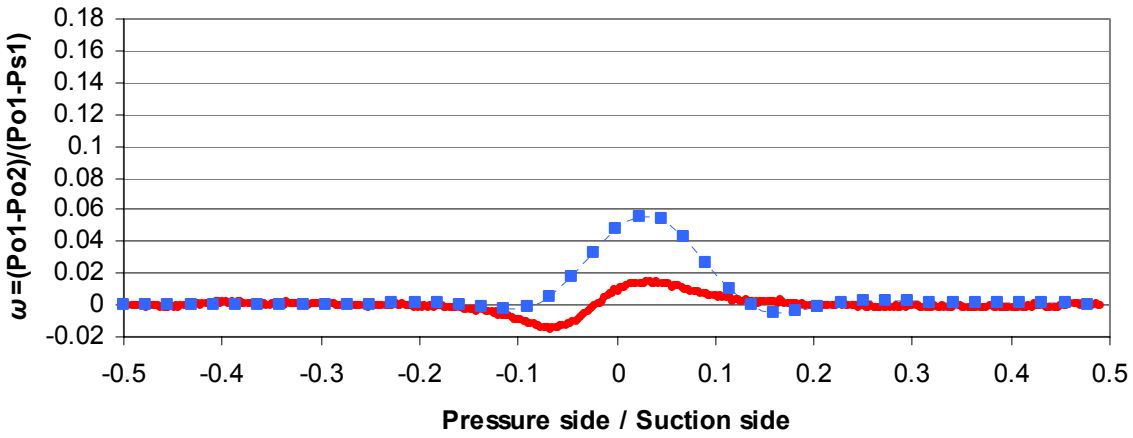

Figure B-10 CFD and experimental pressure loss for slot with 2.25% mass flow rate at 1.0 chords

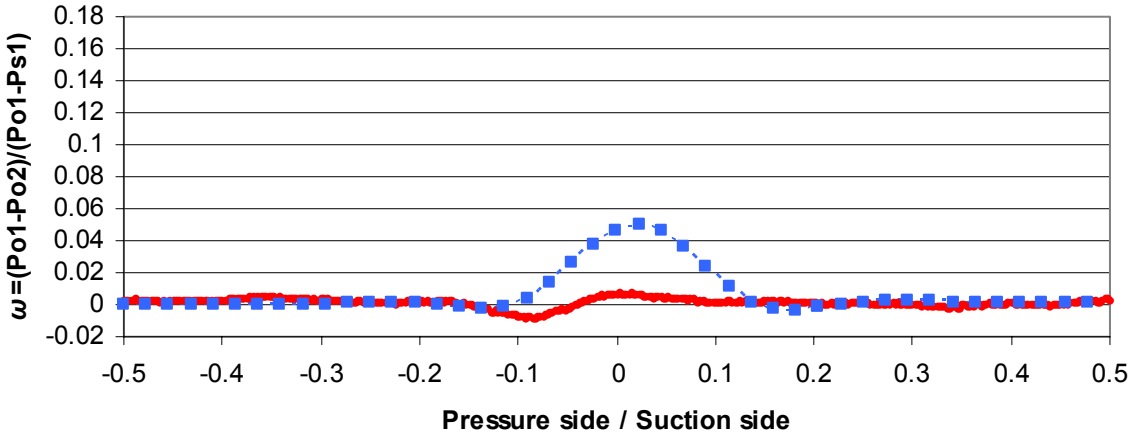

Figure B-11 CFD and experimental pressure loss for slot with 2.25% mass flow rate at 1.4 chords

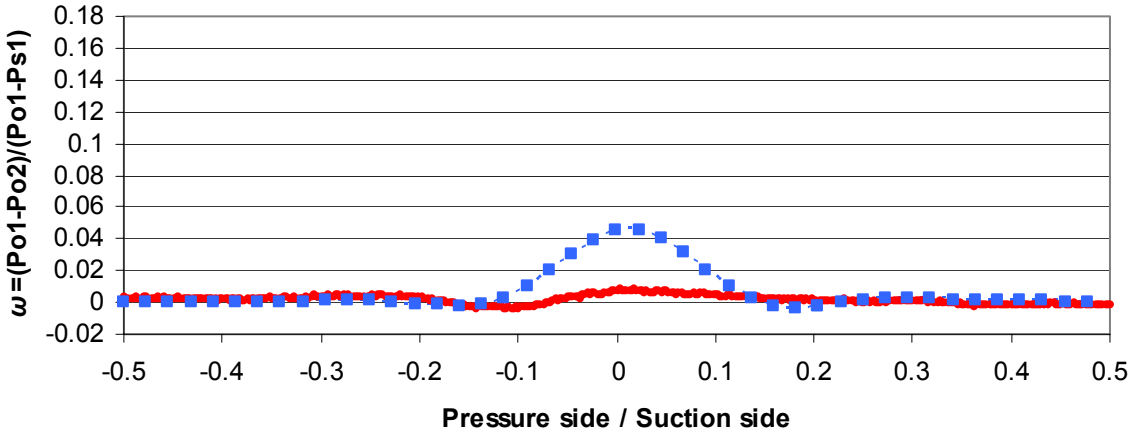

Figure B-12 CFD and experimental pressure loss for slot with 2.25% mass flow rate at 1.8 chords

The previous results display a lack of coincidence between the CFD and experimental results. The lack of conformity is especially evident in the 2.25% mass flow rate case (Figure B-10 through Figure B-12) where the experimental case displays an overblown wake profile and CFD does not. Also evident in all cases shown for the slot is that the CFD data shows a much deeper and narrower wake, whereas the experimental data displays a shallower and wider wake. Even though some difference between the cases is expected, this is not acceptable.

The difference between the cases can further be studied by observing the average wake pressure loss coefficient. These can be seen in Figure B-13, which shows the average loss coefficient versus downstream location. Under-prediction of losses by CFD is an accepted term of the technology and its current limitations. However, for the case shown, average loss coefficient plots show a trend of CFD over-predicting of losses as the mass flow through the slot is increased.

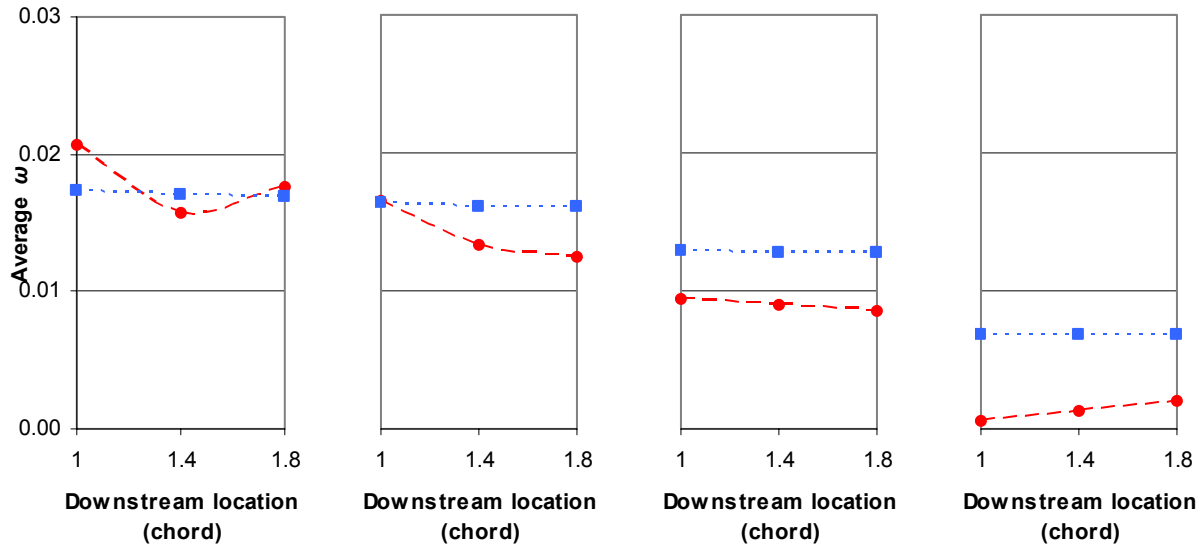

Figure B-13 Average pressure loss coefficient for slot shown at 0.75%, 1.25%, 1.75%, and 2.25% mass flow from left to right, respectively

This error and lack of coincidence can be explained by examining the interior of the blade. A sketch of the interior of the blade highlighting the flow control plenum is shown in Figure B-14. The sketch shows an accurate representation of the interior of the blade along the trailing edge with plenum areas and sealed passages shown.

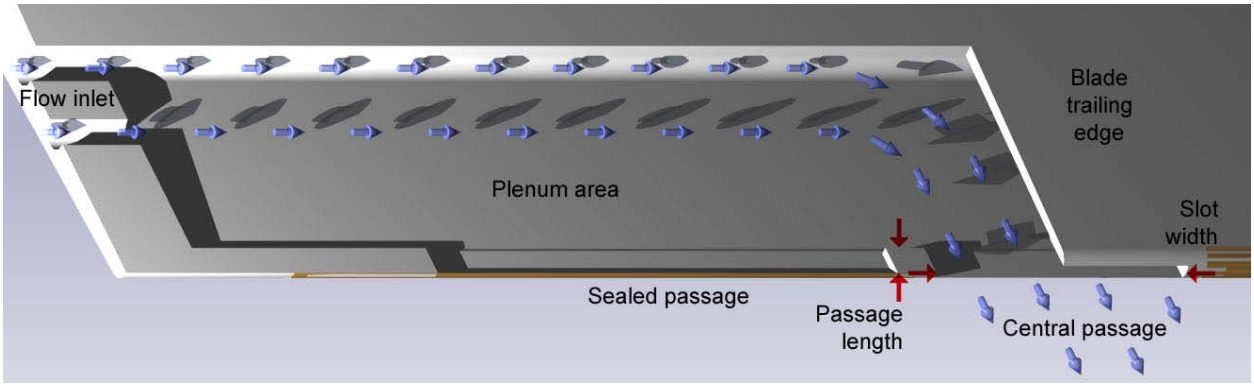

Figure B-14 Trailing edge of slot showing flow control plenum cross section

As seen in the previous sketch, a small passage length to slot width ratio is evident and is about 1:8; the passage is not long enough for straightening the slot's air flow through such a large opening. The plenum area also does little to hinder and settle the high speed flow entering the blade on both sides. This high speed flow will mix violently towards the center of the blade plenum assuming air is coming in at similar rates through all four flow control air supply inlets.

Since the internal geometry of the blade does not settle the flow entering the plenum, nor straighten it when coming out, it is probable that the flow is not exiting the slot uniformly in the span-wise direction. Regarding what was discussed previously concerning the slot experimental results, the flow is probably favoring the middle portion of the central passage creating a stronger flow through the center section. The occurring flow conditions are effectively creating a high pressure jet via the center of the slot. This would explain why the conditions seen during cascade testing performed better than what was seen from CFD. This would also explain why the lack of coincidence between CFD and experimental wakes worsens for higher pressure flows.

As seen in the results, disagreement between CFD and experimental increases with higher supply pressures. If what is speculated above is true, then this trend could be expected. Higher pressure supply flow will undergo less settling than lower pressure flows, thus any effects seen at low pressure will be further pronounced at higher pressures.

Despite similar plenum design, this effect will not manifest itself with discrete jet flow control, where the passage length to hole diameter ratio is at least 2:1. Due to the small sizes of the holes and the losses associated with them, the settling chamber will perform more adequately than it has for the slot case. This brings up an interesting point regarding the application of the slot configuration in a 3D and more realistic setting. As seen in studies by Brookfield and Waitz [2000], flow control passage design of a blade is an important aspect towards the applicability of a flow

control system. Properly designed passages will allow the flow control system to function correctly while providing little change to the blade untwist characteristics.

The opening created by the slot along the trailing edge greatly changes the structure for the blade, affecting the blade untwist characteristics. Because it requires large amounts of mass flow, the flow supply into the blade must have a large area or receive high pressure air, which must be settled and straightened in order to perform as designed. Because the trailing edge would present such a large opening, the air must be properly settled and straightened, or it will suffer from poor uniformity. As seen by Brookfield and Waitz, despite careful analysis and design of interior passages so that the flow control would create a momentumless wake, a momentumless wake was not achieved when tested.

Appendix C. TEJ Wake Data

The following section contains a wake based brief comparison between CFD and experimental results obtained for the TEJ flow control configuration. Note that for the following section, when comparing CFD and experimental data, CFD wake data is shown in blue squares and experimental wake data is shown in red circles.

The results from cascade testing plotted with corresponding CFD results for the pressure loss coefficient are presented next to show wake propagation for the TEJ. Pressure loss coefficient wakes for 0.50% fan though-flow are shown in Figure C-1 through Figure C-3. Figure C-4 through Figure C-6 show the wake propagation for 0.75%. Loss coefficient propagation at TEJ design is presented from Figure C-7 to Figure C-9. Lastly, Figure C-10 through Figure C-12 illustrate the spread of the wake with 1.25% fan through-flow. For all cases, the wakes are shown at 1.0, 1.4, and 1.8 chords downstream of the trailing edge.

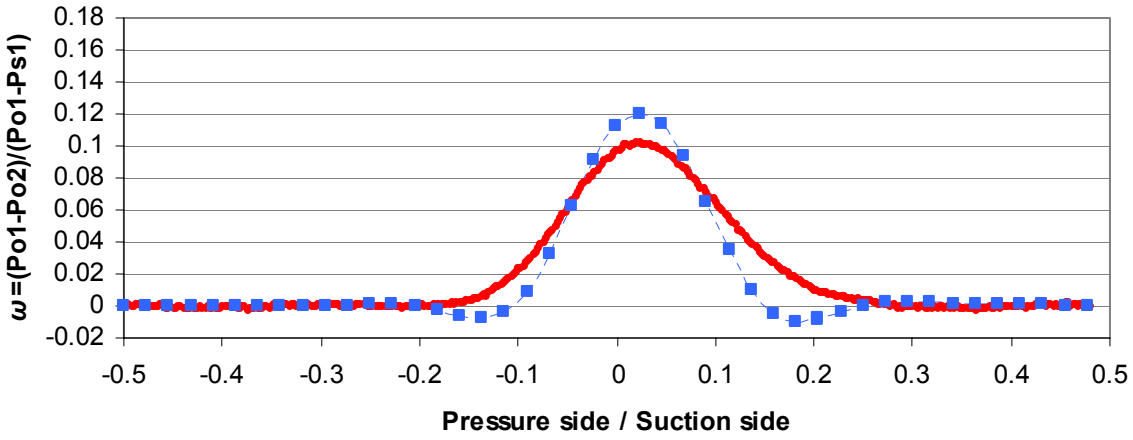

Figure C-1 CFD and experimental pressure loss for TEJ with 0.50% mass flow rate at 1.0 chords

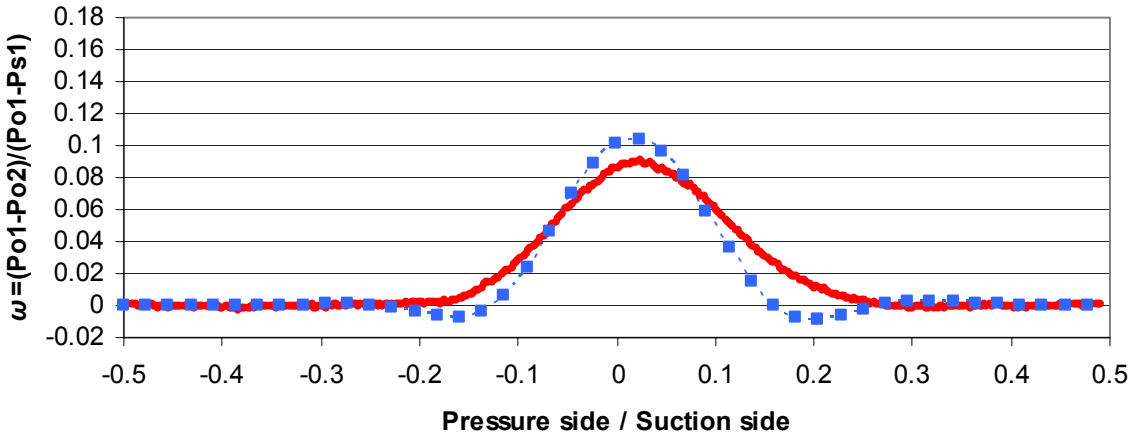

Figure C-2 CFD and experimental pressure loss for TEJ with 0.50% mass flow rate at 1.4 chords

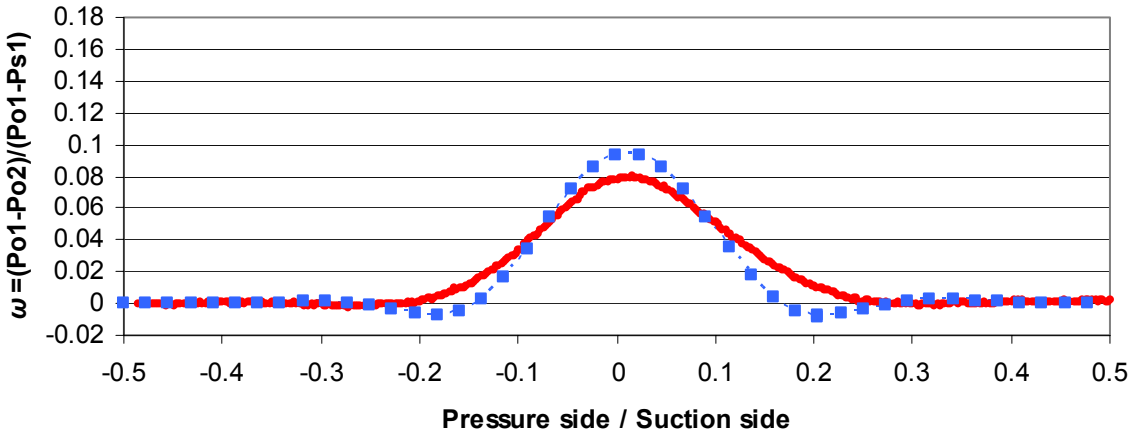

Figure C-3 CFD and experimental pressure loss for TEJ with 0.50% mass flow rate at 1.8 chords

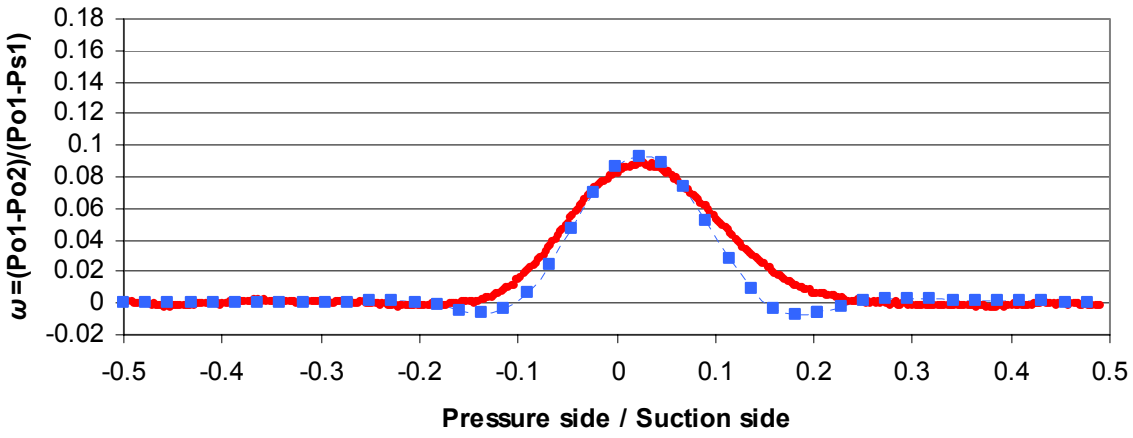

Figure C-4 CFD and experimental pressure loss for TEJ with 0.75% mass flow rate at 1.0 chords

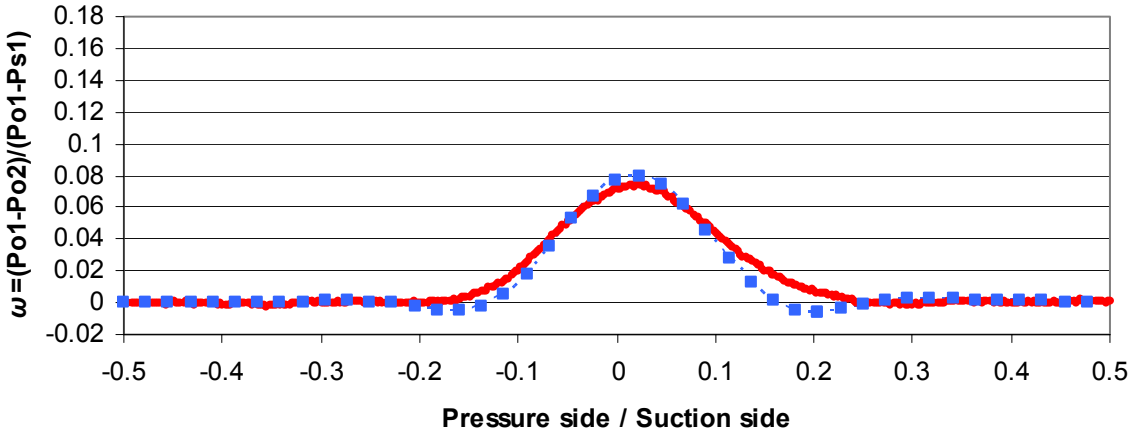

Figure C-5 CFD and experimental pressure loss for TEJ with 0.75% mass flow rate at 1.4 chords

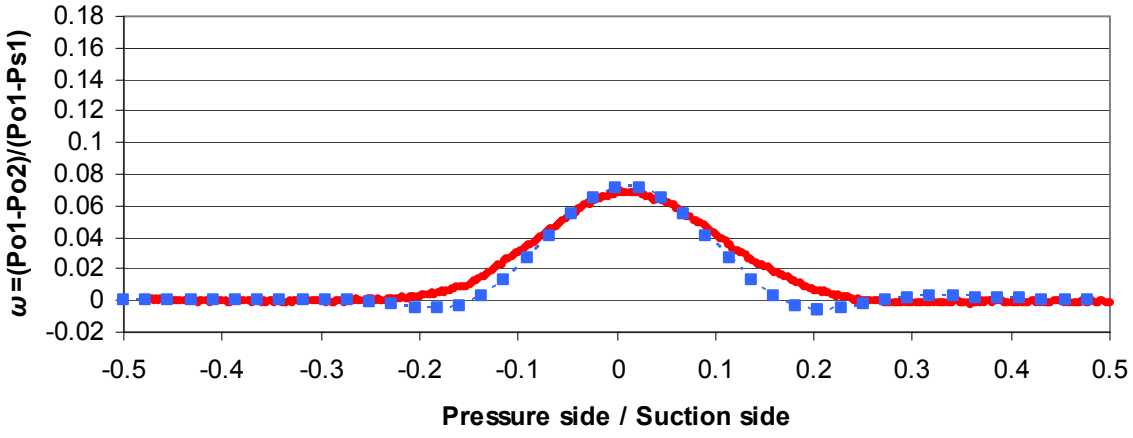

Figure C-6 CFD and experimental pressure loss for TEJ with 0.75% mass flow rate at 1.8 chords

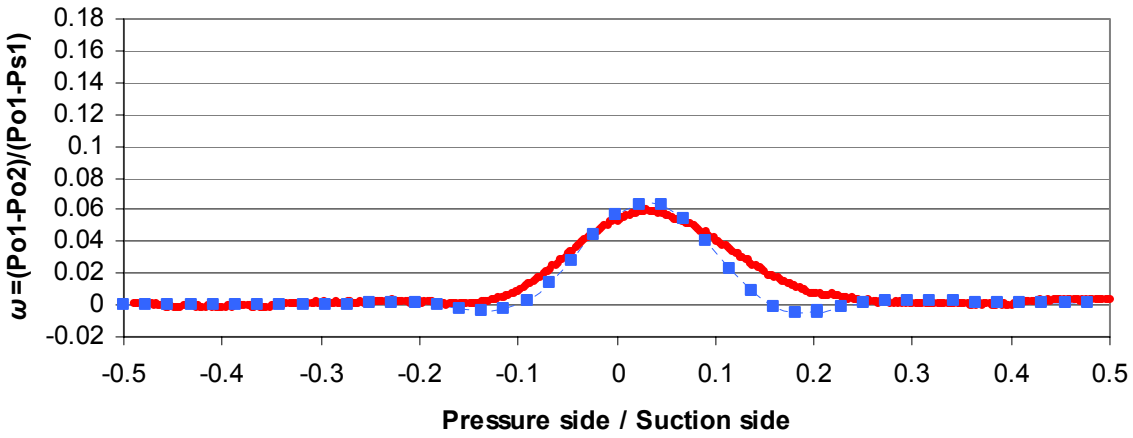

Figure C-7 CFD and experimental pressure loss for TEJ with 1.00% mass flow rate at 1.0 chords

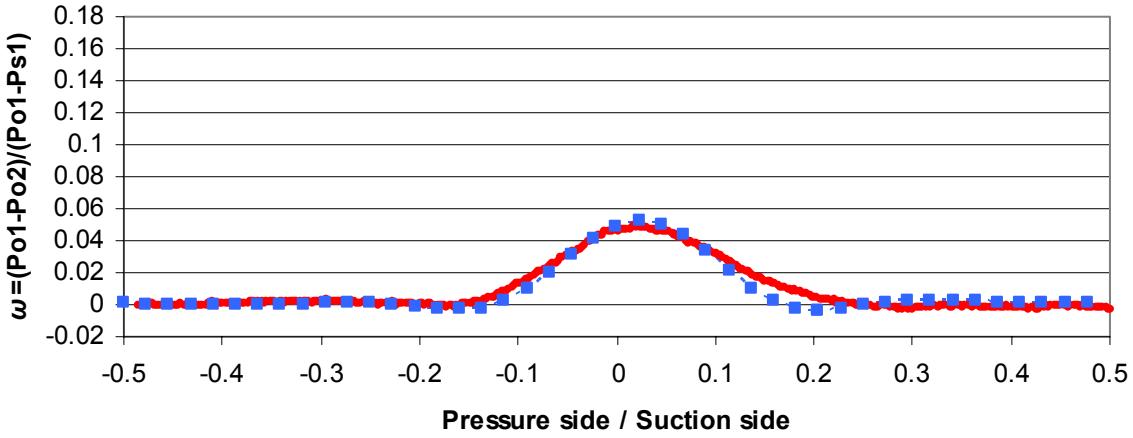

Figure C-8 CFD and experimental pressure loss for TEJ with 1.00% mass flow rate at 1.4 chords

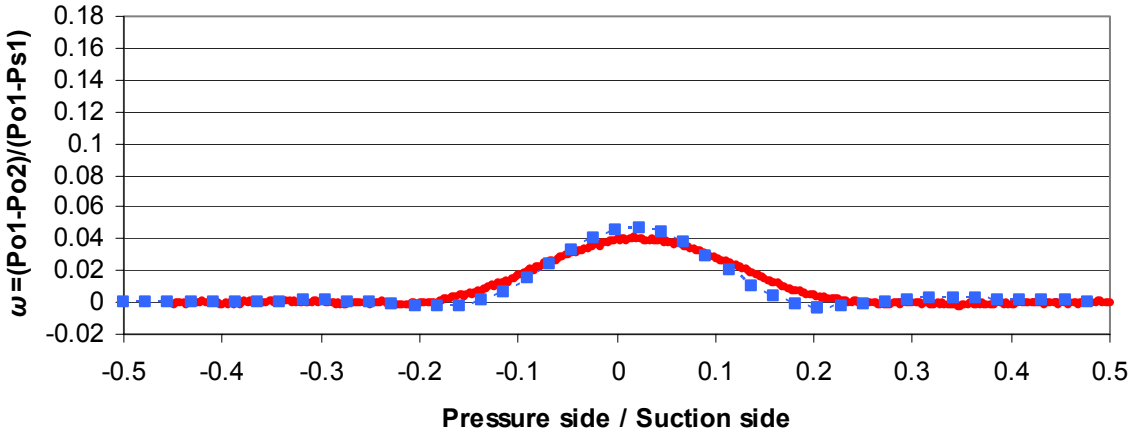

Figure C-9 CFD and experimental pressure loss for TEJ with 1.00% mass flow rate at 1.8 chords

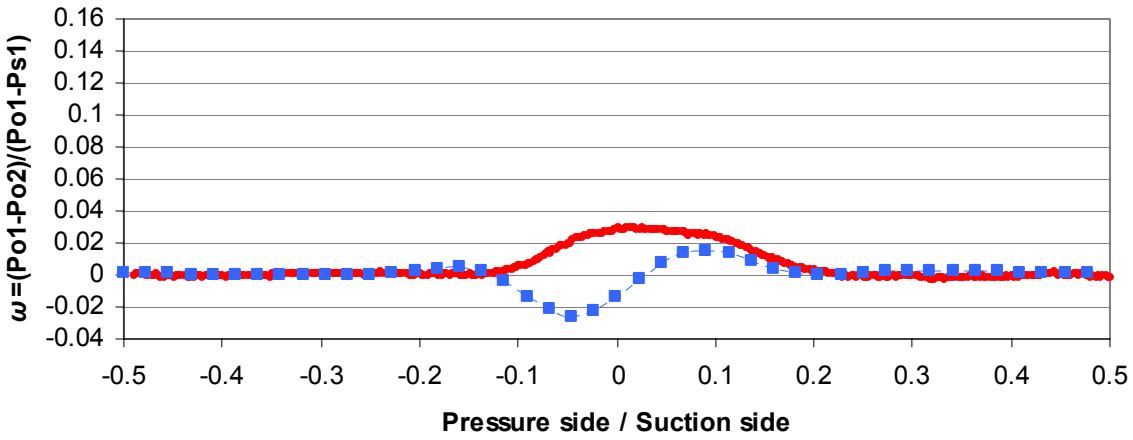

Figure C-10 CFD and experimental pressure loss for TEJ with 1.25% mass flow rate at 1.0 chords

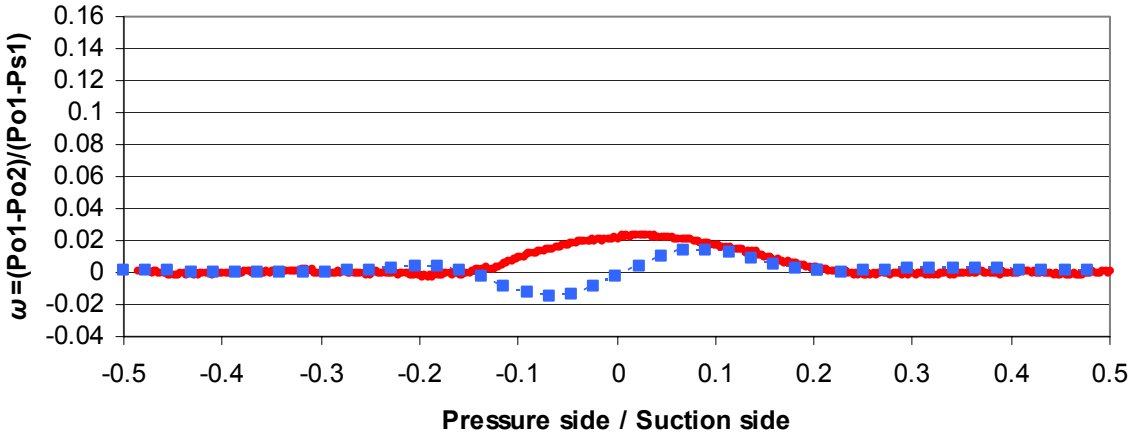

Figure C-11 CFD and experimental pressure loss for TEJ with 1.25% mass flow rate at 1.4 chords

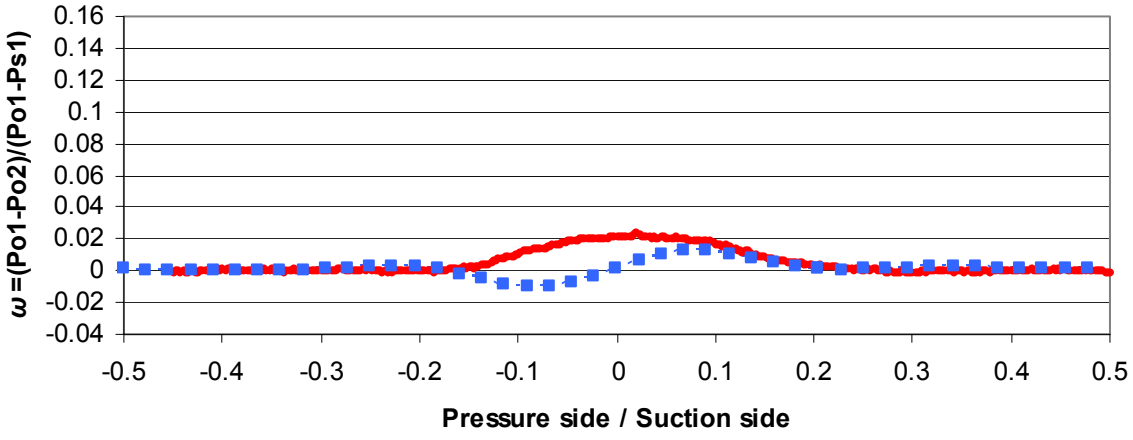

Figure C-12 CFD and experimental pressure loss for TEJ with 1.25% mass flow rate at 1.8 chords

Unlike the comparison of Slot experiment to CFD, the TEJ displayed excellent coincidence between the two cases, with the TEJ at 1.25% showing the largest deviation. Experimental wakes tend to be a little shallower and wider than CFD wakes.

An explanation for the discrepancy of the 1.25% case can be addressed by considering the total pressure within the tubing necessary to produce the fan through-flow rate. Unlike the slot case, where the maximum total pressure used to produce 2.25% mass flow rate was 40 psig, an air supply total pressure of 80 psig was required to produce 1.25% mass flow rate for the TEJ. A leak in the tubing under higher pressures may explain why the 1.25% case differs more greatly from CFD than the other TEJ cases studied. When testing was conducted, leakage was known to be present within the flow control system near the blade air supply flow inlet tubes. Little could be done during the test period to rid the system from leakage. Steps were taken to reduce leakage, but at total pressures above those required by 1.00% mass flow rate, ~65 psig, there was some audible leakage in the system (while the wind tunnel was not running). This problem was rectified when testing was conducted with the SSJ.

It can be concluded from the data gathered that the jet is affecting the middle portion of the wake primarily, bringing in slower moving flow towards the middle to fill in the high energy zone created by the TEJ. Because the jets are discrete holes, the high energy flow pulls lower energy flow towards itself more efficiently than the slot, creating a three-dimensional, viscous ramp that surrounds the jet. This allows the jet to quickly energize surrounding flow near the trailing edge while mixing rapidly into the surrounding flow. This yields a shallower and wider wake than with the slot, which unintentionally maintains a two-dimensional flow with little mixing.

Appendix D. SSJ Wake Data

The following section contains a wake based brief comparison between CFD and experimental results obtained for the SSJ flow control configuration. Note that for the following section, when comparing CFD and experimental data, CFD wake data is shown in blue squares and experimental wake data is shown in red circles.

Pressure loss coefficients from cascade testing are shown plotted against corresponding CFD results are presented on the following pages. It should be noted that the SSJ were tested at a later date after initial bench testing showed that the first set of blades suffered from a flow control manufacturing flaw. This change in test date shows up as small differences seen in freestream values between these cases and the previously presented ones (average pressure losses will be slightly greater for these cases). Wake propagation for fan-through flow of 0.50% is shown from Figure D-1 to Figure D-3. Pressure loss coefficients from 0.75% are plotted in Figure D-4 through Figure D-6. Figure D-7 through Figure D-9 display the results for mass flow rate of 1.00%. And Figure D-10 through Figure D-12 present the pressure loss coefficients for the 1.25% case. For all cases, the wakes are shown at 1.0, 1.4, and 1.8 chords downstream of the trailing edge.

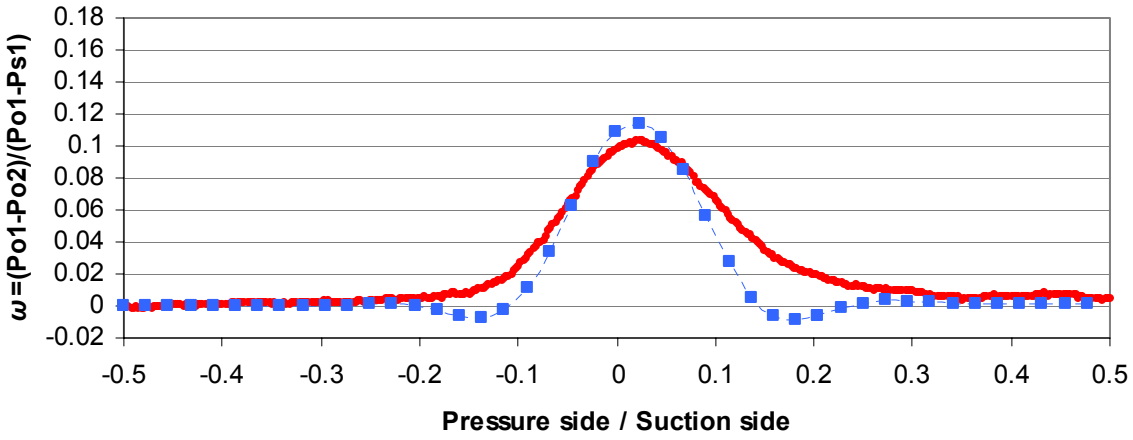

Figure D-1 CFD and experimental pressure loss for SSJ with 0.50% mass flow rate at 1.0 chords

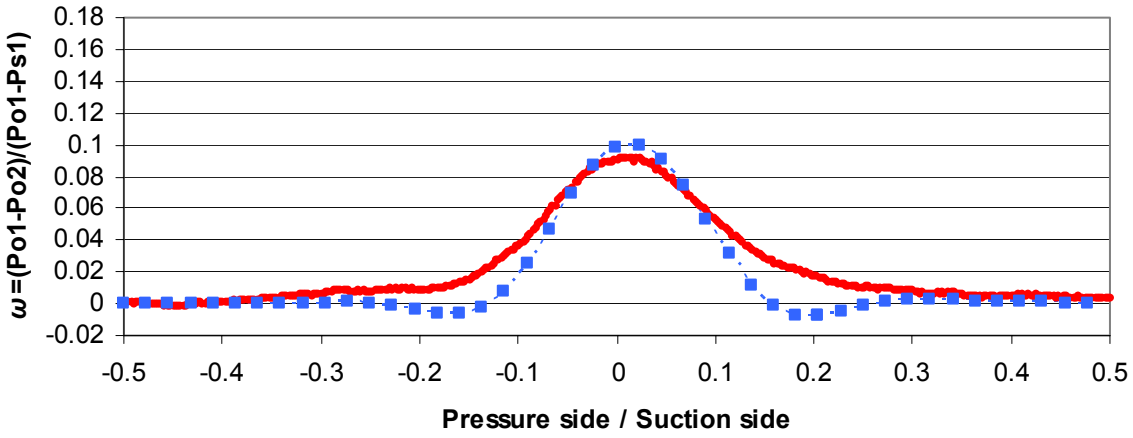

Figure D-2 CFD and experimental pressure loss for SSJ with 0.50% mass flow rate at 1.4 chords

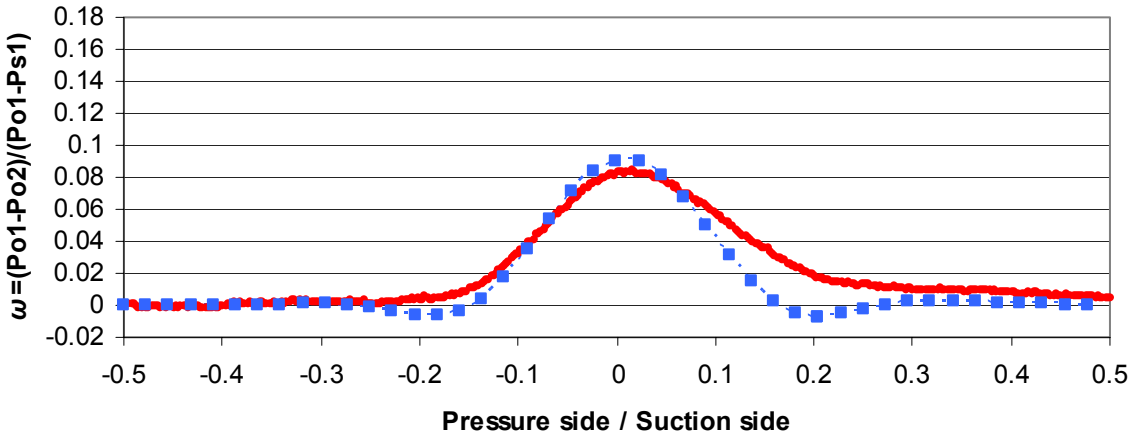

Figure D-3 CFD and experimental pressure loss for SSJ with 0.50% mass flow rate at 1.8 chords

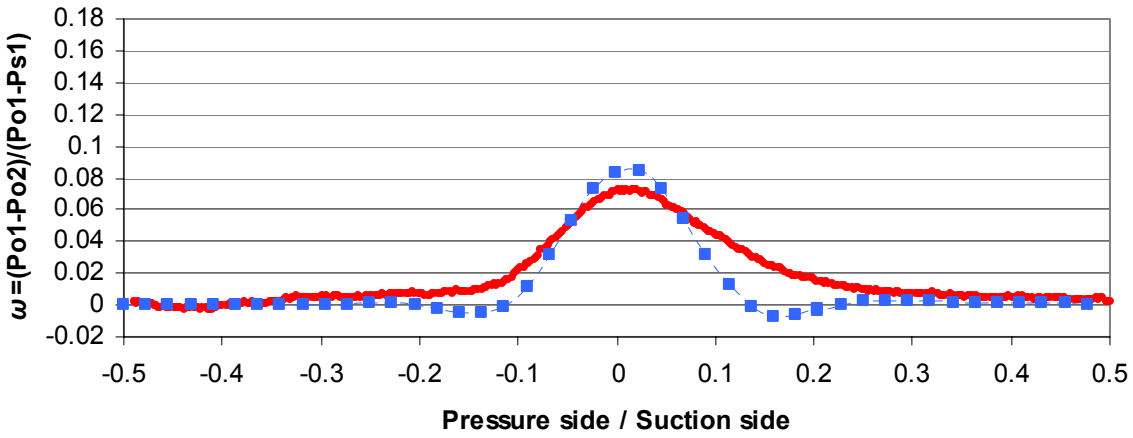

Figure D-4 CFD and experimental pressure loss for SSJ with 0.75% mass flow rate at 1.0 chords

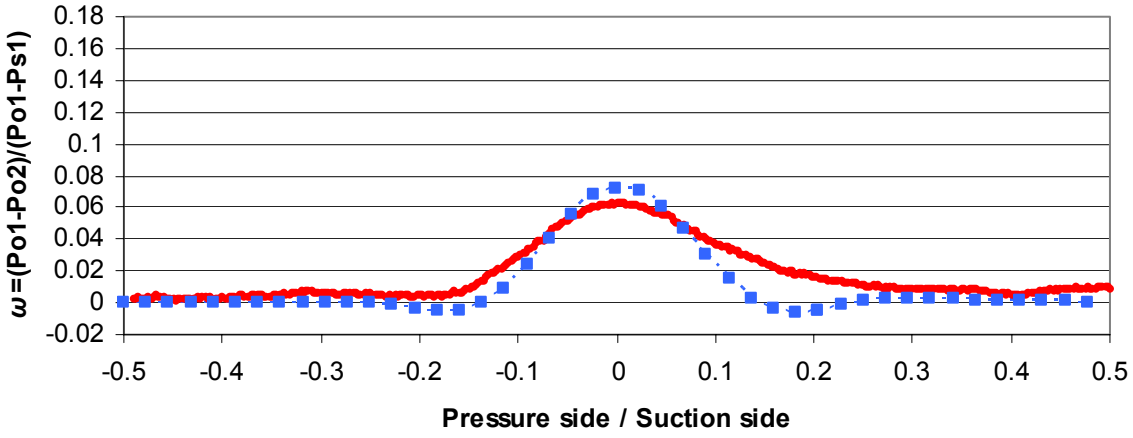

Figure D-5 CFD and experimental pressure loss for SSJ with 0.75% mass flow rate at 1.4 chords

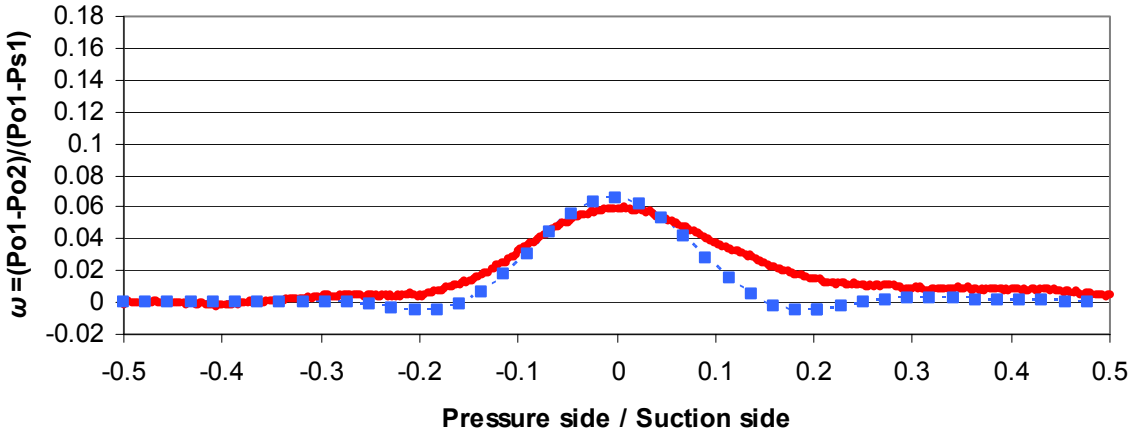

Figure D-6 CFD and experimental pressure loss for SSJ with 0.75% mass flow rate at 1.8 chords

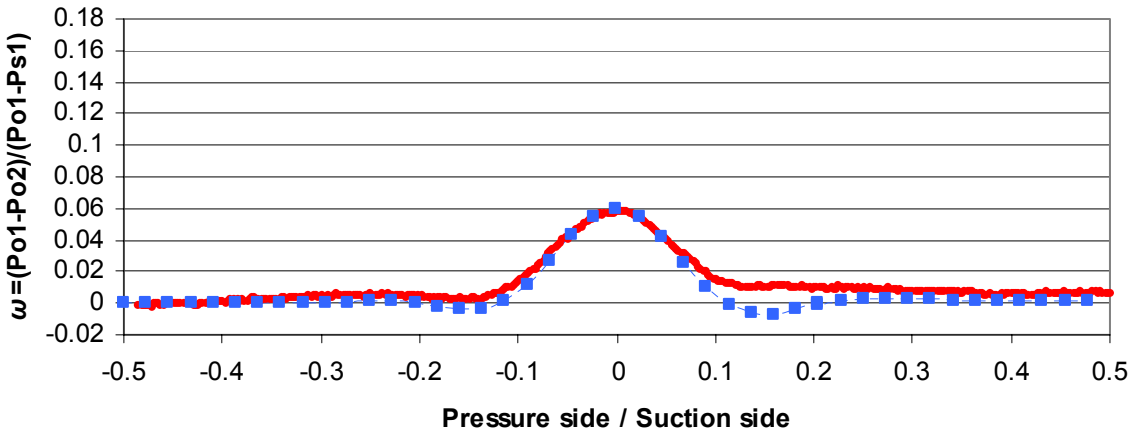

Figure D-7 CFD and experimental pressure loss for SSJ with 1.00% mass flow rate at 1.0 chords

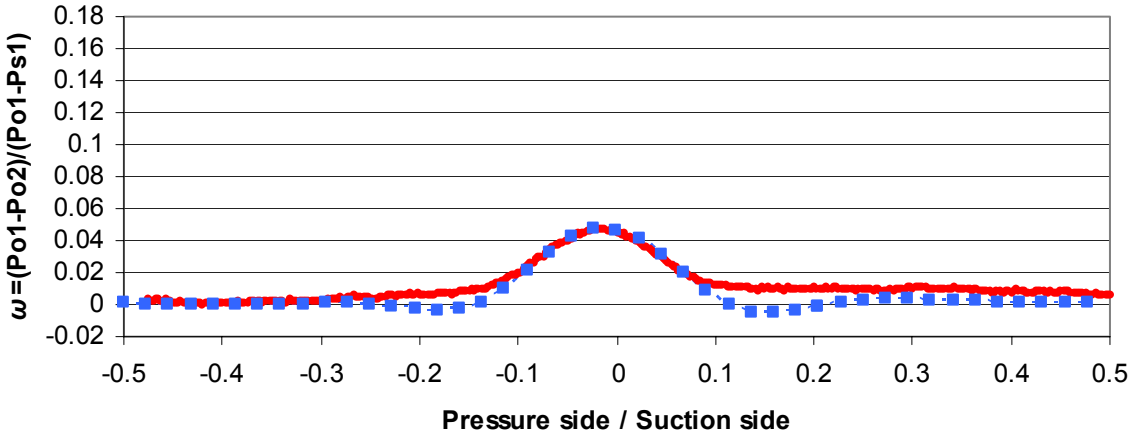

Figure D-8 CFD and experimental pressure loss for SSJ with 1.00% mass flow rate at 1.4 chords

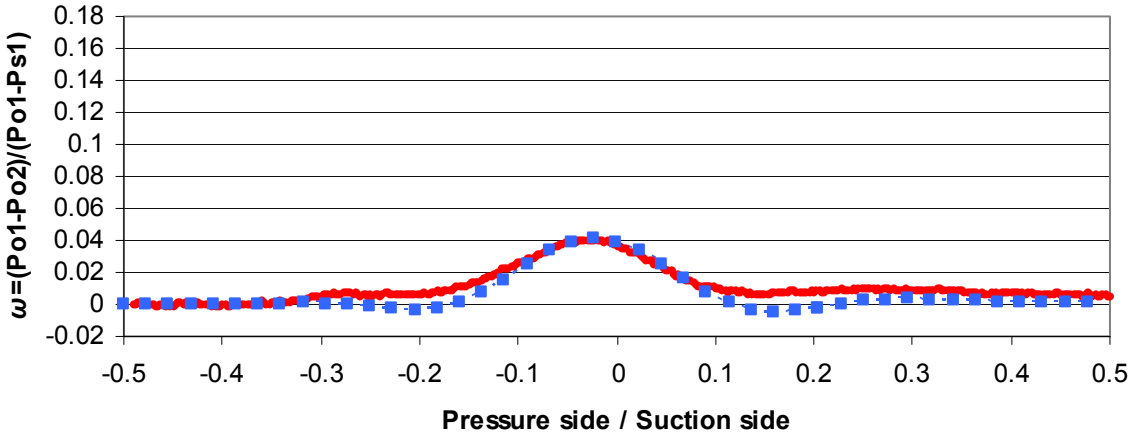

Figure D-9 CFD and experimental pressure loss for SSJ with 1.00% mass flow rate at 1.8 chords

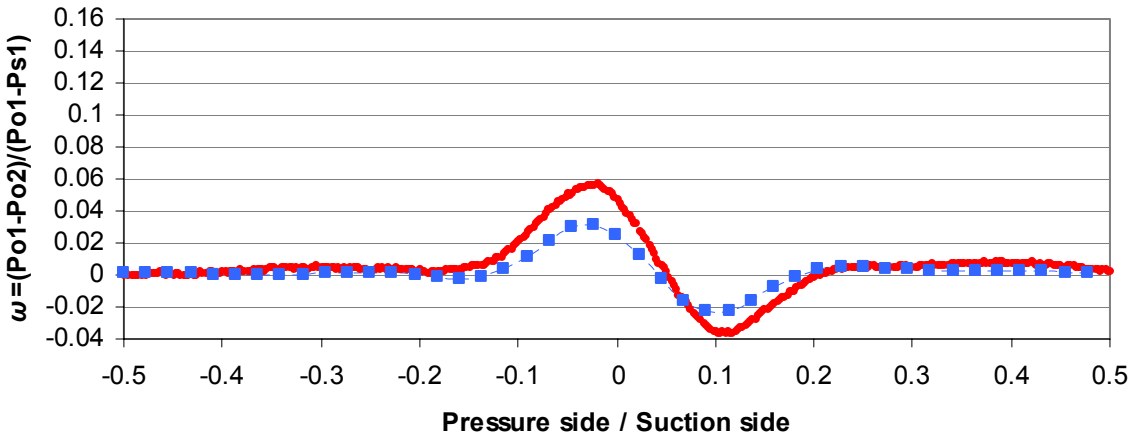

Figure D-10 CFD and experimental pressure loss for SSJ with 1.25% mass flow rate at 1.0 chords

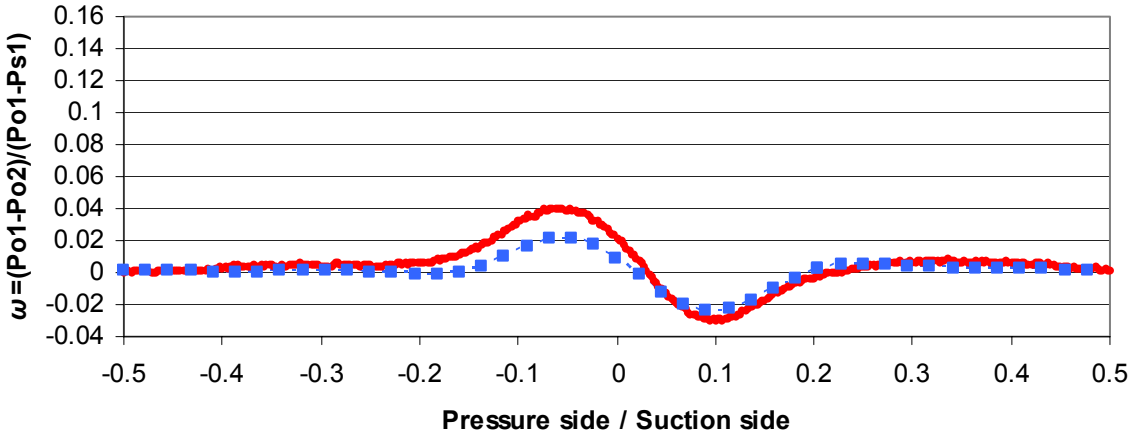

Figure D-11 CFD and experimental pressure loss for SSJ with 1.25% mass flow rate at 1.4 chords

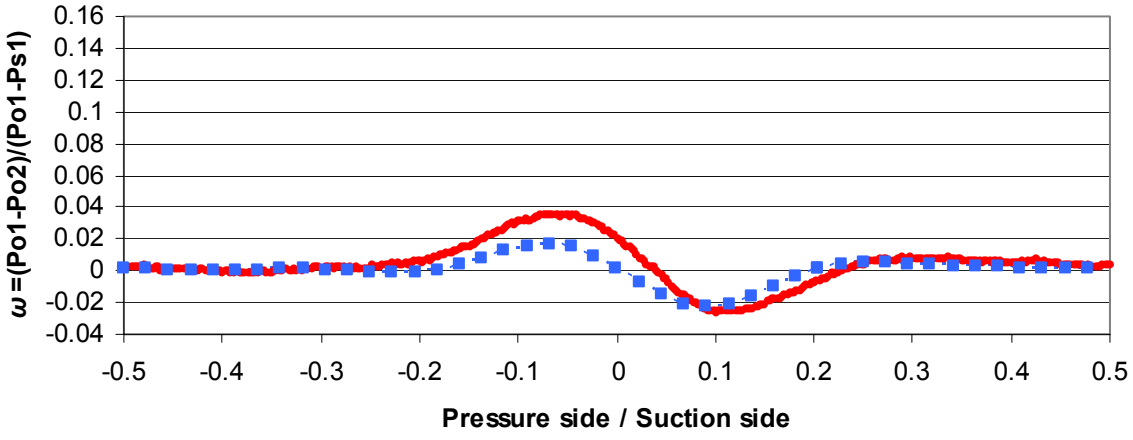

Figure D-12 CFD and experimental pressure loss for SSJ with 1.25% mass flow rate at 1.8 chords

Appendix E. Vortex Generating Jets

The results of the Vortex Generating Jets are presented in this section. As mentioned in section 2.2, more complex flow control configurations were modeled after the study of the SSJ was conducted. These designs implemented variations in pitch and span angles in order to induce additional mixing while still attempting to energize the surrounding fluid. Although CFD modeling did not yield the desired results instead creating wakes worse than those seen with the solid blade, it was decided to test one VGJ configuration in order to further validate CFD. Shown first are CFD results for various configurations attempted, followed by experimental results of a chosen design.

E.1 CFD Results

After SSJ modeling in CFD was completed, the use of angles into the span was attempted. The purpose of this effort was to increase mixing and subsequently increase the width of the wake while still providing the addition of high energy fluid into the retarded boundary layer flow. As such, VGJ were modeled using a variety of span and pitch angles along with different flow rates and hole diameters. Total pressure contours normalized by free stream total pressure of some of these conceptual configurations are shown in Figure E-1. All of the cases shown use the same hole diameter and spacing as the final design of SSJ and TEJ. All of these VGJ were centered at 95.5% span. The large difference between the cases lies in the angles used and the flow rates implemented.

When compared to the SSJ and solid blade cases, it can be stated that changes in angle into the span create additional losses on the flow conditions. No matter the angle chosen, losses were increased considering that at this stage the VGJ are a manipulation of the SSJ into different angles. None of the cases behave better than the SSJ. Some of them behave worse than solid blade. Not only do the VGJ shown here fail to vastly improve flow from conditions already tested, but they also fail to increase the width of the wake by any significant means. The only case that shows a significant increase in the wake width is the case using 90° angle into the span and 30° of pitch angle at 0.34% fan through flow. This case, however, produces a wake much larger than the solid blade.

Following these VGJ configurations, another attempt was made using smaller diameter holes and shifting the location of the holes further upstream. Despite CFD modeling showing that the case would not offer any performance improvement over solid blade, this configuration was chosen for testing in the wind tunnel and is highlighted in the following section.

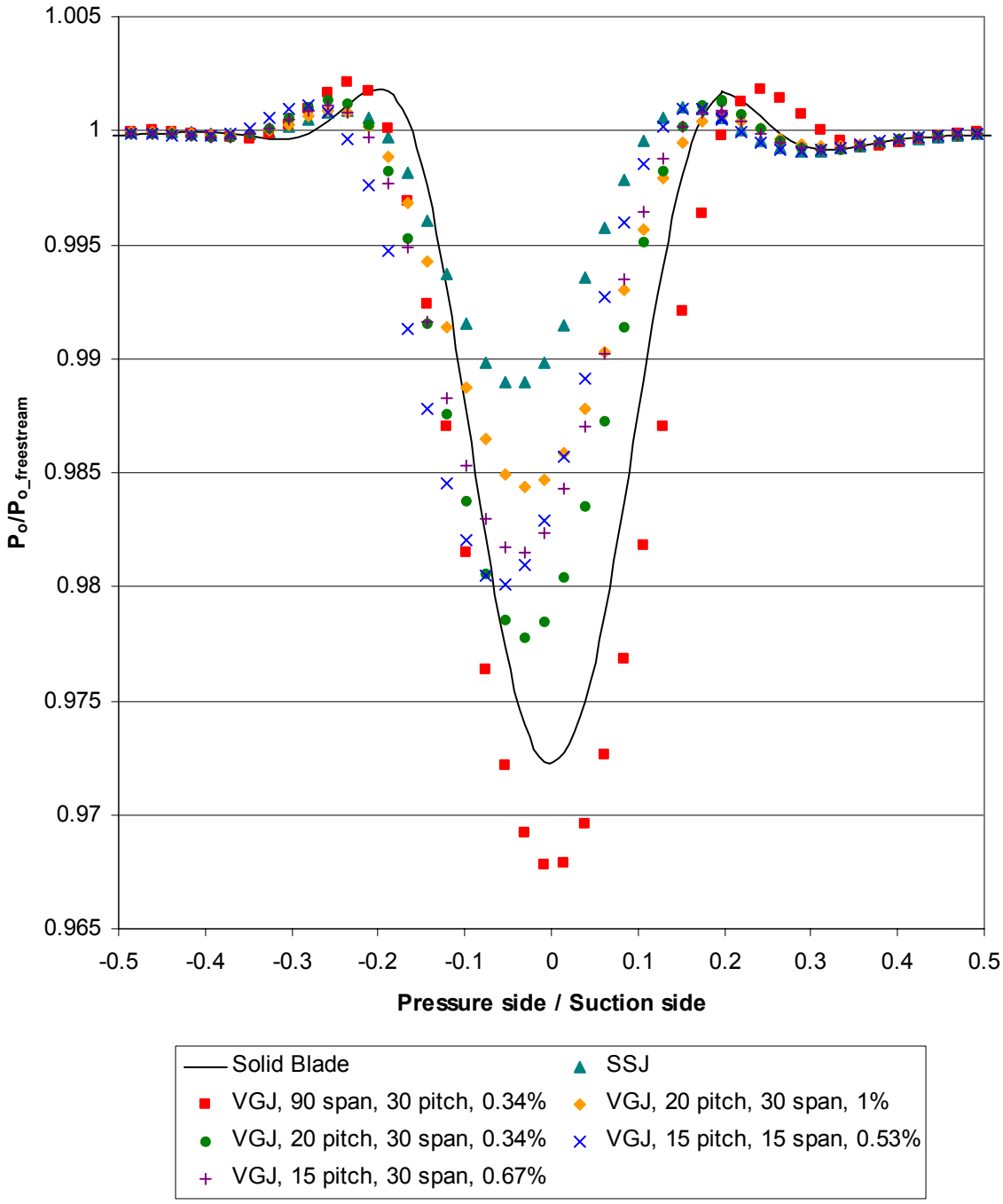

Figure E-1 Normalized total pressure wakes for various VGJ configurations compared to solid blade and SSJ

E.2 Experimental Results

The design chosen for testing consisted of a jet aimed 25° from the blade surface and 45° into the span. Unlike previous cases, a smaller diameter jet size of 0.02 inches was chosen, due to the nature of the VGJ. Larger jet sizes would increase viscous drag created by the flow control fluid.

The jets were spaced 0.3 inches apart and located at 90% chord. The blade manufactured for testing is shown below in Figure E-2 with ten jets made to the previous specifications.

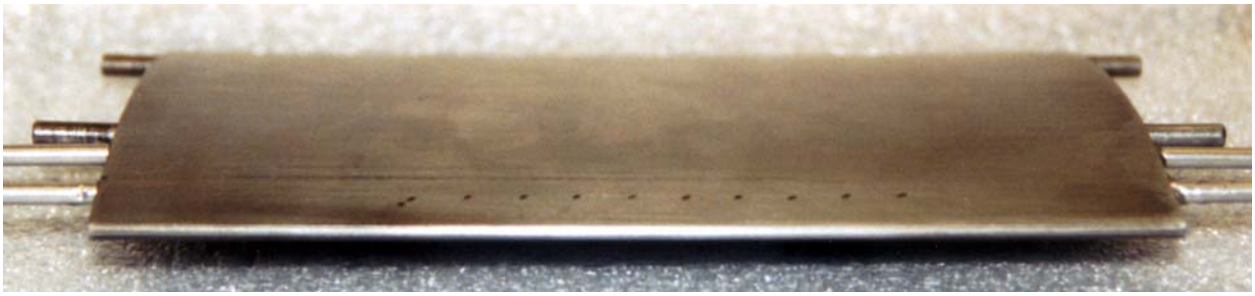

Figure E-2 Photograph of blade used for testing with VGJ

Results obtained from the VGJ in the wind tunnel experiments are shown below. However, unlike with previous flow control configurations, the experimental results will not be compared to CFD pressure loss coefficient, because that is not the most relevant conclusion. Instead, the VGJ are compared in this section to the solid blade. The solid blade results are shown in black and the VGJ is represented in a thicker green line. Figure E-3 to Figure E-5 show the VGJ operating with 0.30% of the fan though flow. The VGJ test results at 0.50% fan through flow are shown in Figure E-6 to Figure E-8.

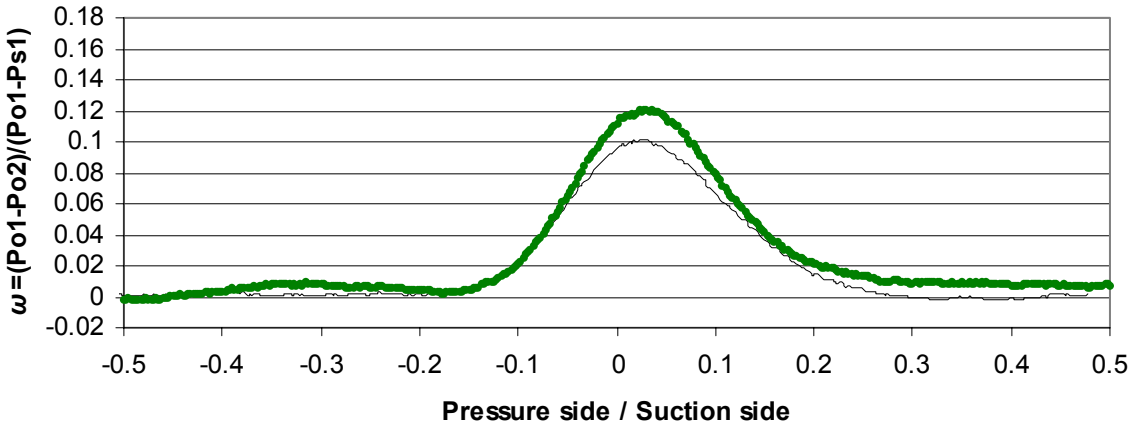

Figure E-3 Pressure loss for solid blade and VGJ with 0.30% mass flow rate at 1.0 chords

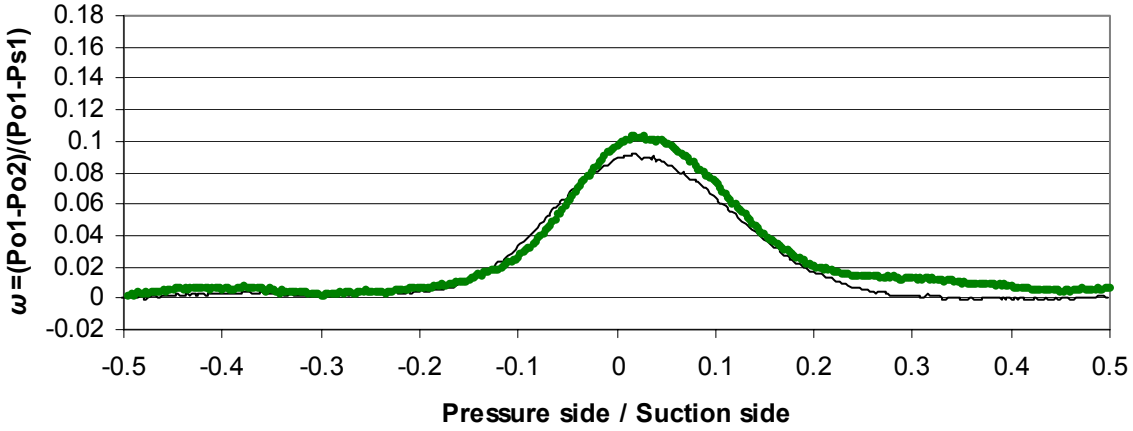

Figure E-4 Pressure loss for solid blade and VGJ with 0.30% mass flow rate at 1.4 chords

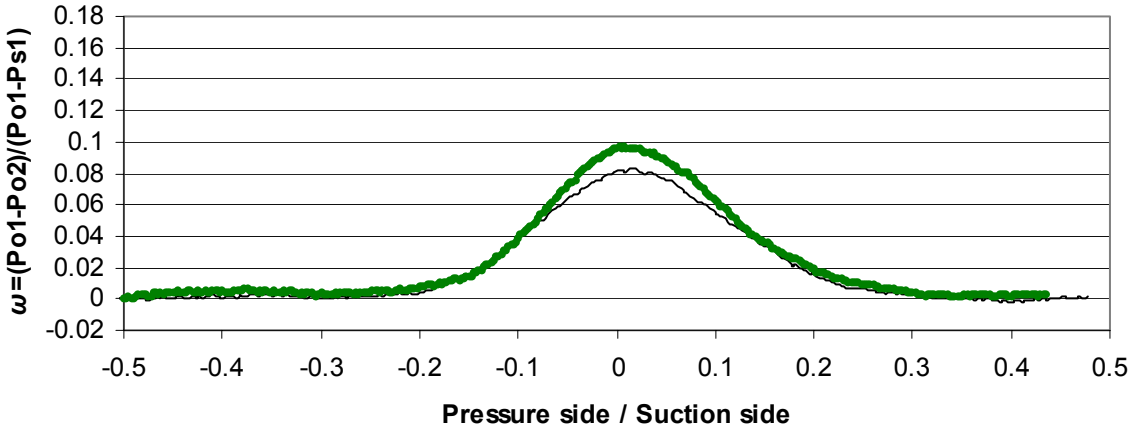

Figure E-5 Pressure loss for solid blade and VGJ with 0.30% mass flow rate at 1.8 chords

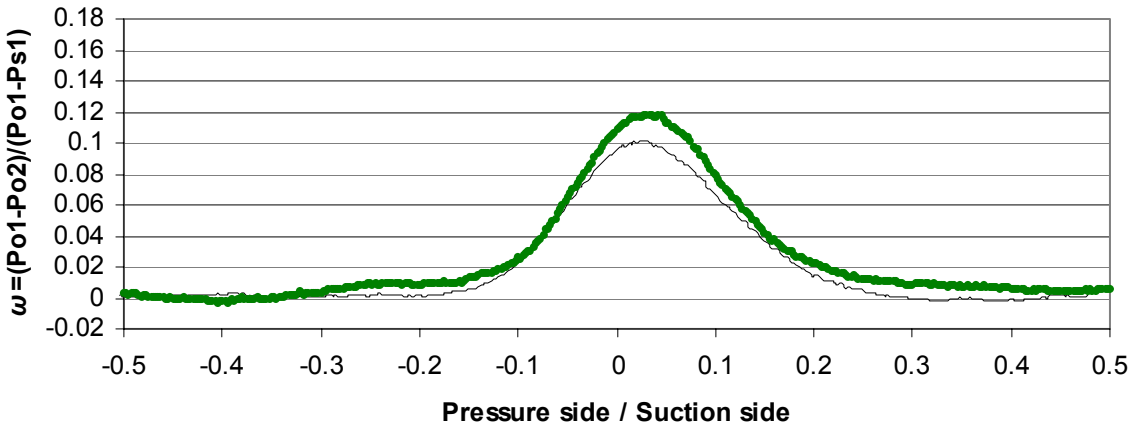

Figure E-6 Pressure loss for solid blade and VGJ with 0.50% mass flow rate at 1.0 chords

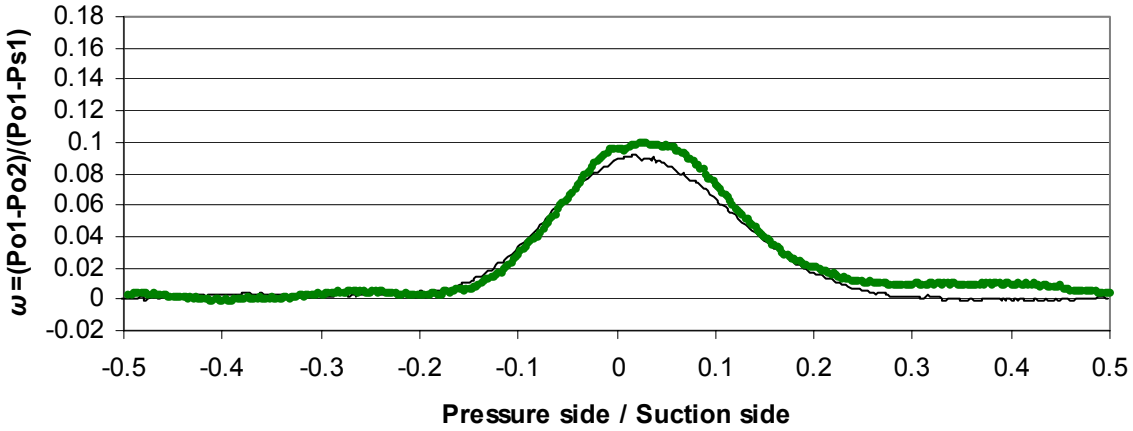

Figure E-7 Pressure loss for solid blade and VGJ with 0.50% mass flow rate at 1.4 chords

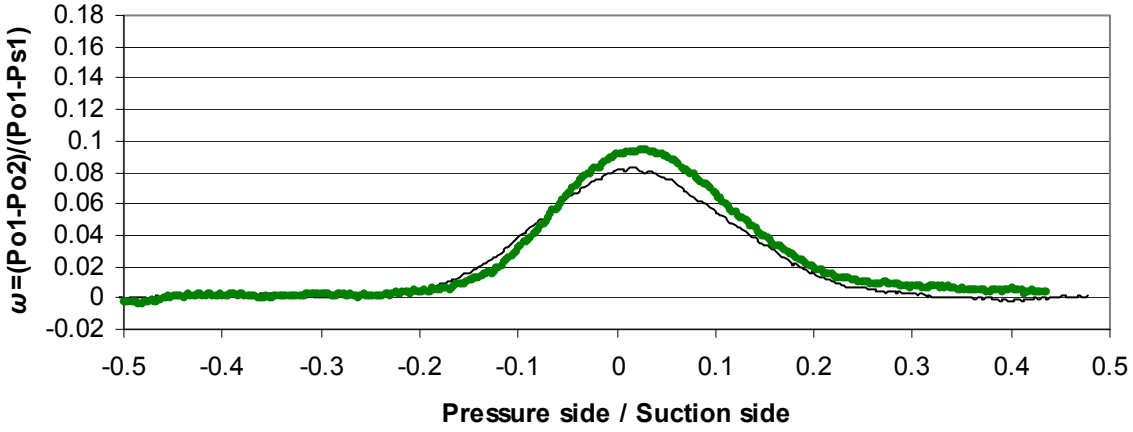

Figure E-8 Pressure loss for solid blade and VGJ with 0.50% mass flow rate at 1.8 chords

It had been thought that perhaps CFD had not managed to capture accurately the mixing generated by the complex flow of the VGJ and that perhaps the VGJ would yield better results in the wind tunnel. That was obviously not the case. From the results it can be easily seen that the VGJ performed worse than baseline, creating deeper wakes and increasing losses. Losses were increased by approximately 25%. There is little evidence of a large increase in mixing since the wake width does not propagate much in the same way that baseline does. In fact, wake width does not increase much more from baseline. A shift in the wake towards the suction surface shows that the VGJ are generating additional losses on the suction surface.

If VGJ have been a proven method of generating additional mixing and preventing separation in certain applications, particularly in LPT, why didn't they work for this blade at least producing a wider wake or additional mixing?

> "[VGJ rely] …on vortices to mix high-energy fluid from the freestream with the retarded fluid in the outer region of the boundary layer. Using this technique shock induced boundary layer separation can be suppressed at the cost of a viscous drag penalty" (Qin, et al, 2000)

Thus, VGJ have proven to be successful at preventing separation on high-turning LPT surfaces. However, in the case of the blade studied, separation control was not an issue. It was hoped that the mixing caused by the VGJ would outweigh the viscous drag penalty, but that was not the case.

Appendix F. Solid Blade Comparison

The performance of the flow control is not the only point that needs to be considered when implementing flow control. Another aspect considered is whether or not the blade still behaves like the solid blade when the flow control is disabled. This is a desirable aspect, because the use of flow control for fan noise reduction will not be needed for the entire operating range of the turbofan engine, for example at cruise altitudes. Thus, it is important that the blade not suffer large performance penalties due to the addition of flow control.

Each of the blades tested in the wind tunnel were also assessed without the use of flow control in order to compare performance to that of a solid blade. These solid blade comparisons were not performed using a range of operating conditions since this was not the primary focus of this study. Nevertheless, this test was performed for a preliminary evaluation of the performance of the flow controlled blades compared to the solid blade.

A comparison of the pressure loss coefficient for the solid and flow control blades is shown at two downstream locations. The first, Figure F-1, is of all four blades at 1.0 chord downstream of the trailing edge of the blade. The second, Figure F-2, is at 1.8 chords downstream.

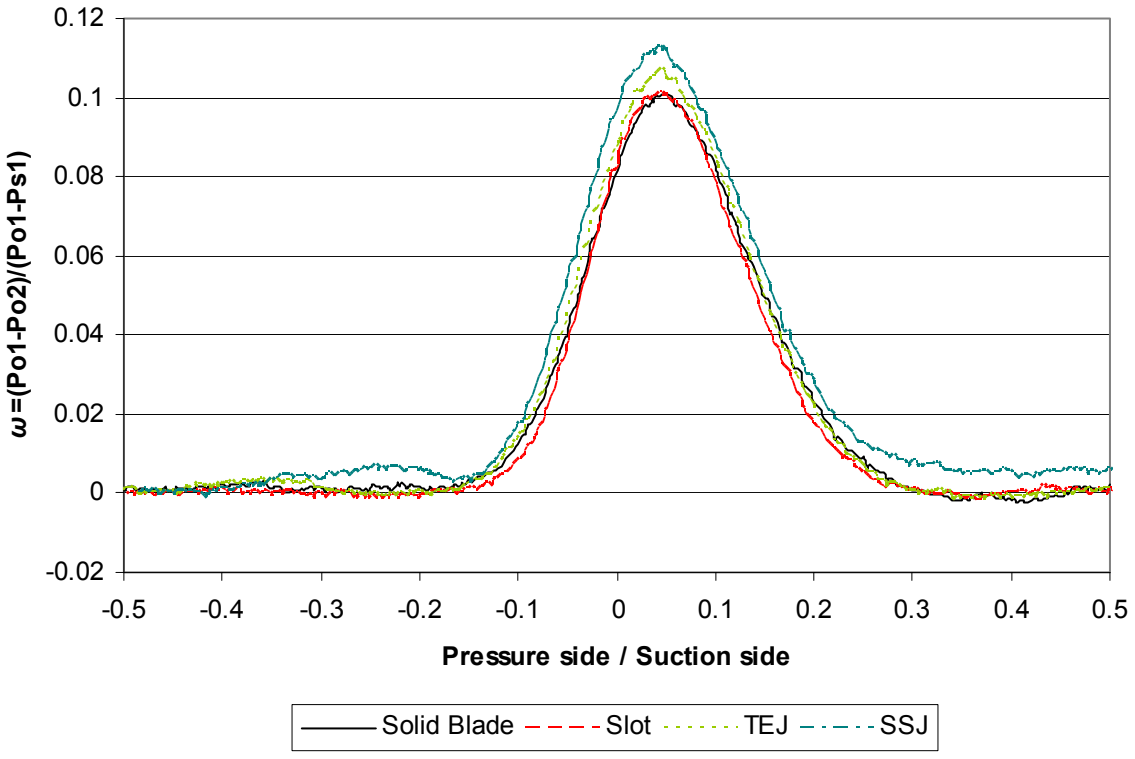

Figure F-1 Solid blade comparison to flow control blade with no flow at 1.0 chords downstream

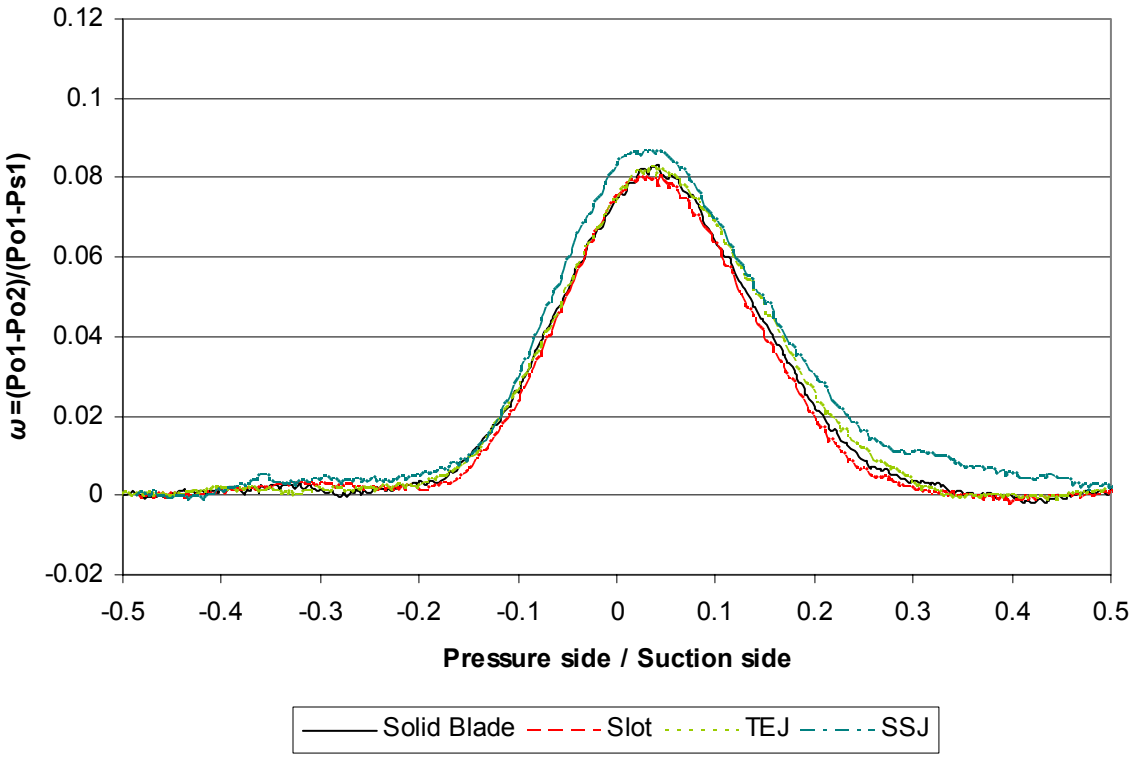

Figure F-2 Solid blade comparison to flow control blade with no flow at 1.8 chords downstream

The performance differences between the blades are most pronounced at 1 chord. However, both plots show that the holes created for flow control do affect the flow of the solid blade. The SSJ has the most pronounced effect followed by the TEJ and lastly the Slot. Due to the small ridges formed on the suction surface by the holes for SSJ, this additional loss might be expected. However, two things should be contemplated. First, the SSJ was tested at a different date than the other three blades, and conditions, such as the freestream values, are different. Second, the behavior of the Slot must be considered.

The Slot performs very close to solid blade at both locations, but this needs to be carefully analyzed before assumptions are made. Both the TEJ and SSJ contain holes spaced evenly throughout most of the span of the trailing edge (about two-thirds). For both of these cases, the area of the flow control opening measures 0.01 in^2 per inch span. The Slot contains an opening along the trailing edge that is more than 4 times that number: 0.045 in^2 per inch span. So, why does the Slot perform better than the SSJ?

Unfortunately, when the Slot was tested with no flow control, its open area had already been nearly quartered when the two side slots were sealed (see Section 2.2.1). In order to have been properly evaluated, the Slot's passages should have been unobstructed. In actuality, the Slot may

have performed worse than the SSJ due to the significant size of the opening, but this was not caught during testing.

If the small openings on the trailing edge created by the TEJ have a small detrimental effect on the blade's performance, an even larger detrimental effect should be expected from a flow control scheme with an area opening more than four times in area at the same location. Thus, despite small additional losses associated with the holes generated by the flow control of 2% for the TEJ and roughly 10% for the SSJ, the SSJ and TEJ not only outperform the Slot when flow control is in use but also when the flow control is deactivated.

Appendix G. Uncertainty Analysis

Outlined in this appendix is the experimental uncertainty analysis for the study presented. Tools used for measurement in any study have inherent bias errors associated with them that affect the accuracy of the data collected by these tools. Shown in Table G-1 are measurements performed in this study with the respective instrument or method used to perform the measurement and the inherent bias error of each instrument. Accuracy values have been gathered from specifications provided by instrument manufacturers. Only the bias error of the manual probe setup was estimated for use in this study. However, this value was of little importance in the study of fan noise reduction.

Table G-1 Accuracy of instruments and methods

Measurement	***Instrument or Method***	***Accuracy***
Static pressures wall taps P	Pressure Systems ESP 32 HD, ±15 psi	±0.03% of full scale or ±0.009 psi
Total pressure upstream P_{o1}	MKS Type 223B Baratron® Differential Capacitance Manometer, 0 – 20 psid	±0.5% of full range or ±0.1 psi
Differential total pressure $P_{o2} - P_{o1}$	MKS Type 223B Baratron® Differential Capacitance Manometer, 0 – 3 psid	±0.5% of full range or ±0.015 psi
Flow control mass flow through orifice meter ΔP	Validyne pressure transducer, 0 – 3 psid	±0.008 psi
Flow control mass flow supply total pressure	Analog pressure gage, 0 – 150 psi	±5 psi
Total temperature T_o	K-type Thermocouple	±2°K
Pitch	Manual probe setup	±0.18 in or ±5%
	Traverse mechanism	±0.0162 in or 0.45%
Incidence angle	Digital protractor	±0.05°

Quantization error due to the National Instruments© A/D PC board was neglected when compared to other bias errors considered. The precision error in the wind tunnel facility's repeatability was monitored through the average inlet Mach number and its standard deviation. A tolerance of ±0.01 of the desired average inlet Mach number was allowed. The maximum standard deviation of the inlet Mach number accepted was ±0.01. Most cases contained a standard deviation of about ±0.005. Cases that did not meet one or both of these requirements were retested.

Therefore, the precision error associated with the repeatability of the tunnel is not considered in the uncertainty analysis.

Each of the bias errors listed in Table G-1 will propagate into the uncertainty of parameters dependent of these measurements. If the assumption is made that uncertainties behave like standard deviations, the uncertainty propagation of the function f can be calculated using Equation G-1 [Beckwith], where x_n is the nth-dependent variable of the function and u is its respective uncertainty.

Equation G-1 $$f\left(x_1, x_2, \cdots, x_n\right) \Rightarrow u_f = \sqrt{\left(\frac{\partial f}{\partial x_1} u_1\right)^2 + \left(\frac{\partial f}{\partial x_2} u_2\right)^2 + \cdots + \left(\frac{\partial f}{\partial x_n} u_n\right)^2}$$

Using this equation, the uncertainty associated with dependent values discussed in this study, such as the pressure loss coefficient, inlet Mach number, and orifice meter mass flow rate, can be calculated. The maximum propagation of uncertainty of key parameters calculated is shown in Table G-2.

Table G-2 Maximum propagation of uncertainty

Parameter	***Maximum propagation of uncertainty***
Pressure loss coefficient ω	±0.003
Inlet Mach number M_1	±0.0056
Orifice meter mass flow rate $\dot{m}$	±0.0005 lbm/s or ±10.0% of value for low $\dot{m}$ or ±1.5% of value for high $\dot{m}$

References

Bailie, S.T., Ng, W.F., Wicks, A.L., "Effects of Flow Control on Forced Response and Performance of a Transonic Compressor," ASME Turbo Expo 2002, Amsterdam, Netherlands, GT-2002-30008, June, 2002.

Beckwith, T.G., Marangoni, R.D., Liendard V., J.H., Mechanical Measurements. 5th ed. Reading, MA: Addison-Wesley Publishing Company, 1995.

Bons, J.P., Sondergaard, R., Rivir, R.B., "The Fluid Dynamics of LPT Blade Separation Control Using Pulsing Jets," *Journal of Turbomachinery*, Vol. 124, pp. 77-85, 2002.

Brookfield, J.M., Waitz, I.A., "Trailing Edge Blowing for Reduction of Turbomachinery Fan Noise," *Journal of Propulsion and Power*, Vol. 16, No. 1, pp. 57-64, 2000.

Brookfield, J.M., Waitz, I.A., Sell, J., "Wake Decay: Effect of Freestream Swirl," *Journal of Propulsion and Power*, Vol. 14, No.2, pp. 215-224, 1998.

Carter, C.J., "Aerodynamic Performance of a Flow Controlled Compressor Stator Using an Imbedded Ejector Pump," Master's Thesis, Virginia Polytechnic Institute and State University, Blacksburg, VA, 2001.

Carter, C.J., Guillot, S.A., Ng, W.F., Copenhaver, W.W., "Aerodynamic Performance of a High Turning Compressor Stator with Flow Control," 37th AIAA/ASME/SAE/ASEE Joint Propulsion Conference & Exhibit, Salt Lake City, Utah, AIAA 2001-3973, July, 2001.

Corcoran, T.E., "Control of Wake from a Simulated Blade by Trailing Edge Blowing," Master's Thesis, Lehigh University, Bethlehem, PA, 1992.

Envia, E., "Fan Noise Reduction: An Overview," *AIAA Paper* 01-0661, 2001.

Hall, E.J., Heidegger, N.J., Delaney, R.A., "ADPAC v1.0 – User's Manual," NASA/CR-1999-206600, 1999.

Leitch, T.A., Saunders, C.A., Ng, W.F., "Reduction of Unsteady Stator-Rotor Interaction using Trailing Edge Blowing," *AIAA Paper* 99-1952, 1999.

"Making Future Commercial Aircraft Quieter," NASA Facts, FS-1999-07-003-GRC, or see http://www.grc.nasa.gov/WWW/PAO/PAIS/fs03grc.htm, 1999.

Munson, B.R., Young, D.F., Okiishi, T.H., Fundamentals of Fluid Mechanics. 3rd update ed. New York: John Wiley & Sons, Inc., 1998.

Naumann, R.G., "Control of Wake from a Simulated Blade by Trailing Edge Blowing," Master's Thesis, Lehigh University, Bethlehem, PA, 1992.

Ng, W.F., Burdisso, R.A., "Active Acoustic and Flow Control for Aeropropulsion," 38th AIAA Aerospace Sciences Meeting & Exhibit, Reno, NV, AIAA 2001-0220, January, 2001.

Oosthuizen, P.H., Carscallen, W.E., Compressible Fluid Flow. New York: McGraw-Hill, 1997.

Park, W.J., Cimbala, J.M., "The Effect of Jet Injection Geometry on Two-Dimensional Momentumless Wakes," *Journal of Fluid Mechanics*, Vol. 224, pp. 29-47, 1991.

Qin, N., Zhu, Y., Ashill, P., Shaw, S.T., "Active Control of Transonic Aerodynamics Using Suction, Blowing, Bumps, and Synthetic Jets," *AIAA Paper* 00-4329, 2000.

Rao, N.M., Feng, J., Burdisso, R.A., Ng, W.F., "Active Flow Control to Reduce Fan Blade Vibration and Noise," *AIAA Paper* 99-1806, 1999.

Sabersky, R.H., Acosta, A.J., Hauptmann, E.G., Gates, E.M., Fluid Flow. 4th ed. Upper Saddle River, NJ: Prentice Hall, 1999.

Sell, J., "Cascade Testing to Assess the Effectiveness of Mass Addition/Removal Wake Management Strategies for Reduction of Rotor-Stator Interaction Noise," Master's Thesis, MIT, Cambridge, MA, 1997.

Waitz, I.A., Brookfield, J.M., Sell, J., Hayden, B.J., "Preliminary Assessment of Wake Management Strategies for Reduction of Turbomachinery Fan Noise," *Journal of Propulsion and Power*, Vol. 12, No.5, pp. 958-66, 1996.

Wilcox, D.C., Turbulence Modeling for CFD. 2nd ed. DCW Industries, 1998.

Vita

HANS R RAVEN E

Hans completed his Bachelors of Science in Mechanical Engineering at Virginia Polytechnic Institute and State University in May of 2001 and went on to attain his Masters of Science in Mechanical Engineering at the same institution. He defended his M.S.M.E. in May of 2004. He was born on November 17, 1977 in Managua, Nicaragua, to Hans R Raven W and Vida Espinosa, and grew up in beautiful Costa Rica where his parents still reside.